A Simplified Method for Estimating the Performance of Supersonic Ram-Jets

A. B. P. BEETON

(National Gas Turbine Establishment)

SUMMARY: Curves are presented which, together with a knowledge of the intake performance, enable ram-jet thrust coefficients and specific consumption figures to be obtained quickly and accurately in the range $M = 1{\cdot}0$ to $3{\cdot}0$.

1. Introduction

The component parts of a typical ram-jet are indicated diagrammatically in Fig. 1. For the purposes of performance estimation, it is convenient to consider the cycle in two stages, the division being made at Station 1.

The first phase therefore consists of the air intake, in which the flight kinetic energy is converted into pressure. The total temperature T_{1t} at the diffuser exit can be calculated from flight conditions only and does not depend on intake performance. The corresponding total pressure P_{1t}, however, depends also on the aerodynamic design of the intake and on the mass flow demand, and therefore involves considerations which come outside the scope of the present paper. It has, therefore, to be assumed that pressure recovery characteristics are available elsewhere for the intake in question.

In the remainder of the ram-jet cycle, the air is first passed through the stabilising baffles, thereby suffering a certain loss of pressure. Then it passes through the parallel combustion chamber in which a typical hydrocarbon fuel is burnt, and in which there is assumed to be no further friction drag on the walls. The resulting gases are finally expanded isentropically through a convergent-divergent nozzle.

As the ram-jet is fundamentally so very simple a form of propulsion system, it might be expected that the presentation of its thrust characteristics would be an equally simple matter. Perhaps the main reason why this is not so is that the high gas temperatures used mean that the concept of a constant specific heat (and at

Received May 1958.

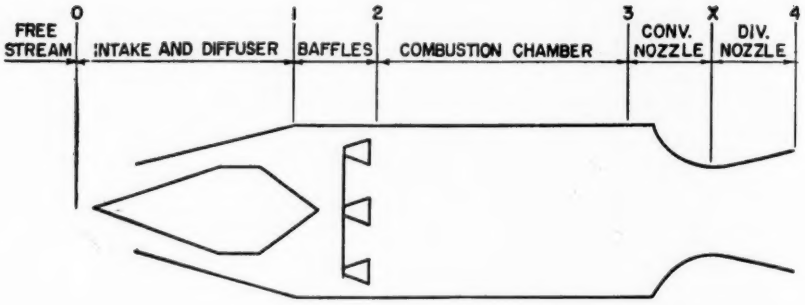

FIGURE 1. Diagram showing the components of a ram-jet engine and the notation used.

the very highest temperatures indeed the concept of a constant gas composition also), in terms of which the performance of other types of power plant can be so successfully expressed, is no longer valid.

In attempting to determine the theoretical thrust direct from fundamental data, it would therefore first be necessary to make a complicated analysis of the combustion gas composition at various parts of the cycle, and then to calculate therefrom the mean molecular weights, pressures, temperatures, velocities, and so on. The majority of these quantities, however, are of no direct importance from the performance point of view. A very great saving in time is therefore to be made by a graphical presentation which eliminates all or most of these superfluous variables. The aim is to devise a system using the minimum number of parameters which can both be read off curves against the basic ram-jet design data (area ratios, baffle loss, and so on), and which will also enable the required thrust coefficient to be calculated from a simple formula.

In addition, the presentation should be such that there is no significant loss in accuracy due to any interpolation necessary, or by having an unduly high ratio of maximum ordinate to minimum ordinate in any one diagram. A further desirable object is thought to be a treatment that is as far as possible non-dimensional in application, so that potential users do not have to cast aside their favourite systems of units.

NOTATION

A flow area

C_T thrust coefficient

F stream thrust, $= \dfrac{mv\,(1+\alpha)}{g} + AP$

g standard gravitational acceleration

m air mass flow per second

M Mach number

P static pressure

P_t total pressure

R gas constant for air

T_t total temperature (°K)

v velocity

α fuel/air ratio

γ ratio of specific heats for air, $=1{\cdot}400$

η combustion efficiency

θ_G gross thrust

θ_N net thrust

λ baffle loss coefficient

ρ density

Suffixes

These correspond to the stations shown in Fig. 1.

2. Definition of Stream Thrust F

For ram-jet calculations it is convenient to introduce a flow function F known as the stream thrust and defined as

$$F=\frac{mv\,(1+\alpha)}{g}+AP. \quad . \quad . \quad . \quad . \quad . \quad (1)$$

This function has the property of remaining constant during frictionless flow in a duct of constant area, however much heat is added. With the suffix notation corresponding to the stations shown in Fig. 1, therefore,

$$F_2=F_3.$$

A further useful property is that the value of F goes through a minimum during isentropic expansion through a choked nozzle, and this minimum value can be predicted by theory as a function of the air inlet temperature and the fuel/air ratio in the combustion chamber. Since, moreover, it is only necessary to measure the test bed thrust developed under the prescribed conditions in order to deduce the actual value of F at the nozzle throat, a convenient yardstick of combustion chamber performance is thereby available.

3. Formula for the Thrust Coefficient

With reference to an atmospheric datum pressure P_0, the gross thrust at the exit section is given by

$$\theta_G = \frac{m(1+\alpha)v_4}{g} + A_4(P_4 - P_0).$$

Since the value of the stream thrust F at this point is by definition

$$F_4 = \frac{m(1+\alpha)v_4}{g} + A_4P_4,$$

we have $$\theta_G = F_4 - A_4P_0 \quad . \quad . \quad . \quad . \quad . \quad . \quad . \quad (2)$$

The net thrust θ_N is the difference between θ_G and the momentum of the intake air under free-stream conditions, *i.e.*

$$\theta_N = \theta_G - \frac{mv_0}{g}$$

$$= F_4 - A_4P_0 - \frac{mv_0}{g} \quad . \quad . \quad . \quad . \quad . \quad (3)$$

The thrust coefficient C_T is usually evaluated on the maximum area A_1, so that

$$C_T = \frac{\theta_N}{\frac{1}{2g}\rho_0 v_0^2 A_1}$$

$$= \frac{2}{\gamma M_0^2}\frac{\theta_N}{A_1P_0} \quad . \quad . \quad . \quad . \quad . \quad . \quad . \quad (4)$$

Substituting the expression for θ_N from equation (3), and putting $\gamma = 1{\cdot}400$, this will be found to reduce to

$$C_T = \frac{10}{7}\left[\frac{\left(\frac{P_{1t}}{P_{0t}}\right)\left(\frac{1}{M_0^2}\frac{P_{0t}}{P_0}\right)}{\left(\frac{A_1P_{1t}}{F_3}\right)}\left\{\frac{\left(\frac{F_4}{F_X}\right)}{\left(\frac{F_3}{F_X}\right)} - \frac{\left(\frac{v_0}{g\sqrt{(T_{1t})}}\right)}{\left(\frac{F_3}{m\sqrt{(T_{1t})}}\right)}\right\} - \frac{1}{M_0^2}\frac{A_4}{A_1}\right] \quad . \quad (5)$$

4. Formula for the Nozzle Exit Pressure

The expression for C_T given in equation (5) was derived on the assumption that the nozzle exit pressure P_4 was either greater than the atmospheric ambient pressure P_0, or at least not sufficiently below it to cause the supersonic flow in the diverging part of the nozzle to break down. It will also have been observed that P_4 is not evaluated in the process of calculating C_T, and so a check may have to be

made periodically to ensure that the jet is not being over-expanded. It is in fact quite easily found from the relation

$$\frac{P_4}{P_0} = \frac{M_0^2\left(\frac{P_{1t}}{P_{0t}}\right)\left(\frac{1}{M_0^2}\frac{P_{0t}}{P_0}\right)\left(\frac{A_X P_{3t}}{F_X}\right)\left(\frac{A_3}{A_X}\right)}{\left(\frac{P_{3t}}{P_4}\right)\left(\frac{A_1 P_{1t}}{F_3}\right)\left(\frac{F_3}{A_X}\right)}.$$

Since $A_X P_{3t}/F_X = 0{\cdot}80 \pm 1$ per cent for all air inlet temperatures and fuel/air ratios, and there is certainly no need to work out P_4 to any greater accuracy than this, we have

$$\frac{P_4}{P_0} = \frac{0{\cdot}8M_0^2\left(\frac{1}{M_0^2}\frac{P_{0t}}{P_0}\right)\left(\frac{P_{1t}}{P_{0t}}\right)\left(\frac{A_3}{A_X}\right)}{\left(\frac{P_{3t}}{P_4}\right)\left(\frac{A_1 P_{1t}}{F_3}\right)\left(\frac{F_3}{F_X}\right)} \quad . \quad . \quad . \quad . \quad (6)$$

5. Formula for the Specific Fuel Consumption

The specific fuel consumption (per hour) is given by

$$\frac{3{,}600\alpha m}{\theta_N} = \frac{7{,}200\alpha m}{\gamma M_0^2 A_1 P_0 C_T}$$

$$= \frac{5{,}143\alpha\left(\frac{1}{M_0^2}\frac{P_{0t}}{P_0}\right)\left(\frac{P_{1t}}{P_{0t}}\right)}{C_T\left(\frac{F_X}{m}\right)\left(\frac{F_3}{F_X}\right)\left(\frac{A_1 P_{1t}}{F_3}\right)}. \quad . \quad . \quad . \quad . \quad (7)$$

6. Derivation of the Curves

It is not proposed to explain here in great detail the methods by which the combustion data of Figs. 2, 3, 4 and 5 were derived. The following brief description indicates the general procedure.

The fuel was assumed to consist of 15 per cent hydrogen and 85 per cent carbon, with a lower calorific value of 10,350 C.H.U./lb.; this can be taken as typical of a liquid fuel of the kerosine type. Combustion was supposed to occur in an atmosphere made up of 76·8 per cent nitrogen and 23·2 per cent oxygen by weight.

The combustion gases were assumed to consist of an equilibrium mixture of N_2, O_2, CO_2, CO, H_2O and H_2, for which total heat and entropy data were available as functions of temperature every 100 degrees up to 2500°K. Equilibrium constants consistent with these values were also worked out over the same range of temperatures. At various gas temperatures and pressures for a given fuel/air ratio, the first thing to do was to work out the gas composition, and hence the mean

STATE UNIVERSITY LIBRARIES
CHARLES E. HOOKER SCIENCE LIBRARY

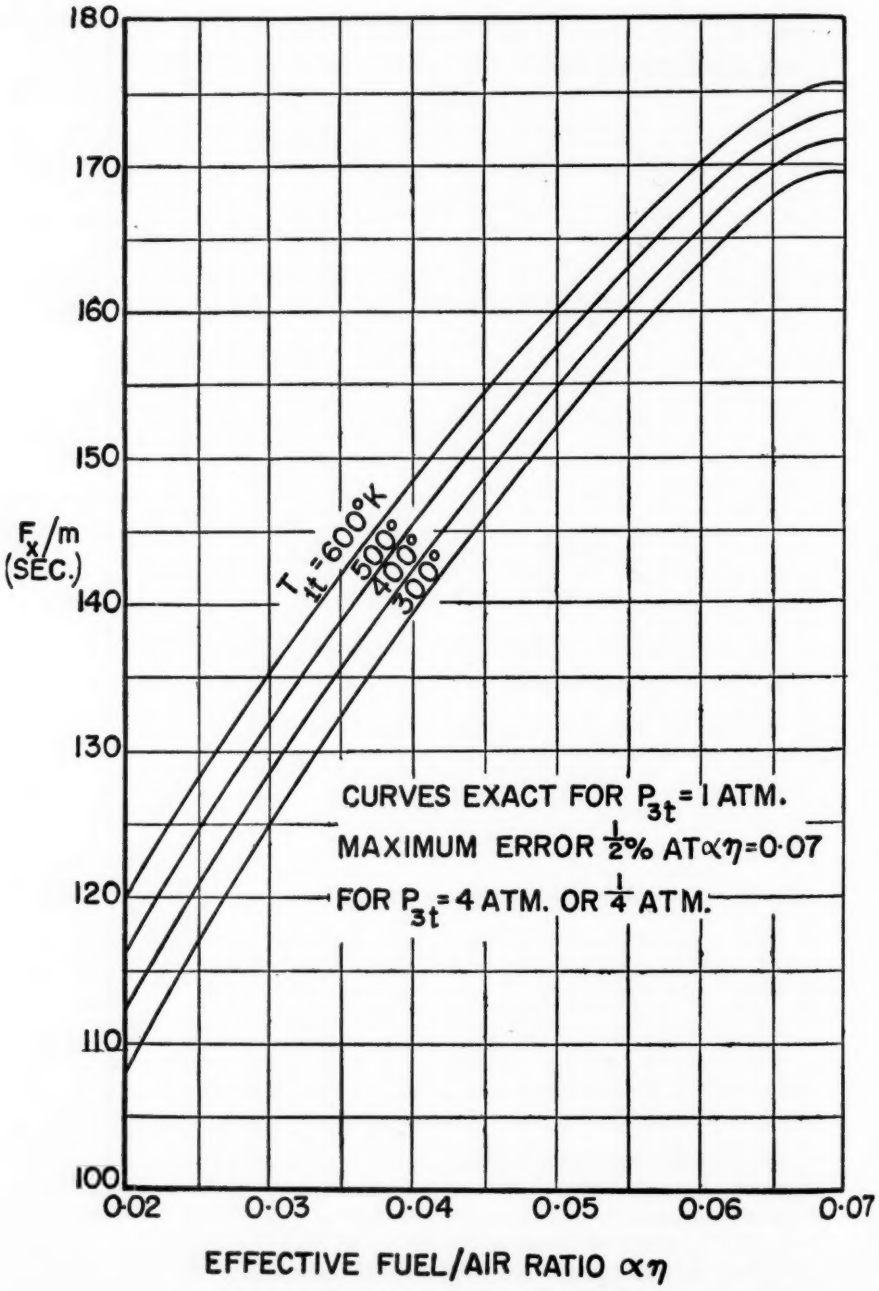

FIGURE 2. Calculated air specific stream thrusts.

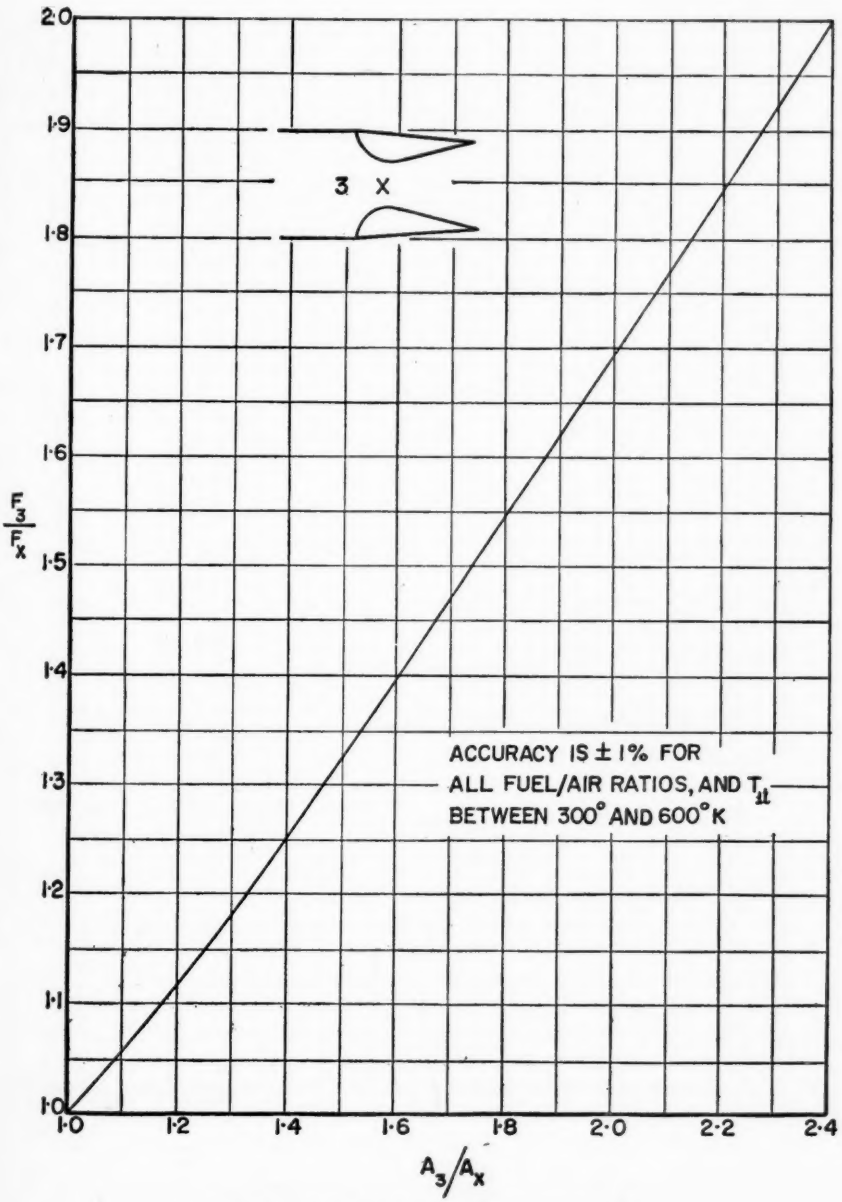

FIGURE 3. Stream thrust ratios for convergent nozzle.

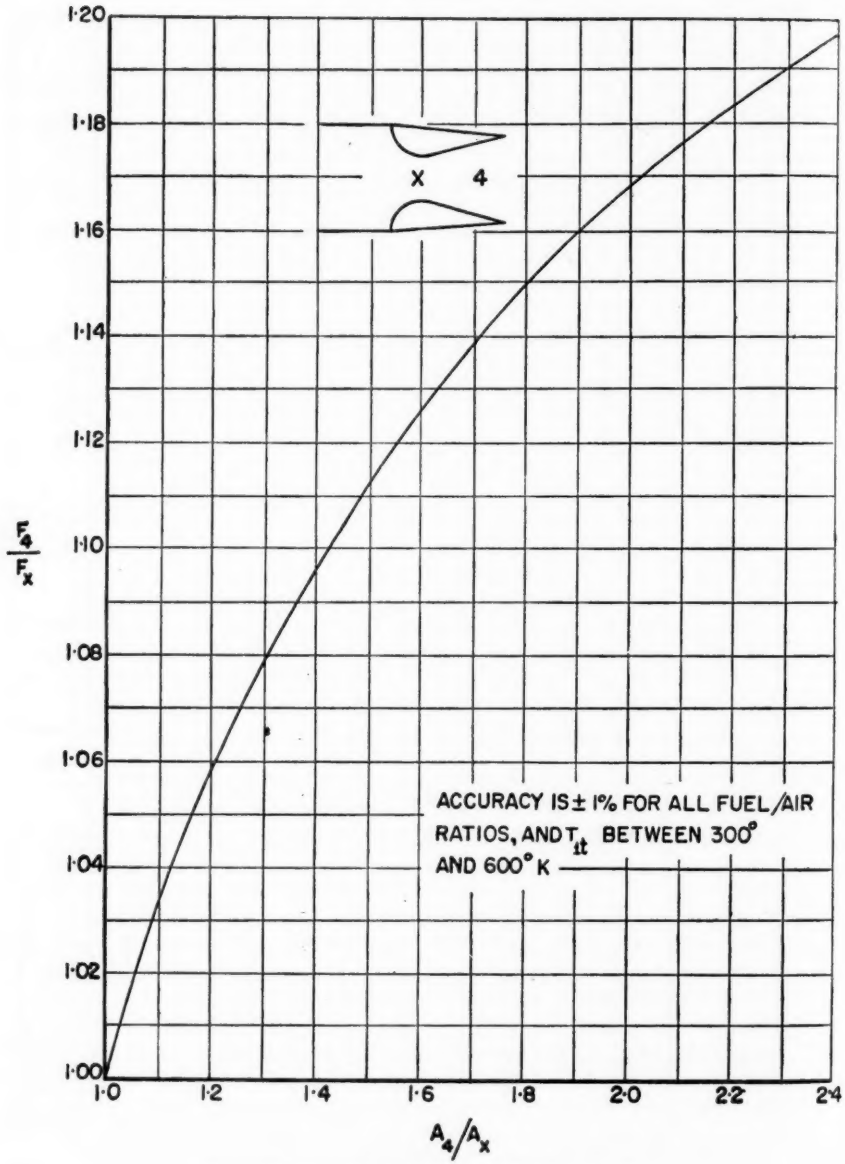

FIGURE 4. Stream thrust ratios for divergent nozzle.

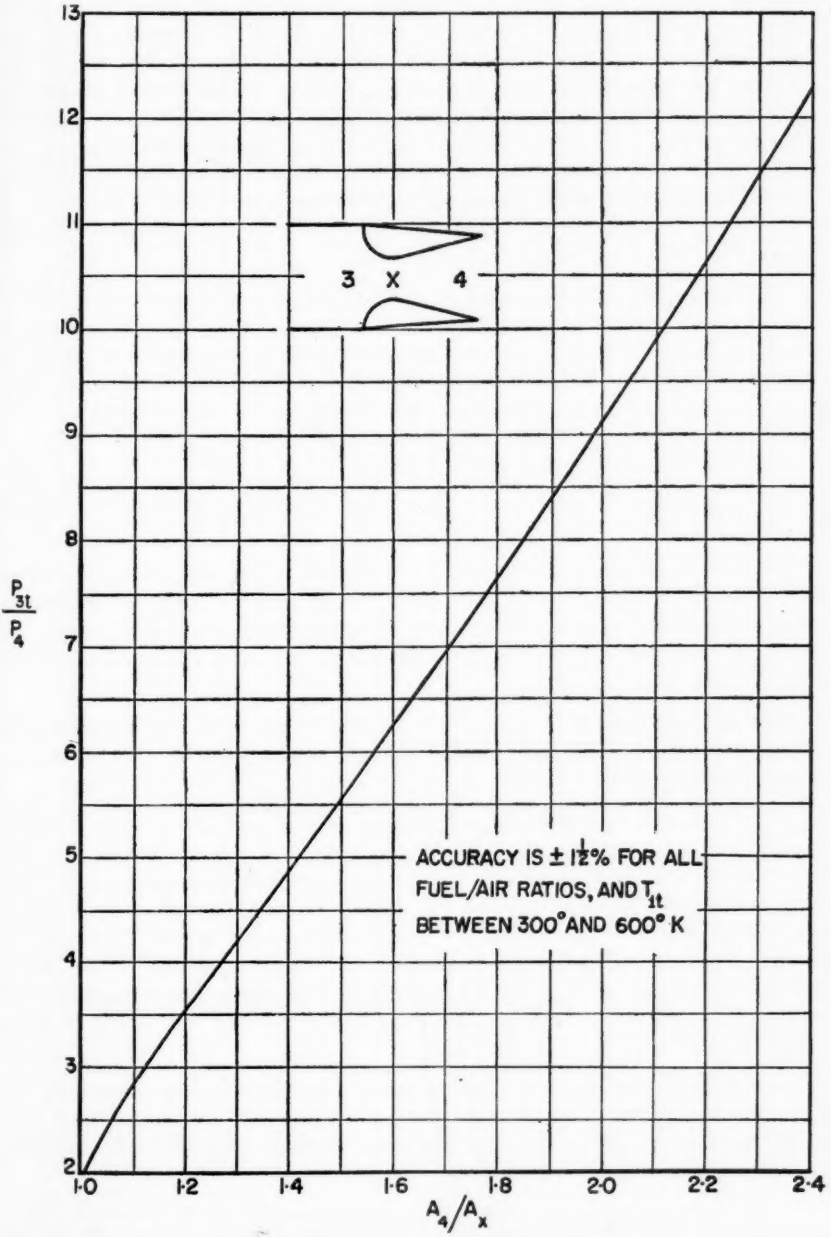

FIGURE 5. Pressure ratios for diverging nozzle.

molecular weight, total heat and entropy. This enabled a total heat/entropy diagram to be plotted in the region of one atmosphere total pressure and at a level of total heat corresponding to air inlet temperatures between 300° and 600°K. The next step was to use this diagram to find the variations in gas velocity, temperature, pressure and mean molecular weight during isentropic expansion from the various input levels of total heat. Finally these values were used to deduce the required parameters F/m and A/A_X down the expansion line. A series of such expansions was considered at total pressures of 4 atm., 2 atm., 1 atm., $\frac{1}{2}$ atm., and $\frac{1}{4}$ atm., at air inlet temperatures of 300°, 400°, 500° and 600°K, and at eight fuel/air ratios between 0·02 and 0·07.

Any measurable effect of absolute pressure on the flow parameters is limited to those fuel/air ratios close to chemically-correct in which dissociation is both considerable and also varies as expansion proceeds. It was found that a maximum error of about $\frac{1}{2}$ per cent resulted from using the 1 atm. curve at either 4 atm. or $\frac{1}{4}$ atm., which represent the approximate practical limits of operation. For fuel/air ratios less than 0·05, the error was negligible.

Figure 2 shows the minimum (*i.e.* throat) value of F/m down the expansion line as a function of T_{1t} and the theoretical fuel/air ratio $\alpha\eta$ at a total pressure of one atmosphere.

Figure 3 gives the required data for expansion in the converging portion of the nozzle as a single curve of F_3/F_X against A_3/A_X. It was found that this would cover all the fuel/air ratios and air inlet temperatures investigated ± 1 per cent, which was considered good enough for the present purpose. The maximum area ratio considered was 2·4 to 1.

Similarly Figures 4 and 5 show, for the diverging part of the nozzle, the corresponding ratio F_4/F_X and the total to static pressure ratio P_{3t}/P_4. The same range of area ratios was covered as for the converging part of the nozzle.

It will always be possible to sacrifice accuracy in order to gain in simplicity and, in the present instance, the unique curves given in Figs. 2, 3, 4 and 5 could have been elaborated upon to give corrections for different fuel/air ratios, air inlet temperatures and absolute pressures. As already stated, exact values were worked out over the range of $\alpha\eta = 0{\cdot}02$ to 0·07, $T_{1t} = 300°K$ to 600°K and $P_{3t} = 4$ atm. to $\frac{1}{4}$ atm. abs. The maximum differences between these theoretically exact values and the curves in Fig. 2 were found to be $\pm\frac{1}{2}$ per cent (due to the effect of pressure only in this case), ± 1 per cent in Figs 3 and 4, and $\pm 1\frac{1}{2}$ per cent in Fig. 5, which is only used as a relatively rough check.

It would be unrealistic to suppose that small effects such as these have any significant importance in performance estimations, and they have accordingly been suppressed here in view of the very considerable gain in simplicity of presentation that is thereby obtained.

Figure 6 merely expresses the baffle loss in terms of quantities which can be used directly in the thrust coefficient formula: it does not depend in any way on the thermodynamics of combustion.

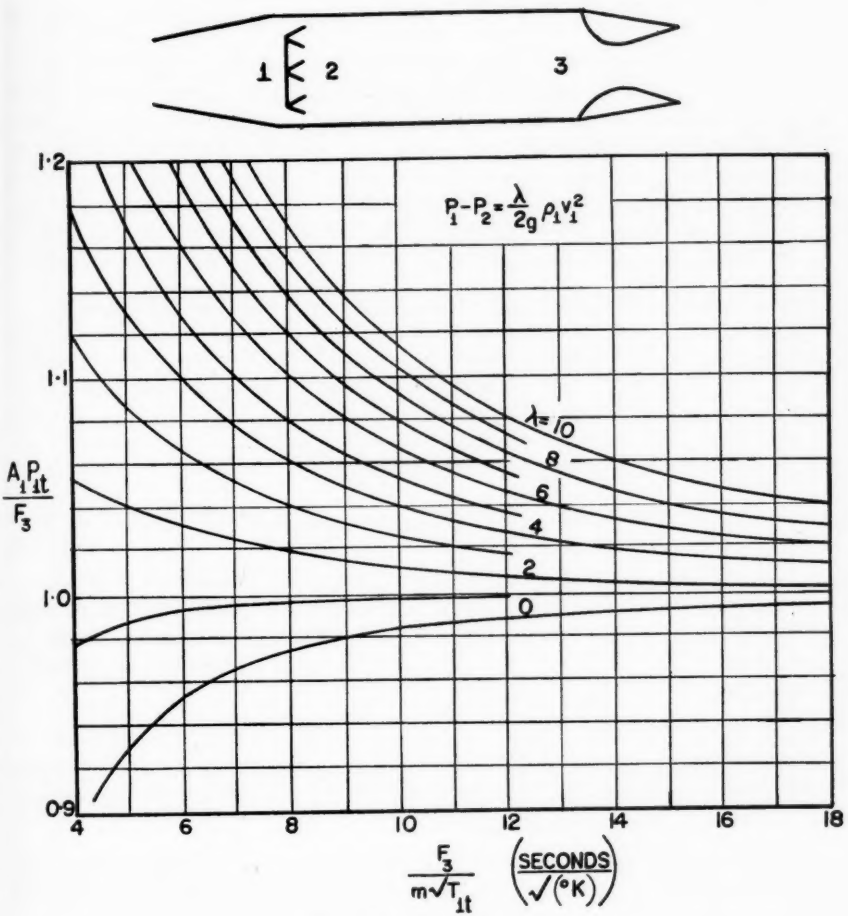

FIGURE 6. Baffle loss curves.

Defining λ as the pressure loss per unit inlet velocity head, we have

$$P_1-P_2=\frac{\lambda}{2g}\rho_1 v_1^2. \quad . \quad . \quad . \quad . \quad . \quad . \quad (8)$$

Since the mass flow, total temperature and flow area are all unaltered, it is possible to write λ in terms of the Mach numbers M_1 and M_2 in front of and behind the baffles respectively:—

$$\frac{M_1}{M_2}=\left(1-\tfrac{1}{2}\gamma\lambda M_1^2\right)\sqrt{\left[\frac{1+\frac{1}{2}(\gamma-1)M_2^2}{1+\frac{1}{2}(\gamma-1)M_1^2}\right]}. \quad . \quad . \quad . \quad . \quad (9)$$

The stream thrust after the baffles is given by

$$F_2 = \frac{mv_2}{g} + A_1 P_2,$$

which will be found to reduce to

$$\frac{F_2}{m\sqrt{(T_{1t})}} = \frac{\sqrt{(R/\gamma g)}\,(1+\gamma M_2^2)}{M_2\sqrt{\{1+\tfrac{1}{2}(\gamma-1)\,M_2^2\}}} \quad . \quad . \quad . \quad . \quad . \quad . \quad (10)$$

Finally, in front of the baffles a flow function can be evaluated in terms of M_1 as

$$\frac{A_1 P_{1t}}{m} = \frac{1}{M_1}\sqrt{\left(\frac{RT_{1t}}{\gamma g}\right)}\left(1+\tfrac{1}{2}(\gamma-1)\,M_1^2\right)^{\frac{1}{2}(\gamma+1)/(\gamma-1)} \quad . \quad . \quad (11)$$

Combining this with the previous expression gives

$$\frac{A_1 P_{1t}}{F_2} = \frac{M_2}{M_1}\,\frac{\{1+\tfrac{1}{2}(\gamma-1)\,M_2^2\}^{1/2}\{1+\tfrac{1}{2}(\gamma-1)\,M_1^2\}^{\frac{1}{2}(\gamma+1)/(\gamma-1)}}{(1+\gamma M_2^2)} \quad . \quad (12)$$

Now it is known that the value of F after the baffles is equal to the value found for the nozzle at the other end of the combustion chamber. Hence calculating

$$\frac{F_3}{m\sqrt{(T_{1t})}} = \frac{F_2}{m\sqrt{(T_{1t})}}$$

specifies M_2, from equation (10). So if the baffle loss λ is known, M_1 is uniquely determined by equation (9). Finally with both M_1 and M_2 known, the value of $A_1P_{1t}/F_3 = A_1P_{1t}/F_2$ is given by equation (12).

Since M_1 and M_2 have no significance from the performance point of view, they can be eliminated and the results merely expressed as values of A_1P_{1t}/F_3 for different values of λ and $F_3/\{m\sqrt{(T_{1t})}\}$, as in Fig. 6.

The quantity $(1/M_0^2)(P_{0t}/P_0)$ given in Fig. 7 is a simple function of Mach number. It is a more suitable function to plot than P_{0t}/P_0 in that it covers a relatively small range of values (between 1·6 and 4·1) for M_0 between 1 and 3, and can therefore be read off the curve reasonably accurately. Otherwise it can be evaluated to any accuracy desired from the relation

$$\frac{P_{0t}}{P_0} = \left(1+\tfrac{1}{2}(\gamma-1)\,M_0^2\right)^{\gamma/(\gamma-1)}.$$

Similarly $v_0/\{g\sqrt{(T_{1t})}\}$ is plotted as another function of M_0 in Fig. 8:—

$$\frac{v_0}{g\sqrt{(T_{1t})}} = M_0\sqrt{\left[\frac{\gamma R/g}{1+\tfrac{1}{2}(\gamma-1)\,M_0^2}\right]}.$$

7. Notes on Using the Curves

In general, the pressure recovery factor P_{1t}/P_{0t} is determined by the aerodynamics of the intake, as affected by the degree of matching with the engine. For many purposes the intake can be considered to be ideally matched to engine requirements at all the points it is necessary to investigate, and the design-point recovery can then be expressed straight away as some function of the flight Mach number. The likely variation of this maximum recovery with M_0 is fairly well known, but typical values would be given with more authority in a book on practical aerodynamics than in a purely theoretical treatment such as this.

When off-design conditions are required with an intake of known characteristics, it is best to re-plot them, if necessary, to show the flow function A_1P_{1t}/m against P_{1t}/P_{0t}. The value of this flow function can be found from the engine operating conditions as the product

$$\left(\frac{A_1P_{1t}}{F_3}\right)\left(\frac{F_3}{F_X}\right)\left(\frac{F_X}{m}\right),$$

which thus enables P_{1t}/P_{0t} to be picked off the intake characteristic.

Another usual case is one in which the intake is known to be running supercritically and the critical condition at the given flight Mach number has been previously worked out, so that $(A_1P_{0t}/m)_{crit}$ can be determined. The thrust coefficient then becomes

$$C_T = \frac{10}{7}\left[\frac{\left(\frac{1}{M_0^2}\frac{P_{0t}}{P_0}\right)}{\left(\frac{A_1P_{0t}}{m}\right)_{crit}}\left\{\left(\frac{F_4}{F_X}\right)\left(\frac{F_X}{m}\right) - \sqrt{(T_{1t})}\left(\frac{v_0}{g\sqrt{(T_{1t})}}\right)\right\} - \left(\frac{1}{M_0^2}\right)\left(\frac{A_4}{A_1}\right)\right] \quad (13)$$

It is therefore unnecessary to work out either P_{1t}/P_{0t}, F_3/F_X, $F_3/\{m\sqrt{(T_{1t})}\}$ or A_1P_{1t}/F_3 in order to derive C_T in this case.

Similarly the specific fuel consumption formula (7) reduces to

$$\frac{5{,}143\,\alpha\left(\frac{1}{M_0^2}\frac{P_{0t}}{P_0}\right)}{C_T\left(\frac{A_1P_{0t}}{m}\right)_{crit}}, \quad . \quad . \quad . \quad . \quad . \quad . \quad (14)$$

while the expression for the nozzle exit pressure is now

$$\frac{P_4}{P_0} = \frac{0{\cdot}8M_0^2\left(\frac{1}{M_0^2}\frac{P_{0t}}{P_0}\right)\left(\frac{F_X}{m}\right)\left(\frac{A_3}{A_X}\right)}{\left(\frac{A_1P_{0t}}{m}\right)_{crit}\left(\frac{P_{3t}}{P_4}\right)} \quad . \quad . \quad . \quad (15)$$

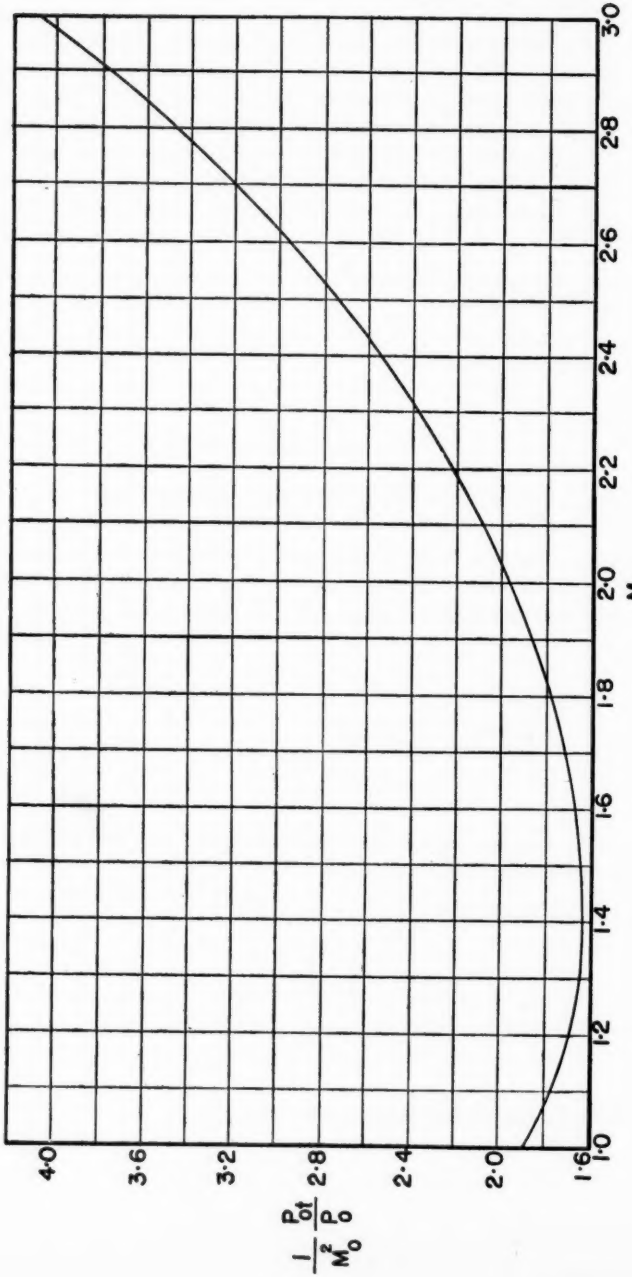

FIGURE 7. Isentropic pressure recovery function.

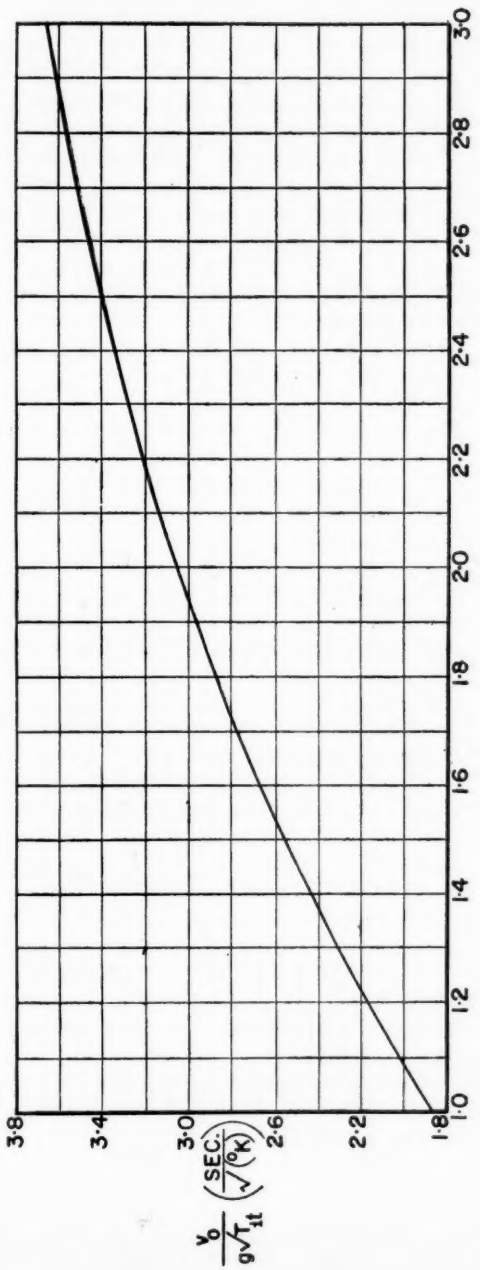

FIGURE 8. Flight velocity function.

Figure 2 shows the ratio F_X/m, also known as the air specific stream thrust, in terms of the air inlet temperature T_{1t} and the effective or theoretical fuel/air ratio $\alpha\eta$. It will be seen how this parameter approaches a maximum at approximately chemically-correct mixture. In practice, however, the greatest value measured on the test bed is somewhat less than the theoretical limit at the given air inlet temperature, and the peak performance of the engine can conveniently be expressed as the maximum air specific stream thrust actually developed. Calculation of $C_{T\max}$ then proceeds directly from this value of F_X/m, without reference to Fig. 2.

In general, it is clear that the combustion chamber operating conditions can be specified by an one of the following:—

(*i*) F_X/m and α,

(*ii*) F_X/m and η,

(*iii*) $\alpha\eta$ and α,

(*iv*) $\alpha\eta$ and η,

(*v*) α and η.

For calculating the thrust coefficient, it is only necessary either to know F_X/m or to be able to obtain it from a given value of $\alpha\eta$ from the curves in Fig. 2. For calculating the specific fuel consumption, the value of the true fuel/air ratio α also has to be deduced from the further information supplied in any of the five ways listed.

It should be noticed, however, that those quantities obtained directly from test-bed results, namely F_X/m and α, are also those which lead to the most direct determination of thrust coefficient and specific consumption. It would nevertheless be more reasonable to specify instead some typical value of η when considering a "hypothetical" engine of unknown characteristics.

Of the remaining terms in the expressions derived for C_T, P_4/P_0 and specific consumption, it will be seen that F_3/F_X, F_4/F_X, P_{3t}/P_4, $(1/M_0^2)(P_{0t}/P_0)$, and $v_0/\{g\sqrt{(T_{1t})}\}$ are obtainable directly from Figs. 3, 4, 5, 7 and 8 respectively. $F_3/\{m\sqrt{(T_{1t})}\}$ then has to be calculated from the three quantities T_{1t}, F_3/F_X and F_X/m. As well as appearing in the formula for C_T, this parameter is used to evaluate A_1P_{1t}/F_3, the only quantity so far undetermined, from the curves in Fig. 6.

It will be observed that the only units specified in this paper are the second and the degree Centigrade absolute. All the figures and formulae are therefore equally well suited for working in metric as in ft.-lb.-sec. units.

8. Example

Any doubts as to the exact method of using Figs. 2 to 8 should be resolved by following through the example in this section.

Data

Flight Mach number	$M_0 = 2{\cdot}30$
Inlet total temperature	$T_{1t} = 450°\text{K}$
Intake pressure recovery ratio	$P_{1t}/P_{0t} = 0{\cdot}75$
Baffle loss coefficient	$\lambda = 6$
Effective fuel/air ratio	$\alpha\eta = 0{\cdot}045$
Combustion efficiency	$\eta = 0{\cdot}80$
Nozzle contraction ratio	$A_3/A_X = 1{\cdot}50$
Nozzle divergence ratio	$A_4/A_X = 1{\cdot}30.$

Hence:—

from Fig. 2,	$F_X/m = 150{\cdot}0$ sec.
from Fig. 7,	$(1/M_0^2)(P_{0t}/P_0) = 2{\cdot}36$
from Fig. 8,	$v_0/\{g\sqrt{(T_{1t})}\} = 3{\cdot}275$ sec. $(°\text{K})^{-1/2}$
from Fig. 3,	$F_3/F_X = 1{\cdot}322$
from Fig. 4,	$F_4/F_X = 1{\cdot}078$
and from Fig. 5,	$P_{3t}/P_4 = 4{\cdot}20.$

Therefore

$$\frac{F_3}{m\sqrt{(T_{1t})}} = \frac{1}{\sqrt{(T_{1t})}}\frac{F_3}{F_X}\frac{F_X}{m} = \frac{1{\cdot}322 \times 150{\cdot}0}{\sqrt{(450)}} = 9{\cdot}34 \text{ sec. } (°\text{K})^{-1/2},$$

Hence from Fig. 6, $$\frac{A_1 P_{1t}}{F_3} = 1{\cdot}0775.$$

Therefore
$$C_T = \frac{10}{7}\left[\frac{\left(\frac{P_{1t}}{P_{0t}}\right)\left(\frac{1}{M_0^2}\frac{P_{0t}}{P_0}\right)}{\left(\frac{A_1 P_{1t}}{F_3}\right)}\left\{\frac{\left(\frac{F_4}{F_X}\right)}{\left(\frac{F_3}{F_X}\right)} - \frac{\left(\frac{v_0}{g\sqrt{(T_{1t})}}\right)}{\left(\frac{F_3}{m\sqrt{(T_{1t})}}\right)}\right\} - \frac{1}{M_0^2}\frac{A_4}{A_3}\right]$$

$$= \frac{10}{7}\left[\frac{0{\cdot}75 \times 2{\cdot}36}{1{\cdot}0775}\left\{\frac{1{\cdot}078}{1{\cdot}322} - \frac{3{\cdot}275}{9{\cdot}34}\right\} - \frac{1{\cdot}30}{2{\cdot}30 \times 2{\cdot}30 \times 1{\cdot}50}\right] = 0{\cdot}857.$$

Also
$$\frac{P_4}{P_0} = \frac{0{\cdot}80\,M_0^2\left(\frac{P_{1t}}{P_{0t}}\right)\left(\frac{1}{M_0^2}\frac{P_{0t}}{P_0}\right)\left(\frac{A_3}{A_X}\right)}{\left(\frac{P_{3t}}{P_4}\right)\left(\frac{A_1P_{1t}}{F_3}\right)\left(\frac{F_3}{F_X}\right)}$$

$$= \frac{0{\cdot}800 \times 2{\cdot}30 \times 2{\cdot}30 \times 0{\cdot}75 \times 2{\cdot}36 \times 1{\cdot}50}{4{\cdot}20 \times 1{\cdot}0775 \times 1{\cdot}322}$$

$$= 1{\cdot}88,$$

indicating that there is still plenty of pressure ratio in hand at the nozzle exit.

Finally, the specific fuel consumption is

$$\frac{5{,}143\,(\alpha\eta)\left(\frac{1}{M_0^2}\frac{P_{0t}}{P_0}\right)\left(\frac{P_{1t}}{P_{0t}}\right)}{\eta C_T\left(\frac{F_X}{m}\right)\left(\frac{F_3}{F_X}\right)\left(\frac{A_1P_{1t}}{F_3}\right)}$$

$$= \frac{5{,}143 \times 0{\cdot}045 \times 2{\cdot}36 \times 0{\cdot}75}{0{\cdot}80 \times 0{\cdot}857 \times 150{\cdot}0 \times 1{\cdot}322 \times 1{\cdot}0775}$$

$$= 2{\cdot}80 \text{ lb./hr./lb. (or kg./hr./kg.)}$$

Variably Reinforced Circular Holes in Stressed Plates

RAYMOND HICKS, Ph.D., M.Sc.

(G.E.C. Simon-Carves Atomic Energy Group)

SUMMARY: Expressions are obtained for the radial, tangential, and shear stresses in an infinite plate containing a variably reinforced circular hole. The variation in the cross-sectional area of the reinforcement is chosen so that the maximum tensile resistance of the reinforcement occurs at points around the hole where the stresses in the plate tend to be high. It is shown that when the reinforcement has a given weight, the effect of varying its cross section is to reduce the stress concentration in the plate.

The following particular applied stress systems are considered:—

(*i*) Uniform tension or compression in one direction.

(*ii*) Uniform shear.

(*iii*) Unequal principal stresses.

For the particular cases of uniform end loading and unequal applied stresses in the ratio 2: 1, data have been obtained which enable the designer to determine the stress distribution in plates with reinforcements having a reasonably wide range of practical dimensions.

1. Introduction

The presence of a circular hole in a flat plate loaded in its own plane results in a stress concentration. If the hole is small compared with the lateral dimensions of the plate its effect on the stress distribution will be local, whereas a large hole may appreciably alter the stress distribution in the whole plate. For example, Kirsch[1] found that the effect of a circular hole in an infinite plate uniformly stressed in one direction is to cause a stress concentration of three, while Timoshenko[2] showed that Kirsch's solution can be applied to a finite plate provided that its least lateral dimension is several times the diameter of the hole. Thus, when the width of the plate is four times the diameter of the hole, the error in the solution when calculating the maximum stress is six per cent.

A bibliography of some important papers dealing with unreinforced circular holes in stressed plates is given in Ref. 3.

Received February 1958

It has been shown by Gurney[4], Timoshenko[5], Beskin[6] and many others (*see*, for example, Ref. 3) that the effect of suitably reinforcing the hole is to decrease the maximum stress in the plate. Thus, when the maximum stress is nowhere to exceed a given value, the presence of the reinforcement results in a decrease in the necessary weight of the structure. The design of the reinforcement is therefore an important problem when the weight of the structure must be as low as possible, for example, with holes in the skin of an aircraft.

It is worth noting that Gurney used a relatively thin annular type of reinforcement and determined the stress distributions in the plate and reinforcement due to various load systems applied at infinity. Timoshenko, however, used a compact ring as a reinforcement, the radial width of which was small compared with the diameter of the hole. That is, a reinforcement with a negligible bending stiffness in the plane of the plate.

Reinforced holes which do not alter the stress distribution in a plate are said to be neutral. The problem of a neutral hole in a plate loaded in its own plane has been considered by Mansfield[7] who found that such holes are possible if there is a choice for the shape of the hole and the tensile stiffness of the reinforcement.

For many practical problems the necessary cross-sectional area of the reinforcement which makes the hole neutral is sufficiently large to be prohibitive, while the necessary shape of the hole in some cases is defined by a curve which does not close.

Mansfield[8] also considered the problem of a variably reinforced circular hole in an end-loaded plate. Using an inverse method of solution and taking stress functions which gave two independent stress pertubations around the hole, he found expressions for the cross-sectional areas of reinforcements corresponding to the chosen number of stress pertubations. He found that the necessary cross-sectional areas of the reinforcements were defined by

$$A_R = \frac{\lambda_1 + \lambda_2 \cos n\theta}{\lambda_3 + \lambda_4 \cos n\theta} ,$$

where n is 0, 2 or 4, depending on the applied stress distribution.

The problem of a reinforced elliptical hole in an end-loaded plate has been considered by Wells[9] for several important applied stress distributions, while the author[10] has considered the design of similar reinforced holes for stress systems of the type found in cylindrical and ellipsoidal pressure vessels.

This investigation deals with a reinforced hole in an infinite plate under the action of the following applied stress systems:—

(*i*) Uniform tension in one direction.

(*ii*) Uniform shear.

(*iii*) Unequal principal stresses.

The reinforcement has a variable cross-sectional area, so designed that its tensile resistance increases at points around the hole where the stresses in the plate tend to be high. The advantage of a reinforcement of this type is that no material is wasted in reinforcing parts of the hole where the accompanying stresses are relatively small.

Expressions are obtained for the radial, tangential, and shear stresses in the plate. These expressions are written in terms of a set of constants which can be evaluated readily for any particular numerical problem. As would be expected, the concentration of stress is local, so that the solution can be applied to a finite plate provided that its least lateral dimension is several times the diameter of the hole.

For the problem of a plate uniformly pulled in one direction, the constants appearing in the expressions for the stress components have been evaluated for a wide range of reinforcements with practical dimensions, it being assumed that Poisson's ratio is 0·3. Furthermore, curves have been obtained for the maximum tangential stresses around holes in plates having reinforcements of a constant weight, but with different variations in their cross-sectional areas. It has been found that, for a given maximum tangential stress, the weight of the reinforcement can be reduced by as much as 50 per cent by suitably varying its cross-sectional area.

Similarly, for the important case of unequal applied principal stresses in the ratio 2:1, values of the constants appearing in the expressions for the stress components have been calculated for the same range of practical reinforcements.

NOTATION

$\widehat{rr}, \widehat{\theta\theta}, \widehat{r\theta}$	stress components
f_x, f_y	principal stresses
f	applied stress
q	applied shear stress
F	tensile force in reinforcement
r, θ	polar co-ordinates
x, y	Cartesian co-ordinates
b	radius of hole
h	thickness of plate
A_R	area of variable reinforcement
A_{CR}	area of constant reinforcement
ϕ	stress function
E	Young's modulus
M, N	parameters defined in equations (19) and (36)

ν Poisson's ratio

ε strain

$\alpha', \beta', \alpha, \beta$ constants

R, ω parameters introduced in Section 7.

Suffix

b denotes boundary conditions.

2. Uniform Tension

For an infinite plate uniformly stressed in the direction of the x-axis, the boundary conditions at infinity are

$$\left.\begin{aligned}(\widehat{rr})_\infty &= \frac{f}{2}(1+\cos 2\theta)\\ (\widehat{r\theta})_\infty &= -\frac{f}{2}\sin 2\theta\end{aligned}\right\} \quad \ldots\ldots \quad (1)$$

where the θ co-ordinate is measured from the direction of the x-axis.

Referring to Fig. 1, around the hole the boundary conditions are obtained by considering an elemental length of the reinforcement subtended by an angle $d\theta$. There is assumed to be no radial shear on a radial cross section of the reinforcement, because its bending stiffness in the plane of the plate is small. This follows from the work of Reissner and Morduchow[11], who concluded that reinforcements which have a relatively small bending stiffness in the plane of the plate experience primarily tensile and compressive stresses as opposed to bending stresses.

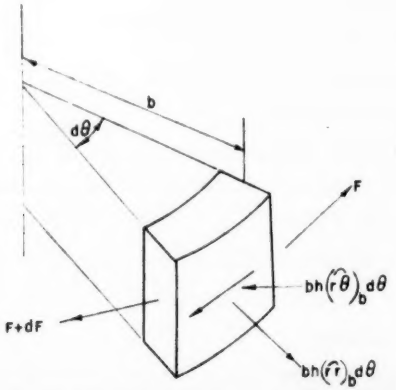

FIGURE 1. Forces acting on an elemental length of reinforcement.

For force equilibrium in a radial and tangential direction respectively, it can be shown that

$$\left.\begin{aligned} F &= bh\,(\widehat{rr})_b \\ \frac{dF}{d\theta} &= -hb\,(\widehat{r\theta})_b \end{aligned}\right\} \quad . \quad . \quad . \quad . \quad . \quad (2)$$

Also, equating the strain in the reinforcement to the tangential strain in the adjacent part of the plate, it is found that

$$\frac{F}{A_R} = (\widehat{\theta\theta} - \nu\widehat{rr})_b, \quad . \quad . \quad . \quad . \quad . \quad (3)$$

it being assumed that the materials of the reinforcement and the plate are the same.

Combining (2) and (3), the following boundary condition is obtained

$$(\widehat{\theta\theta} - \nu\widehat{rr})_b \frac{A_R}{bh} - (\widehat{rr})_b = 0 \quad . \quad . \quad . \quad . \quad (4)$$

From Ref. 1, the stresses around an unreinforced hole in a plate uniformly stressed in one direction are

$$\left.\begin{aligned} (\widehat{rr})_b &= 0 \\ (\widehat{r\theta})_b &= 0 \\ (\widehat{\theta\theta})_b &= f\,(1 - 2\cos 2\theta) \end{aligned}\right\} \quad . \quad . \quad . \quad . \quad (5)$$

Thus the presence of the hole increases the maximum stress in the plate by a factor of three. The effect of suitably reinforcing the hole is to decrease the stress concentration in the plate, and in this analysis the reinforcement is designed so that its cross-sectional area varies in a similar manner to the tangential stress given by (5), that is

$$A_R = \alpha' + \beta' \cos 2\theta, \quad . \quad . \quad . \quad . \quad . \quad (6)$$

where α' and β' are constants so that $\alpha' + \beta'$ is the area of the reinforcement at the point $\theta = 0$, and $\alpha' - \beta'$ is the area of the reinforcement at the point $\theta = \pi/2$. It is clear that α' is the cross-sectional area of a reinforcement having the same weight as the variable reinforcement defined by expression (6). Comparing (5) and (6), it can be seen that the advantage of the variable reinforcement is that its effectiveness in decreasing the tangential stress around the hole increases as the tangential stress tends to increase.

Using the expression for A_R given by (6), the boundary condition specified by (4) can be written as

$$(\widehat{\theta\theta} - \nu\widehat{rr})_b\,(\alpha + \beta\cos 2\theta) - (\widehat{rr})_b = 0, \quad . \quad . \quad . \quad . \quad (7)$$

where α has been written for α'/bh and β for β'/bh.

If ϕ is a function which satisfies the equation

$$\left(\frac{\partial^2}{\partial r^2}+\frac{1}{r}\frac{\partial}{\partial r}+\frac{1}{r^2}\frac{\partial^2}{\partial\theta^2}\right)^2\phi=0 \quad . \quad . \quad . \quad . \quad . \quad (8)$$

the stresses in the plate are given by

$$\left.\begin{aligned}\widehat{rr}&=\frac{1}{r}\frac{\partial\phi}{\partial r}+\frac{1}{r^2}\frac{\partial^2\phi}{\partial\theta^2}\\ \widehat{\theta\theta}&=\frac{\partial^2\phi}{\partial r^2}\\ \widehat{r\theta}&=-\frac{\partial}{\partial r}\left(\frac{1}{r}\frac{\partial\phi}{\partial\theta}\right)\end{aligned}\right\} \quad . \quad . \quad . \quad . \quad . \quad (9)$$

The solution of (8) which can be made to satisfy the boundary conditions is

$$\phi=A_0\log r+B_0r^2\log r+C_0r^2+D_0+\sum_{n=2}^{\infty}\left[A_n'r^n+B_n'r^{n+2}+\frac{A_n}{r^n}+\frac{B_n}{r^{n-2}}\right]\cos n\theta, \quad (10)$$

where n is even and A_0, A_n', B_n', etc., are arbitrary constants. It is worth noting that if A_0, B_0, C_0 and D_0 are zero and $\sin n\theta$ is substituted for $\cos n\theta$, the resulting stress function can be used to solve the problem of a variably reinforced hole in a plate having a pure shear distribution applied at infinity.

Substituting (10) in (9), the stress components become

$$\left.\begin{aligned}\widehat{rr}&=\frac{A_0}{r^2}+B_0(1+2\log r)+2C_0-\sum_{n=2}^{\infty}\left[n(n-1)A_n'r^{n-2}+(n+1)(n-2)B_n'r^n+\right.\\ &\qquad\left.+n(n+1)\frac{A_n}{r^{n+2}}+(n+2)(n-1)\frac{B_n}{r^n}\right]\cos n\theta\\ \widehat{\theta\theta}&=-\frac{A_0}{r^2}+B_0(3+2\log r)+2C_0+\sum_{n=2}^{\infty}\left[n(n-1)A_n'r^{n-2}+\right.\\ &\qquad\left.+(n+2)(n+1)B_n'r^n+n(n+1)\frac{A_n}{r^{n+2}}+(n-2)(n-1)\frac{B_n}{r^n}\right]\cos n\theta\\ \widehat{r\theta}&=\sum_{n=2}^{\infty}n\left[(n-1)A_n'r^{n-2}+(n+1)B_n'r^n-(n+1)\frac{A_n}{r^{n+2}}-(n-1)\frac{B_n}{r^n}\right]\sin n\theta.\end{aligned}\right\} \quad (11)$$

Using these expressions, for the stresses to remain finite as r approaches infinity it is found that

$$\left.\begin{aligned}B_0&=0\\ A_n'&=0 \quad \text{when } n\neq 2\\ B_n'&=0 \quad \text{when } n\geqslant 2\end{aligned}\right\} \quad . \quad . \quad . \quad . \quad (12)$$

Also, from (1),
$$C_0 = -A_2' = \frac{f}{4} \quad . \quad . \quad . \quad . \quad . \quad (13)$$

Eliminating F from the equilibrium equations given by (2), the following boundary condition is obtained

$$\frac{\partial}{\partial\theta}(\widehat{rr})_b + (\widehat{r\theta})_b = 0. \quad . \quad . \quad . \quad . \quad . \quad (14)$$

This condition is satisfied when

$$B_n = \left\{ \frac{f\delta_2}{4} - \frac{A_n}{b^{n+2}} \right\} b^n \quad . \quad . \quad . \quad . \quad . \quad (15)$$

where $\delta_2 = 1$ when $n = 2$

$\delta_2 = 0$ when $n \neq 2$.

Using the values of the constants given by (12), (13) and (15), the stress components become

$$\left.\begin{aligned}
\widehat{rr} &= \frac{A_0}{r^2} + \frac{f}{2} - \sum_{n=2}^{\infty} \left\{ \frac{A_n}{r^n}\left[\frac{n(n+1)}{r^2} - \frac{(n+2)(n-1)}{b^2}\right] + f\delta_2\left[\frac{b^2}{r^2} - \frac{1}{2}\right] \right\} \cos n\theta \\
\widehat{\theta\theta} &= -\frac{A_0}{r^2} + \frac{f}{2} + \sum_{n=2}^{\infty} \left\{ \frac{A_n}{r^n}\left[\frac{n(n+1)}{r^2} - \frac{(n-1)(n-2)}{b^2}\right] - \frac{f\delta_2}{2} \right\} \cos n\theta \\
\widehat{r\theta} &= -\sum_{n=2}^{\infty} \left\{ n\frac{A_n}{r^n}\left[\frac{(n+1)}{r^2} - \frac{(n-1)}{b^2}\right] + \frac{f\delta_2}{2}\left[1 + \frac{b^2}{r^2}\right] \right\} \sin n\theta
\end{aligned}\right\} \quad (16)$$

$$\text{Also} \quad F = bh\left\{ \frac{A_0}{b^2} + \frac{f}{2} - \sum_{n=2}^{\infty} \left[\frac{2A_n}{b^{n+2}} + \frac{f\delta_2}{2}\right] \cos n\theta \right\}. \quad . \quad . \quad . \quad (17)$$

It is worth noting that these expressions are independent of the cross-sectional area of the reinforcement. They are, therefore, valid for any type of reinforcement provided its bending stiffness in the plane of the plate is negligible. Furthermore, by applying the principle of superposition, these expressions can be used to find corresponding expressions for the stress distribution in a plate subjected to a pure shear or an unequal principal stress distribution at infinity.

The arbitrary constants appearing in the expressions for the stress components must be chosen to satisfy the boundary condition given by (7). Thus, substituting the appropriate expressions for $(\widehat{rr})_b$ and $(\widehat{\theta\theta})_b$ in (7) and equating to zero the coefficients of each $\cos n\theta$ term in the resulting form of the boundary condition, the following set of equations is obtained for the arbitrary constants A_0 and A_n.

$$\left\{N\delta_0+M\delta_2+2\frac{A_n}{b^{n+2}}[\alpha(2n-1+\nu)+1]\gamma_0+\beta\left[(2n-5+\nu)\frac{A_{n-2}}{b^n}\gamma_2-\frac{(1-\nu)}{4}f\delta_4+\right.\right.$$
$$\left.\left.+(2n+3+\nu)\frac{A_{n+2}}{b^{n+4}}\right]=0\right\}_{n=0,\,2,\,4,\,\ldots} \qquad (18)$$

$$\text{where}\quad N=\frac{f}{2}[(1-\nu)\alpha-1]-\frac{A_0}{b^2}[(1+\nu)\alpha+1]-\frac{\beta f}{4}(1-\nu)$$
$$M=\frac{\beta f}{2}(1-\nu)-\frac{A_0}{b^2}\beta(1+\nu)-\frac{f}{2}[(1-\nu)\alpha-1] \qquad (19)$$

and

$$\delta_m=1 \text{ when } n=m, \qquad \gamma_m=0 \text{ when } n=m,$$
$$\delta_m=0 \text{ when } n\neq m, \qquad A_{-2}=0.$$
$$\gamma_m=1 \text{ when } n\neq m,$$

From (4) and (16), it follows that, for any given set of values for the constants A_n, the solution of the problem is exact provided that the reinforcement is chosen so that the variation in its cross-sectional area is given by the expression

$$A_R\left\{f(1-\nu)\sin^2\theta-(1+\nu)\frac{A_0}{b^2}+2\sum_{n=2}\frac{A_n}{b^{n+2}}[(2n-1)+\nu]\cos n\theta\right\}$$
$$=bh\left\{\frac{A_0}{b^2}+f\sin^2\theta-2\sum_{n=2}\frac{A_n}{b^{n+2}}\cos n\theta\right\}. \qquad (20)$$

Thus, if there is no restriction on the variation of the cross-sectional area of the reinforcement, and if there is only one particular stress system applied to the plate, the expression (20) can be used to design variable reinforcements corresponding to any reasonable number of stress perturbations. However, when dealing with particular problems the constants A_n must be chosen to satisfy certain design conditions. For example, the chosen values for the constants must correspond to reinforcements having practical dimensions and with stress concentrations which are relatively low for a reinforcement of a given weight. As previously stated, this method of solution has been used by Mansfield.

In this analysis it is proposed to use an inverse method of solution. Thus, when dealing with practical problems it is assumed initially that the stress distribution in the plate is given with sufficient accuracy by taking a finite number of terms in the expression for the stress function. The constants A_n are then determined from (18) and the cross-sectional area of the reinforcement necessary to make the solution exact is determined from (20). Finally, it is verified that the cross-sectional area of the reinforcement calculated from (20) does not differ appreciably from the given cross-sectional area of the reinforcement defined by (6).

As an example, consider the following extreme case where $\beta = -\alpha$ and $\alpha = 0{\cdot}1$. Assuming $A_n = 0$ when $n > 8$, the solution of the first five of equations (18) gives

$$\left.\begin{aligned} A_0 &= -0{\cdot}352182\ b^2 f \\ A_2 &= -0{\cdot}150104\ b^4 f \\ A_4 &= -0{\cdot}020629\ b^6 f \\ A_6 &= -0{\cdot}003843\ b^8 f \\ A_8 &= -0{\cdot}000858\ b^{10} f \end{aligned}\right\} \quad . \quad . \quad . \quad . \quad . \quad (21)$$

Substituting from (21) into (20), the stress distribution associated with these constants is exact when the variation in the cross-sectional area of the reinforcement is given by (20). It can be verified that this distribution in cross-sectional area of the reinforcement is virtually the same as

$$A_R = 0{\cdot}1\ bh\,(1 - \cos 2\theta),$$

which is the given expression for the variation in the cross-sectional area of the reinforcement. Thus, for this particular example, the inverse method of obtaining the arbitrary constants A_n is justified.

Substituting from (21) into (16), it is found that, when r is several times greater than the hole diameter, the stress components reduce to

$$\left.\begin{aligned} \widehat{rr} &= \frac{f}{2}(1 + \cos 2\theta) \\ \widehat{\theta\theta} &= \frac{f}{2}(1 - \cos 2\theta) \\ \widehat{r\theta} &= -\frac{f}{2}\sin 2\theta. \end{aligned}\right\} \quad . \quad . \quad . \quad . \quad . \quad (22)$$

That is, the effect of the hole is local, and for this reason the solution can be applied to a finite plate provided that its width is several times greater than the diameter of the hole.

3. Design Data for Uniform Tension

For design purposes, values of a_n ($a_n f\, b^{n+2} = -A_n$) are given in Table I for a wide range of reinforcements with practical dimensions. Using these values for the constants, it can be verified that the cross-sectional areas of the variable reinforcements defined by (20) are virtually the same as the cross-sectional areas of the reinforcements defined by (6). That is, the inverse method of determining the stress distribution is justified for all reinforcements given in Table I.

TABLE I

VALUES OF a_n ($a_n\ b^{n+2} f = -A_n$) FOR VARIOUS VALUES OF α AND β WHEN $\nu = 0{\cdot}3$

	β/α					α
	$-1{\cdot}0$	$-0{\cdot}8$	$-0{\cdot}7$	$-0{\cdot}5$	$-0{\cdot}3$	
a_0	0·35218	0·36321	0·36883	0·38035	0·39235	0·1
a_2	0·15010	0·15368	0·15574	0·16036	0·16563	
a_4	0·02063	0·01639	0·01435	0·01032	0·00629	
a_6	0·00384	0·00237	0·00179	0·00090	0·00033	
a_8	0·00086	0·00042	0·00028	0·00010	0·00002	
a_0	0·19992	0·21485	0·22280	0·23776	0·25470	0·3
a_2	0·06526	0·06864	0·07112	0·07729	0·08492	
a_4	0·02179	0·01668	0·01451	0·01047	0·00650	
a_6	0·00646	0·00370	0·00275	0·00136	0·00049	
a_8	0·00196	0·00090	0·00058	0·00020	0·00004	
a_0	0·11796	0·13104	0·13745	0·15122	0·16715	0·5
a_2	0·02598	0·02938	0·03200	0·03846	0·04638	
a_4	0·01764	0·01331	0·01160	0·00849	0·00537	
a_6	0·00596	0·00332	0·00246	0·00122	0·00045	
a_8	0·00195	0·00087	0·00056	0·00020	0·00004	
a_0	0·04558	0·05359	0·05782	0·06793	0·08097	0·8
a_2	−0·00492	−0·00062	0·00220	0·00865	0·01619	
a_4	0·00226	0·00943	0·00833	0·00627	0·00408	
a_6	0·00450	0·00253	0·00189	0·00096	0·00036	
a_8	0·00154	0·00069	0·00045	0·00016	0·00004	

It is worth noting that when $\alpha = \beta = 0$ the hole is unreinforced and the solution of (18) gives

$$\left.\begin{aligned} A_0 &= -\frac{fb^2}{2} \\ A_2 &= -\frac{fb^4}{4} \\ A_n &= 0 \quad \text{when} \quad n > 2 \end{aligned}\right\} \quad . \quad . \quad . \quad . \quad . \quad (23)$$

Also, for a reinforcement with a constant cross-sectional area, $\beta = 0$ and the expressions for the constants are

$$\left.\begin{aligned} A_0 &= -\frac{f}{2}\left[\frac{1-\alpha(1-\nu)}{1+\alpha(1+\nu)}\right] b^2 \\ A_2 &= -\frac{f}{4}\left[\frac{1-\alpha(1-\nu)}{1+\alpha(3+\nu)}\right] b^4 \\ A_n &= 0 \quad \text{when} \quad n > 2. \end{aligned}\right\} \quad . \quad . \quad . \quad . \quad . \quad (24)$$

Thus, around the hole

$$\left.\begin{aligned}(\widehat{rr})_b &= \frac{\alpha f}{[1+\alpha(1+\nu)]} - \frac{2\alpha f\cos 2\theta}{[1+\alpha(3+\nu)]}\\ (\widehat{\theta\theta})_b &= \frac{(1+\alpha\nu)f}{[1+\alpha(1+\nu)]} - \frac{2(1+\alpha\nu)f\cos 2\theta}{[1+\alpha(3+\nu)]}\\ (\widehat{r\theta})_b &= \frac{-4\alpha f\sin 2\theta}{[1+\alpha(3+\nu)]}\end{aligned}\right\} \quad . \quad . \quad . \quad (25)$$

The expressions show that, when there is no reinforcement, the maximum stress acts in a tangential direction on the boundary of the hole and equals $3f$. Furthermore, this maximum stress decreases as the area of reinforcement increases from zero.

It is outside the scope of this paper to determine the maximum principal stresses or octahedral stress concentration factors for a wide practical range of

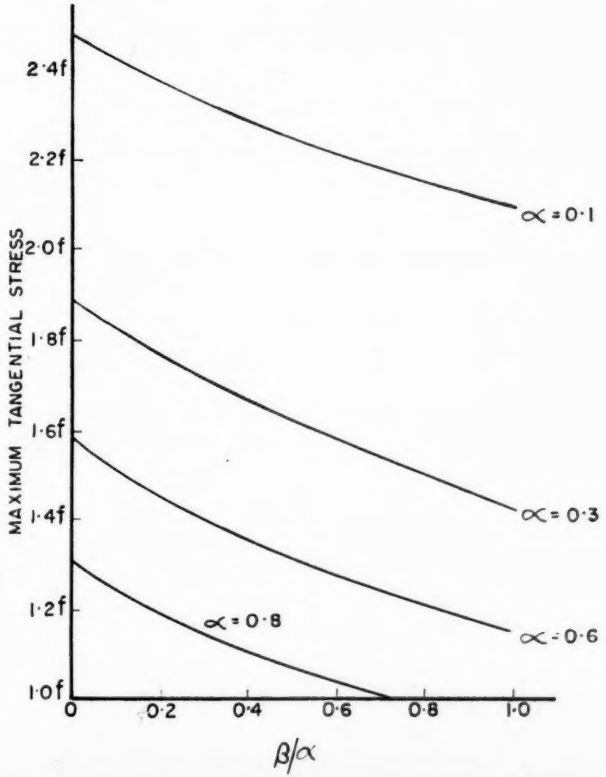

FIGURE 2. Maximum tangential stress for constant weight reinforcements.

reinforcements. Furthermore, for any particular example these can readily be obtained by using the information given in Table I. However, to illustrate the effect of varying the cross-sectional area of the reinforcement, curves showing the variation in the maximum tangential stress for constant weight reinforcements are given in Fig. 2. From these curves it can be concluded that for a given maximum tangential stress, the necessary weight of the reinforcement can be reduced by as much as 50 per cent by suitably varying the cross-sectional area of the reinforcement.

4. Pure Shear

Using the principle of superposition, and rotating the co-ordinate axes through 45°, the stress components given by (16) can be used to obtain the following expressions for the stress components in an infinite plate under the action of a constant shear stress distribution.

Thus, if q is the applied shear stress

$$\left.\begin{aligned}
\widehat{rr} &= -\sum_{n=2}^{\infty}\left\{\frac{A_n}{r^n b^2}\left[n(n+1)\frac{b^2}{r^2}-(n-1)(n+2)\right]+q\left[2\frac{b^2}{r^2}-1\right]\delta_2\right\}\sin n\theta \\
\widehat{\theta\theta} &= \sum_{n=2}^{\infty}\left\{\frac{A_n}{r^n b^2}\left[n(n+1)\frac{b^2}{r^2}-(n-1)(n-2)\right]-q\delta_2\right\}\sin n\theta \\
\widehat{r\theta} &= \sum_{n=2}^{\infty} n\left\{\frac{A_n}{r^n b^2}\left[(n+1)\frac{b^2}{r^2}-(n-1)\right]+\frac{q}{2}\left(1+\frac{b^2}{r^2}\right)\delta_2\right\}\cos n\theta.
\end{aligned}\right\} \quad (26)$$

The stresses around an unreinforced hole in a similarly loaded plate are

$$\left.\begin{aligned}
(\widehat{rr})_b &= (\widehat{r\theta})_b = 0 \\
(\widehat{\theta\theta})_b &= -4q\sin 2\theta
\end{aligned}\right\} \quad . \quad . \quad . \quad . \quad (27)$$

Thus the stress concentrations occur on radial lines which bisect the co-ordinate axis. It therefore follows that a suitable reinforcement would have a variable cross-sectional area given by

$$A_R = \alpha' + \beta' \cos 4\theta. \quad . \quad . \quad . \quad . \quad . \quad (28)$$

From (4) and (28), the compatibility condition becomes

$$(\widehat{\theta\theta} - \nu\widehat{rr})_b\,(\alpha + \beta\cos 4\theta) - (\widehat{rr})_b = 0, \quad . \quad . \quad . \quad . \quad (29)$$

where α and β are given by α'/bh and β'/bh respectively.

Substituting in (29) the appropriate expressions for the stress components, and equating to zero the coefficients of the resulting $\sin n\theta$ terms, we obtain the boundary condition as given by equations (30).

$$\left\{ q\,[1-\alpha(1-\nu)]\,\delta_2+\frac{\beta}{2}q\,(1-\nu)\,\delta_2-\frac{\beta}{2}q\,(1-\nu)\,\delta_6-\beta\frac{A_2}{b^4}(3+\nu)\,\delta_2+2\frac{A_n}{b^{n+2}}[(2n-1+ \right.$$

$$\left. +\nu)\,\alpha+1]+\beta\frac{A_{n-4}}{b^{n-2}}(2n-9+\nu)+\beta\frac{A_{n+4}}{b^{n+6}}(2n+7+\nu)=0 \right\}_{n=0,2,4,\ldots} \qquad (30)$$

where $\delta_m=1$ when $m=n$, $\delta_m=0$ when $m\neq n$,

$A_{-4}=A_{-2}=A_0=0.$

As previously shown, by using an inverse method of solution the set of equations (30) can be used to determine the constants A_n for any particular problem. Also, since the stress distribution is symmetrical with respect to lines inclined at 45° to the directions of the applied shear, the constants A_4, A_8, A_{12} . . . . must be zero.

From (4) and (26), it follows that, for the values of A_n obtained by using an inverse method of solution, the solution of the problem is exact provided that the variation in the cross-sectional area of the reinforcement is given by the expression

$$A_R=\frac{bh\left\{q\sin 2\theta+2\sum_{n=2}\frac{A_n}{b^{n+2}}\sin n\theta\right\}}{\left\{q\,(1-\nu)\sin 2\theta-2\sum_{n=2}\frac{A_n}{b^{n+2}}(2n-1+\nu)\right\}} \qquad (31)$$

Finally, for a reinforcement with a constant cross-sectional area, $\beta=0$ and the constants are given by

$$\left.\begin{aligned} A_2&=-q\left[\frac{1-\alpha(1-\nu)}{1+\alpha(3+\nu)}\right]\frac{b^4}{2}\\ A_n&=0 \quad \text{when} \quad n\neq 2. \end{aligned}\right\} \qquad (32)$$

5. Unequal Principal Stresses

Again using the principle of superposition, it is found from (16) that, for a plate under the action of principal stresses f_x and f_y at infinity, the stress components are given by

$$\left.\begin{aligned} \widehat{rr}&=\frac{A_0}{r^2}+\frac{f_x+f_y}{2}-\sum_{n=2}^{\infty}\left\{\frac{A_n}{r^n b^2}\left[n(n+1)\frac{b^2}{r^2}-(n-1)(n+2)\right]+\right.\\ &\qquad\left.+(f_x-f_y)\left(\frac{b^2}{r^2}-\frac{1}{2}\right)\delta_2\right\}\cos n\theta\\ \widehat{\theta\theta}&=-\frac{A_0}{r^2}+\frac{f_x+f_y}{2}+\sum_{n=2}^{\infty}\left\{\frac{A_n}{r^n b^2}\left[n(n+1)\frac{b^2}{r^2}-(n-1)(n-2)\right]-\right.\\ &\qquad\left.-\frac{(f_x-f_y)}{2}\delta_2\right\}\cos n\theta\\ \widehat{r\theta}&=-\sum_{n=2}^{\infty}\left\{n\frac{A_n}{r^n b^2}\left[(n+1)\frac{b^2}{r^2}-(n-1)\right]+\frac{(f_x-f_y)}{2}\left(1+\frac{b^2}{r^2}\right)\delta_2\right\}\sin n\theta \end{aligned}\right\} \qquad (33)$$

The stresses around an unreinforced hole in a similarly loaded plate are

$$\left.\begin{aligned}(\widehat{rr})_b &= (\widehat{r\theta})_b = 0\\ (\widehat{\theta\theta})_b &= (f_x+f_y) - 2(f_x-f_y)\cos 2\theta\end{aligned}\right\} \quad . \quad . \quad . \quad (34)$$

A suitable reinforcement would therefore have a cross-sectional area defined by (6), in which case the compatibility condition given by (4) can be reduced to the following set of equations:—

$$\left.\begin{aligned}\Big\{ N\delta_0 + M\delta_2 + 2\frac{A_n}{b^{n+2}}[\alpha(2n-1+\nu)+1]\gamma_0 + \beta\Big[(2n-5+\nu)\frac{A_{n-2}}{b^n}\gamma_2 - \\ -(1-\nu)(f_x-f_y)\frac{\delta_4}{4} + (2n+3+\nu)\frac{A_{n+2}}{b^{n+4}}\Big] = 0\Big\}_{n=0,\,2,\,4}\end{aligned}\right\} \quad (35)$$

where

$$\left.\begin{aligned}N &= \frac{(f_x+f_y)}{2}[\alpha(1-\nu)-1] - \frac{(1-\nu)}{4}\beta(f_x-f_y) - \frac{A_0}{b^2}[\alpha(1+\nu)+1]\\ M &= \frac{\beta(1-\nu)}{2}(f_x+f_y) - A_0(1+\nu)\frac{\beta}{b^2} - \frac{(f_x-f_y)}{2}[\alpha(1-\nu)-1]\end{aligned}\right\} \quad (36)$$

and $\gamma_m = 0$ when $m = n$, $\gamma_m = 1$ when $m \neq n$,

$A_{-2} = 0$.

From (4) and (33), it is found that the solution of the problem is exact when the cross-sectional area of the reinforcement is given by

$$A_R\left\{\frac{(f_x+f_y)}{2}(1-\nu) - \frac{A_0(1+\nu)}{b^2} - \frac{(f_x-f_y)}{2}(1-\nu)\cos 2\theta + 2\sum_{n=2}\frac{A_n}{b^{n+2}}[2n-1+\nu]\cos n\theta\right\}$$
$$= bh\left\{\frac{A_0}{b^2} + \frac{(f_x+f_y)}{2} - \frac{(f_x-f_y)}{2}\cos 2\theta - 2\sum_{n=2}\frac{A_n}{b^{n+2}}\cos n\theta\right\}. \quad (37)$$

When the reinforcement has a constant cross-sectional area, the solution of (35) gives

$$\left.\begin{aligned}A_0 &= -\frac{(f_x+f_y)}{2}\left[\frac{1-\alpha(1-\nu)}{1+\alpha(1+\nu)}\right]b^2\\ A_2 &= -\frac{(f_x-f_y)}{4}\left[\frac{1-\alpha(1-\nu)}{1+\alpha(3+\nu)}\right]b^4\end{aligned}\right\} \quad . \quad . \quad . \quad (38)$$

and $A_n = 0$ when $n > 2$.

TABLE II

VALUES OF a_n ($a_n b^{n+2} f_y = A_n$) FOR VARIOUS VALUES OF α AND β WHEN $\nu = 0{\cdot}3$ AND $f_x = 2f_y$.

	β/α					α
	−1·0	−0·8	−0·7	−0·5	−0·3	
a_0	−1·19548	−1·19899	−1·20155	−1·20826	−1·21711	
a_2	−0·08064	−0·09900	−0·10820	−0·12674	−0·14560	
a_4	−0·01357	−0·01206	−0·01108	−0·00870	−0·00571	0·1
a_6	−0·00253	−0·00174	−0·00138	−0·00076	−0·00030	
a_8	−0·00056	−0·00031	−0·00022	−0·00084	−0·00002	
a_0	−0·86146	−0·83843	−0·83173	−0·82621	−0·83009	
a_2	0·06559	0·02830	0·01133	−0·02083	−0·05192	
a_4	0·00231	−0·00339	−0·00487	−0·02593	−0·00495	0·3
a_6	0·00069	−0·00075	−0·00092	−0·00077	−0·00038	
a_8	0·00021	−0·00018	−0·00020	−0·00012	−0·00003	
a_0	−0·66992	−0·61289	−0·59549	−0·57566	−0·57162	
a_2	0·13204	0·08050	0·05957	0·02253	−0·01129	
a_4	0·01764	0·00444	0·00089	−0·00283	−0·00348	0·5
a_6	0·00596	0·00111	0·00019	−0·00041	−0·00029	
a_8	0·00195	0·00029	0·00004	−0·00007	−0·00003	
a_0	−0·48956	−0·38573	−0·35634	−0·32179	−0·30960	
a_2	0·18133	0·11311	0·08925	0·05035	0·01716	
a_4	0·03269	0·01081	0·00547	−0·00027	−0·00211	0·8
a_6	0·01201	0·00290	0·00124	−0·00004	−0·00019	
a_8	0·00410	0·00079	0·00030	−0·00001	−0·00002	

6. Design Data for $f_x = 2f_y$

For the important practical case when $f_x = 2f_y$, values of a_n ($a_n f_y b^{n+2} = A_n$) are given in Table II for a wide range of reinforcements with practical dimensions. As in the problem of a uniform tension in one direction, these values for A_n have been found by using an inverse method of solution.

7. Parameter Solution for Unequal Principal Stresses

When the plate is under the action of a principal stress system of the type found in cylindrical and ellipsoidal pressure vessels, reinforcements having variable cross-sectional areas, which result in reductions in the stress concentrations, can be designed by using the parameter method described in a previous paper[10] dealing with reinforced elliptical holes.

Referring to Fig. 3, the applied stress system shown in State 1 can be resolved with the aid of the parameter ω into the component stress systems shown in State 2 and State 3. Assuming that for State 2 the plate has a circular hole with a reinforcement having a constant cross-sectional area A_{CR}, the stress components are given by equations (39).

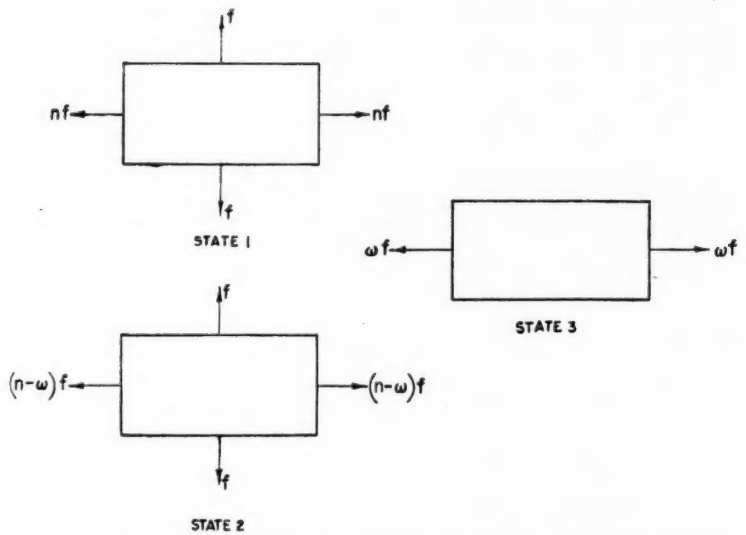

FIGURE 3. Resolution of the applied stress system into two component applied stress systems.

$$\left.\begin{aligned}
\widehat{rr}_2 &= \frac{(n-\omega+1)}{2} f \left\{ 1 - \left[\frac{1-(1-\nu)R}{1+(1+\nu)R}\right]\frac{b^2}{r^2} \right\} + \frac{(n-\omega-1)}{2} f \times \\
&\qquad \times \left\{ 1 - 4\left[\frac{1+(1+\nu)R}{1+(3+\nu)R}\right]\frac{b^2}{r^2} + 3\left[\frac{1-(1-\nu)R}{1+(3+\nu)R}\right]\frac{b^4}{r^4} \right\} \cos 2\theta \\
\widehat{\theta\theta}_2 &= \frac{(n-\omega+1)}{2} f \left\{ 1 + \left[\frac{1-(1-\nu)R}{1+(1+\nu)R}\right]\frac{b^2}{r^2} \right\} - \frac{(n-\omega-1)}{2} f \times \\
&\qquad \times \left\{ 1 + 3\left[\frac{1-(1-\nu)R}{1+(3+\nu)R}\right]\frac{b^4}{r^4} \right\} \cos 2\theta \\
\widehat{r\theta}_2 &= -\frac{(n-\omega-1)}{2} f \left\{ 1 + 2\left[\frac{1+(1+\nu)R}{1+(3+\nu)R}\right]\frac{b^2}{r^2} - 3\left[\frac{1-(1-\nu)R}{1+(3+\nu)R}\right]\frac{b^4}{r^4} \right\} \sin 2\theta
\end{aligned}\right\} \quad (39)$$

$$\text{where} \quad R = \frac{A_{CR}}{bh} .$$

The suffix 2 indicates that the stress components are associated with the applied loading shown in State 2.

Around the hole, the tangential strain in the plate is given by

$$\varepsilon_2 E = \frac{(n-\omega+1)f}{[1+(1+\nu)R]} - \frac{2(n-\omega-1)f}{[1+(3+\nu)R]} \cos 2\theta. \quad . \quad . \quad (40)$$

Assuming that for State 3 the plate has an unreinforced hole, the stress components become

$$\left.\begin{aligned}\widehat{rr}_3 &= \frac{\omega f}{2}\left(1-\frac{b^2}{r^2}\right)+\frac{\omega f}{2}\left(1-4\frac{b^2}{r^2}+3\frac{b^4}{r^4}\right)\cos 2\theta \\ \widehat{\theta\theta}_3 &= \frac{\omega f}{2}\left(1+\frac{b^2}{r^2}\right)-\frac{\omega f}{2}\left(1+3\frac{b^4}{r^4}\right)\cos 2\theta \\ \widehat{r\theta}_3 &= -\frac{\omega f}{2}\left(1+2\frac{a^2}{r^2}-3\frac{a^4}{r^4}\right)\sin 2\theta.\end{aligned}\right\} \quad . \quad . \quad (41)$$

Thus, around the hole,

$$\varepsilon_3 E = \omega f\,(1-2\cos 2\theta). \quad . \quad . \quad . \quad . \quad (42)$$

Finally, assuming that for State 1 the stress distribution in the plate is the sum of the stress distributions for States 2 and 3, the problem reduces to finding the cross-sectional area of the reinforcement necessary to satisfy the boundary conditions around the hole.

From (40) and (42), around the hole the tangential strain in the plate becomes

$$\varepsilon_1 E = \frac{[n+1+(1+\nu)\,\omega R]}{[1+(1+\nu)\,R]} f - 2\,\frac{[n-1+(3+\nu)\,\omega R]}{[1+(3+\nu)\,R]} f\cos 2\theta. \quad . \quad (43)$$

From (2), the normal force acting on a radial cross section of the reinforcement is given by

$$\left.\begin{aligned}F &= bh\,(\widehat{rr}_1)_b \\ &= bhf\left\{\frac{[n-\omega+1]\,R}{[1+(1+\nu)\,R]}-2\,\frac{[n-\omega-1]\,R}{[1+(3+\nu)\,R]}\cos 2\theta\right\}\end{aligned}\right\} \quad . \quad (44)$$

Also, for the reinforcement, $$\varepsilon_1 E = \frac{F}{A_R} \quad . \quad . \quad . \quad . \quad . \quad . \quad (45)$$

From (43), (44), and (45), the variable cross-sectional area of the reinforcement is defined by

$$\begin{aligned}A_R\{&[n+1+(1+\nu)\,\omega R]\,[1+(3+\nu)\,R]-2\,[n-1+(3+\nu)]\,[1+(1+\nu)\,R]\cos 2\theta\} \\ &= A_{CR}\{(n-\omega+1)\,[1+(3+\nu)\,R]-2\,(n-\omega-1)\,[1+(1+\nu)\,R]\cos 2\theta\}. \quad (46)\end{aligned}$$

Thus the stress distribution in the plate and the variation in the cross-sectional area of the reinforcement depend on two arbitrary parameters ω and R (note $A_{CR}=Rbh$). This implies that, when dealing with a particular applied stress system, practical reinforcements can be obtained by choosing the most suitable values for ω and R.

TABLE III

VALUES OF A_R/bh FOR VARIOUS VALUES OF R AND ω WHEN $\nu=0{\cdot}3$.

θ (degrees)	R					ω
	0·2	0·4	0·6	0·8	1·0	
0	0·184	0·366	0·546	0·728	0·893	
15	0·189	0·377	0·569	0·745	0·926	
30	0·200	0·400	0·600	0·800	1·000	
45	0·208	0·421	0·637	0·862	1·080	−0·1
60	0·214	0·434	0·663	0·904	1·143	
75	0·216	0·442	0·678	0·928	1·180	
90	0·217	0·445	0·682	0·936	1·193	
0	0·169	0·337	0·499	0·661	0·806	
15	0·179	0·357	0·530	0·703	0·861	
30	0·200	0·400	0·600	0·807	1·000	
45	0·217	0·442	0·675	0·920	1·168	−0·2
60	0·228	0·472	0·633	1·016	1·315	
75	0·234	0·489	0·768	1·080	1·412	
90	0·235	0·494	0·780	1·100	1·445	
0	0·156	0·310	0·460	0·600	0·735	
15	0·171	0·336	0·500	0·628	0·806	
30	0·200	0·400	0·600	0·797	1·000	
45	0·225	0·464	0·714	0·980	1·265	−0·3
60	0·243	0·512	0·810	1·144	1·528	
75	0·252	0·540	0·876	1·260	1·720	
90	0·254	0·552	0·894	1·300	1·790	

For example, consider the important case of applied principal stresses in the ratio two to one, that is f and $2f$. Then, if the larger of these two principal stresses acts along the radial line where θ is zero, the distribution of tangential stress around an unreinforced hole is

$$\widehat{\theta\theta}_b = f(3-2\cos 2\theta). \quad . \quad . \quad . \quad . \quad . \quad (47)$$

Thus, a suitable reinforcement would have a cross-sectional area which was maximum at the point $\theta=\pi/2$ and minimum at the point $\theta=0$.

For a reasonably wide range of practical reinforcements, values of A_R/bh for various values of R and ω are given in Table III.

ACKNOWLEDGMENTS

The author wishes to express his indebtedness to Mr. R. N. Millar, M.A., B.Com., M.I.Mech.E., Manager of the G.E.C. Simon-Carves Atomic Energy Group, for permission to publish this paper.

REFERENCES

1. KIRSCH, G. Theorie der Elastizitat Bedurfrisse der Festigkeitslehre. *Verein Deutscher Ingenieure*, Vol. 42, p. 113, 1898.
2. TIMOSHENKO, S. Stresses in a Plate with a Circular Hole. *Bulletin of the Polytechnic Institute, Kiew*, 1907.
3. TIMOSHENKO, S. and GOODIER, J. N. *Theory of Elasticity*. McGraw-Hill, New York, 1940.
4. GURNEY, C. An Analysis of the Stresses in a Flat Plate with a Reinforced Circular Hole under Edge Forces. R. & M. 1834, 1938.
5. TIMOSHENKO, S. Stresses on a Plate with a Circular Hole. *Journal of the Franklin Institute*, Vol. 197, p. 508, 1924.
6. BESKIN, L. Strengthening of Circular Holes in Plates under Edge Loads. *Journal of Applied Mechanics*, p. A-140, September 1944.
7. MANSFIELD, E. H. Neutral Holes in Plane Sheet. *Quarterly Journal of Mechanics and Applied Mathematics*, Vol. VI, Part 3, 1953.
8. MANSFIELD, E. H. Optimum Designs for Reinforced Circular Holes. A.R.C. Current Paper 239, 1956.
9. WELLS, A. A. On the Plane Stress-Distribution in an Infinite Plate with a Rim-Stiffened Elliptical Opening. *Quarterly Journal of Mechanics and Applied Mathematics*, Vol. III, Part I, 1950.
10. HICKS, R. Reinforced Elliptical Holes in Stressed Plates. *Journal of the Royal Aeronautical Society*, Vol. 61, p. 688, October 1957.
11. REISSNER, H. and MORDUCHOW, M. Reinforced Circular Cut-Outs in Plate Sheets. N.A.C.A. T.N. 1852, April 1949.

On the Accuracy of the Representation of a Lifting Line by a Finite Set of Horseshoe Vortices

A. R. COLLAR

(*University of Bristol*)

SUMMARY: The paper examines the error involved when the continuous distribution of lift on an unswept lifting surface is represented by a finite number of horseshoe vortices, the strengths of which are determined by a prescribed downwash. Attention is directed mainly to the case of elliptic loading, but an anti-symmetrical case is also studied to ensure that the conclusions are not peculiar to the elliptic case.

If the number of horseshoe vortices is m, it is concluded that

(*a*) when the downwash at the centre of each horseshoe vortex is prescribed equal to that for the continuous case, the total load due to the horseshoe system over-estimates the true load in the ratio $(m+1)/m$,

(*b*) if the circulation is determined for a wing of finite aspect ratio by its geometric incidence, the error will be less than that in case (*a*); a formula involving m and the aspect ratio A is derived.

The analysis involves an unusual method for the reciprocation of the matrix of which the typical element is

$$U_{ij} = \frac{-1}{(k+i-j)(k+i-j-1)}.$$

1. Introduction

Many problems in aeronautics arise in which it is convenient to represent a lifting surface by a lifting line, and further to represent the lifting line by a finite set of horseshoe vortices. Given the strengths of the vortices, the induced downwash is readily written down; but the inverse problem is less easy.

The present note has been written because there are some points of interest in the method of reciprocation of the matrix involved in the solution of the inverse problem, and because the final result sheds some light on the accuracy of the representation.

Received March 1958.

NOTATION

A aspect ratio; *see* also (18) *infra*

B_r *see* (27)

C_r *see* (38) *infra*

D_r *see* (39) *infra*

H triangular matrix

I unit matrix

K circulation

L lift

L_R rolling moment

R_m lift ratio

U square matrix

V fluid speed

a lift coefficient slope

c chord; also matrix

i, j current suffixes

k fraction of width of horseshoe

m number of horseshoes

$n = m + 1$

r, s current suffixes

s semi-span

u square matrix

$v = u^{-1}$

w downwash velocity

α incidence

ρ fluid density

2. The Problem

Suppose we have a set of m horseshoe vortices, of strengths $K_1, K_2, \ldots, K_m$, the bound vortices, each of length $2s/m$, lying on a straight line normal to a stream of density ρ and speed V (Fig. 1). This is perhaps the simplest representation of an unswept lifting wing of span $2s$. The velocities induced by this system of vortices are readily written down; normally we are concerned mainly with the downwash on the lifting line itself. Let w_i be the downwash at a point on the i^{th} bound vortex, distant $2sk/m$ from the left-hand end of that bound vortex. In

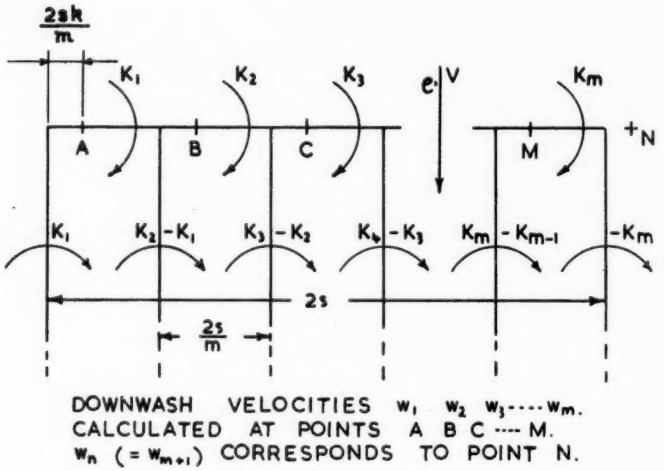

FIGURE 1.

practical cases the fraction k will almost always be given the value $\frac{1}{2}$; but the greater generality is retained here. Then we can write at once

$$\frac{8\pi s}{m} w_i = \frac{K_1}{k+i-1} + \frac{K_2-K_1}{k+i-2} + \ldots\ldots + \frac{K_m-K_{m-1}}{k+i-m} + \frac{(-K_m)}{k+i-1-m} \quad . \quad (1)$$

$$= \frac{-K_1}{(k+i-1)(k+i-2)} - \ldots\ldots\ldots \frac{-K_m}{(k+i-m)(k+i-m-1)} \quad . \quad (2)$$

In matrix notation, equation (2) is

$$\frac{8\pi s}{m} w = UK, \quad . \quad . \quad . \quad . \quad . \quad (3)$$

where the square matrix U, of order m, has the typical element

$$U_{ij} = \frac{-1}{(k+i-j)(k+i-j-1)} \quad . \quad . \quad . \quad . \quad . \quad (4)$$

Given a set of strengths K, equation (3) enables the downwash set w to be calculated. The more difficult problem is, however, the solution of

$$K = \frac{8\pi s}{m} U^{-1} w, \quad . \quad . \quad . \quad . \quad (5)$$

to obtain the set of strengths K for a prescribed downwash set w. We proceed to evaluate the matrix U^{-1} where U is defined by (4).

3. Reciprocation of U

If we return to equation (1), we note that w_i is expressed as a sum of $m+1$ terms, the associated modal column (vector) being

$$\{K_1-0,\quad K_2-K_1,\quad \ldots\ldots,\quad K_m-K_{m-1},\quad 0-K_m\}.$$

Accordingly, let us add to the m equations (1) the $(m+1)^{\text{th}}$ equation

$$\frac{8\pi s}{m}\,w_{m+1}=\frac{K_1}{k+m}+\frac{K_2-K_1}{k+m-1}+\ldots\ldots+\frac{(-K_m)}{k}\qquad(6)$$

Physically, this defines the downwash at a point just outside the lifting line (N, Fig. 1); normally, w_{m+1} will not be prescribed with w. However, we can write the full set of equations (1) and (6) as

$$\frac{8\pi s}{m}\begin{bmatrix} w_1 \\ w_2 \\ \ldots\ldots \\ w_m \\ w_{m+1}\end{bmatrix}=\begin{bmatrix} \frac{1}{k}, & \frac{1}{k-1}, & \ldots\ldots, & \frac{1}{k-m} \\ \frac{1}{k+1}, & \frac{1}{k}, & \ldots\ldots, & \frac{1}{k-m+1} \\ \ldots\ldots & \ldots\ldots & \ldots\ldots & \ldots\ldots \\ \ldots\ldots & \ldots\ldots & \ldots\ldots & \ldots\ldots \\ \frac{1}{k+m}, & \frac{1}{k+m-1}, & \ldots\ldots, & \frac{1}{k}\end{bmatrix}\begin{bmatrix} K_1-0 \\ K_2-K_1 \\ \ldots\ldots \\ \ldots\ldots \\ 0-K_m\end{bmatrix}\qquad(7)$$

The square matrix appearing in (7) is the matrix u of which the reciprocal has been given elsewhere by the author[1]. Since we are now dealing with a square matrix of order $m+1$, it is convenient to write

$$m+1=n.\qquad(8)$$

In this case our symbols accord with those of Ref. 1. The reciprocal of u is v, where the typical $(r, s)^{\text{th}}$ element is

$$v_{rs}=\frac{(-1)^{n+r-s-1}}{k-r+s}\,\frac{(k-r+n)\ldots\ldots(k-r+1)}{(r-1)!\,(n-r)!}\,\frac{(k+s-1)\ldots\ldots(k+s-n)}{(s-1)!\,(n-s)!}\qquad(9)$$

Accordingly, from (7) we obtain

$$\{K_1-0,\ K_2-K_1,\ \ldots\ldots,\ 0-K_m\}=\frac{8\pi s}{m}\,v\,\{w_1,\ w_2,\ \ldots\ldots,\ w_m,\ w_n\}.$$

Pre-multiplication by the "triangular" matrix

$$H=\begin{bmatrix} 1, & 0, & \ldots\ldots, & 0 \\ 1, & 1, & \ldots\ldots, & 0 \\ \ldots\ldots & \ldots\ldots & \ldots\ldots & \ldots\ldots \\ 1, & 1, & \ldots\ldots, & 1\end{bmatrix},$$

gives $$\{K_1, K_2, \ldots, K_m, 0\} = \frac{8\pi s}{m} H v \{w_1, w_2, \ldots, w_m, w_n\}. \quad (10)$$

This, while similar to (5), differs in that we have on the right one unspecified element w_n, and on the left a single specified (zero) element.

Accordingly, write $$Hv = c$$

and partition the matrices so that (10) is written

$$\begin{bmatrix} K \\ \hline 0 \end{bmatrix} = \frac{8\pi s}{m} \begin{bmatrix} c_{ij} & c_{in} \\ \hline c_{nj} & c_{nn} \end{bmatrix} \begin{bmatrix} w \\ \hline w_n \end{bmatrix}. \quad (11)$$

From the last line in (11) we obtain

$$0 = c_{nj} w + c_{nn} w_n \quad (12)$$

and, since c_{nn} is a scalar, the remainder of (11) may be written, on the use of (12),

$$\frac{m}{8\pi s} K = c_{ij} w - \frac{c_{in} c_{nj}}{c_{nn}} w$$

$$= \left[c_{ij} - \frac{c_{in} c_{nj}}{c_{nn}} \right] w. \quad (13)$$

Comparison of (13) with (5) shows that

$$U^{-1} = \left[c_{ij} - \frac{c_{in} c_{nj}}{c_{nn}} \right]. \quad (14)$$

It may be remarked that the last row of H may be written $[\delta, \delta, \ldots, \delta]$, where δ is arbitrary: the analysis is not affected.

4. Evaluation of the Typical Element of U^{-1}

Although (14) provides a formal solution, and is also a result that may be used directly for calculation, it is possible, with a little manipulation, to write down the typical element of U^{-1}. To do this, certain theorems, proved in Ref. 1, are required; they are also required for the further investigation of Section 6. For simplicity, the theorems (all particular cases of a more general theorem) are quoted here:—

Theorem B

$$\sum_{r=1}^{n} \frac{(-1)^{r-1}}{(n-r)!(r-1)!} \frac{(k-r+n)\ldots(k-r+1)}{k-r+s} = 1. \quad (s = 1, 2, \ldots, n).$$

Theorem C

$$\sum_{n}^{r=1} \frac{(-1)^{r-1}}{(n-r)!(r-1)!} (k-r+n)\ldots(k-r+1) = nk.$$

Theorem D

$$\sum_{r=1}^{n} \frac{(-1)^{r-1}}{(n-r)!(r-1)!}(k-r+n)\ldots.(k-r+1)(1-r)=\frac{n(n-1)k(k-1)}{2}.$$

Now, in (14), c_{ij} is the $(i, j)^{\text{th}}$ element of Hv, which is clearly, in view of the expression for H,

$$c_{ij}=\sum_{r=1}^{i} v_{rj}$$

$$=\sum_{r=1}^{i}\frac{(-1)^{n+r-j-1}}{k-r+j}\frac{(k-r+n)\ldots(k-r+1)}{(r-1)!(n-r)!}\frac{(k+j-1)\ldots(k+j-n)}{(j-1)!(n-j)!}$$

$$=(-1)^{n-j}\frac{(k+j-1)\ldots(k+j-n)}{(j-1)!(n-j)!}\sum_{r=1}^{i}\frac{(-1)^{r-1}}{(r-1)!(n-r)!}\frac{(k-r+n)\ldots(k-r+1)}{k-r+j} \quad . \quad . \quad . \quad . \quad . \quad (15)$$

In particular, with $i=n$ the summation in (15) is unity, by Theorem B, so that

$$c_{nj}=(-1)^{n-j}\frac{(k+j-1)\ldots.(k+j-n)}{(j-1)!(n-j)!} \quad . \quad . \quad . \quad (16)$$

With $j=n$, the expression (15) becomes

$$c_{in}=\frac{(k+n-1)\ldots.k}{(n-1)!}\sum_{r=1}^{i}\frac{(-1)^{r-1}}{(r-1)!(n-r)!}\frac{(k-r+n)\ldots(k-r+1)}{k-r+n} \quad . \quad (17)$$

and finally, with $j=n$, the expression (16) gives

$$c_{nn}=\frac{(k+n-1)\ldots.k}{(n-1)!} \quad . \quad . \quad . \quad . \quad . \quad (18)$$

Substitution from (15), (16), (17), (18) in (14) gives, for the typical element of U^{-1},

$$c_{ij}-\frac{c_{in}c_{nj}}{c_{nn}}=(-1)^{n-j}\frac{(k+j-1)\ldots.(k+j-n)}{(j-1)!(n-j)!}A,$$

where $A=\sum_{r=1}^{i}\frac{(-1)^{r-1}}{(r-1)!(n-r)!}(k-r+n)\ldots(k-r+1)\left\{\frac{1}{k-r+j}-\frac{1}{k-r+n}\right\}$

$$=\sum_{r=1}^{i}\frac{(-1)^{r-1}}{(r-1)!(n-r)!}\frac{(k-r+n)\ldots.(k-r+1)}{(k-r+j)(k-r+n)}(n-j).$$

Thus, finally

$$(U^{-1})_{ij}=(-1)^{n-j}\frac{(k+j-1)\ldots(k+j-n)}{(j-1)!(n-j-1)!}\sum_{r=1}^{i}\frac{(-1)^{r-1}(k-r+n-1)\ldots(k-r+1)}{(r-1)!(n-r)!(k-r+j)},$$

$$(i, j=1, 2, \ldots., n-1). \quad . \quad . \quad (19)$$

5. The Special Case $k=1/2$

It will be usual, in practice, to define the downwash at the centre of each bound vortex, since this preserves symmetry. In this case, $k=\frac{1}{2}$, and the matrix U has the typical element

$$U_{ij}=\frac{-4}{(2i-2j+1)(2i-2j-1)} \quad . \quad . \quad . \quad . \quad . \quad (20)$$

From (19), and in view of (8), the reciprocal will be defined by

$$(U^{-1})_{ij}=(\tfrac{1}{2})^{2m}(-1)^{m-j}\frac{(2j-1)\ldots(2j-2m-1)}{(j-1)!(m-j)!}\sum_{r=1}^{i}\frac{(-1)^r(2m+1-2r)\ldots(3-2r)}{(r-1)!(m+1-r)!(2j+1-2r)}$$

$$(i,\ j=1,\ 2,\ \ldots,\ m) \quad . \quad . \quad . \quad (21)$$

As an illustration, let $m=4$. Then

$$U=4\begin{bmatrix} 1 & -\frac{1}{3} & -\frac{1}{15} & -\frac{1}{35} \\ -\frac{1}{3} & 1 & -\frac{1}{3} & -\frac{1}{15} \\ -\frac{1}{15} & -\frac{1}{3} & 1 & -\frac{1}{3} \\ -\frac{1}{35} & -\frac{1}{15} & -\frac{1}{3} & 1 \end{bmatrix} \quad . \quad . \quad . \quad . \quad (22)$$

From (21), the inverse is defined by

$$(U^{-1})_{ij}=(\tfrac{1}{2})^8(-1)^j\frac{(2j-1)\ldots(2j-9)}{(j-1)!(4-j)!}\sum_{r=1}^{i}\frac{(-1)^r(9-2r)\ldots(3-2r)}{(r-1)!(5-r)!(2j+1-2r)}.$$

From this formula, U^{-1} is readily obtained in the form

$$U^{-1}=(\tfrac{1}{2})^{12}\begin{bmatrix} 35.35 & 15.35 & 15.21 & 35.5 \\ 35.15 & 15.95 & 15.41 & 35.9 \\ 35.9 & 15.41 & 15.95 & 35.15 \\ 35.5 & 15.21 & 15.35 & 35.35 \end{bmatrix}$$

It may be noted, for purposes of computation, that there will always be a factor in each column corresponding to the terms preceding the summation.

Thus, in the present illustration, we can write

$$U^{-1}=(\tfrac{1}{2})^{12}\begin{bmatrix}35 & 35 & 21 & 5\\ 15 & 95 & 41 & 9\\ 9 & 41 & 95 & 15\\ 5 & 21 & 35 & 35\end{bmatrix}\begin{bmatrix}35 & 0 & 0 & 0\\ 0 & 15 & 0 & 0\\ 0 & 0 & 15 & 0\\ 0 & 0 & 0 & 35\end{bmatrix},$$

and such a product form will always be possible.

6. Comparison with the Elliptically Loaded Wing

From the general results already given, it is clearly possible to find the distribution of circulation K corresponding to any assigned downwash distribution w. A natural question to ask at this stage is: how many horseshoe vortices should be employed to give a distribution of vorticity leading to a total load correct to some given degree of approximation? This can clearly only be answered for some known case; the simplest and best known is, of course, the elliptically loaded wing.

If the circulation at the centre of an elliptically loaded wing of span $2s$ is K_0, then[2] the induced velocity has the constant value $K_0/(4s)$, while the total load is

$$L=\frac{\pi}{2}\rho V K_0 s. \qquad . \quad . \quad . \quad . \quad . \quad (23)$$

Suppose we represent this case by a system of m horseshoe vortices, prescribing the downwash velocity w_i of equation (1) (and (5)) as $K_0/(4s)$ for each element. Then

$$w=\frac{K_0}{4s}\{1,\ 1,\ \ldots,\ 1\}$$

and, from (5),

$$K=\frac{2\pi K_0}{m}U^{-1}\{1,\ 1,\ \ldots,\ 1\}. \qquad . \quad . \quad . \quad (24)$$

The total load generated by this system of vortices will be

$$L_m=\sum_1^m \rho V K_i\frac{2s}{m}=\frac{2\rho V s}{m}[1,\ 1,\ \ldots,\ 1]K;$$

on use of (24) this becomes

$$L_m=\frac{4\pi\rho V K_0 s}{m^2}[1,\ 1,\ \ldots,\ 1]U^{-1}\{1,\ 1,\ \ldots,\ 1\}. \quad . \quad (25)$$

Accordingly, the ratio of the load derived from the horseshoe vortices to the true elliptic load is

$$R_m=\frac{L_m}{L}=\frac{8}{m^2}[1,\ 1,\ \ldots,\ 1]U^{-1}\{1,\ 1,\ \ldots,\ 1\}. \quad . \quad (26)$$

This quantity will now be evaluated.

Since pre-multiplication and post-multiplication by a row and column of units is equivalent to adding all the elements of the matrix, it is found from (19) and (26) that

$$R_m = \frac{8}{m^2} \sum_{j=1}^{m} \sum_{i=1}^{m} \sum_{r=1}^{i} B_r,$$

where

$$B_r = \frac{(-1)^{m-j+r}(k+j-1)\ldots.(k+j-m-1)(k-r+m)\ldots.(k-r+1)}{(j-1)!(m-j)!(r-1)!(m+1-r)!(k-r+j)} \quad (27)$$

But $\sum_{r=1}^{i} B_r = B_1 + B_2 + \ldots. + B_i$, and therefore

$$\sum_{i=1}^{m} \sum_{r=1}^{i} B_r = B_1 + (B_1 + B_2) + (B_1 + B_2 + B_3) + \ldots.$$

$$= mB_1 + (m-1)B_2 + \ldots. + B_m$$

$$= \sum_{r=1}^{m} (m+1-r) B_r.$$

The factor $(m+1-r)$ appears in the denominator of the expression for B_r; hence

$$\sum_{i=1}^{m} \sum_{r=1}^{i} B_r = \sum_{r=1}^{m} \frac{(-1)^{m-j+r}(k+j-1)\ldots(k+j-m-1)(k-r+m)\ldots(k-r+1)}{(j-1)!(m-j)!(r-1)!(m-r)!(k-r+j)}$$

$$= \frac{(-1)^{m-j+1}(k+j-1)\ldots(k+j-m-1)}{(j-1)!(m-j)!},$$

since the sum of the terms involving r is unity by Theorem B (Section 4). Thus finally

$$R_m = \frac{8}{m^2} \sum_{j=1}^{m} \frac{(-1)^{m-j+1}(k+j-1)\ldots.(k+j-m-1)}{(j-1)!(m-j)!},$$

and if the factor $(k+j-m-1)$ is written as the difference between $(k-m)$ and $(1-j)$ this may be written

$$R_m = \frac{8}{m^2}(k-m) \sum_{j=1}^{m} \frac{(-1)^{j-1}(-k-j+m)\ldots.(-k-j+1)}{(j-1)!(m-j)!} -$$

$$- \frac{8}{m^2} \sum_{j=1}^{m} \frac{(-)^{j-1}(-k-j+m)\ldots.(-k-j+1)(1-j)}{(j-1)!(m-j)!}.$$

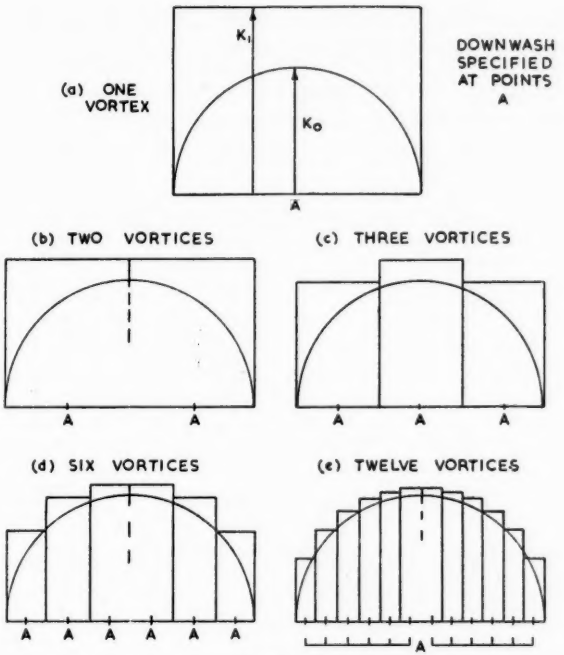

FIGURE 2.

By Theorem C the first summation equals $-mk$ and by Theorem D the second equals $\frac{1}{2}m(m-1)k(k+1)$. Hence

$$R_m = \frac{4}{m^2}\left[(2m-2k)mk - mk(m-1)(k+1)\right]$$

$$= \frac{m+1}{m}2k(2-2k), \quad . \quad . \quad . \quad . \quad . \quad . \quad . \quad (28)$$

on reduction. For this illustration — the symmetrically loaded wing — k will normally be taken as $\frac{1}{2}$, so that then

$$R_m = \frac{m+1}{m} \quad . \quad . \quad . \quad . \quad . \quad . \quad . \quad (29)$$

7. Some Comments

The result (29) is of some interest: it shows, for example, that if ten horseshoe vortices are employed to simulate the continuous distribution, the load generated will be ten per cent too high.

Figure 2 shows some comparisons of loading, with 1, 2, 3, 6, 12 horseshoe vortices to represent the elliptic loading (shown for convenience as circular), and

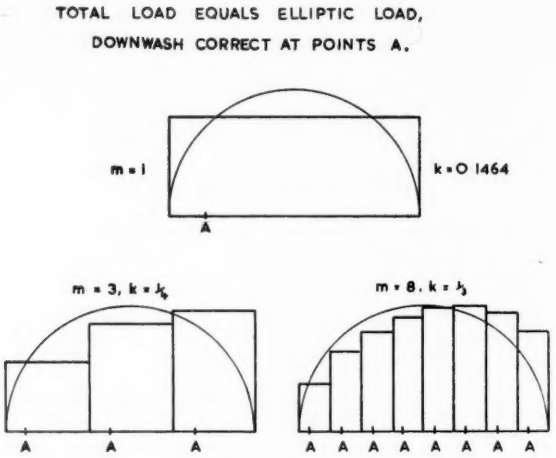

FIGURE 3.

with $k=\frac{1}{2}$ for symmetry. The correctness of the formula (29) is demonstrated in these diagrams.

The result (28) can be used to find a value for k which gives $R_m=1$ for all values of m: it yields on solution for k in this case

$$2k=1\pm(m+1)^{-\frac{1}{2}} . \qquad . \quad . \quad . \quad . \quad (30)$$

As would be expected, k becomes equal to $\frac{1}{2}$ when m is indefinitely large. Some distributions with k as defined by (30) are shown in Fig. 3: they are for $m=1$ ($k=0{\cdot}1464$), $m=3$ ($k=\frac{1}{4}$) and $m=8$ ($k=\frac{1}{3}$). The very considerable asymmetry of the latter two cases is to be noted; it suggests that a choice of k other than $\frac{1}{2}$ is unlikely to be satisfactory. To obtain the results of Fig. 3, it is necessary to evaluate the column $\{K_i\}$ as given by (24). On use of (19), equation (24) becomes (with $n=m+1$)

$$\frac{m}{2\pi}\frac{K_i}{K_0}=\sum_{j=1}^{m}(U^{-1})_{ij}$$

$$=\sum_{j=1}^{m}\sum_{r=1}^{i}\frac{(-1)^{m-j+r}(k-r+1)\ldots(k-r+m)(k+j-1)\ldots(k+j-m-1)}{(m+1-r)!(r-1)!(j-1)!(m-j)!(k-r+j)}$$

and on use of Theorems C and D the summation involving j may be evaluated, so that finally

$$\frac{m}{2\pi}\frac{K_i}{K_0}=\sum_{r=1}^{i}\frac{(-1)^{r-1}(k-r+1)\ldots(k-r+m)(m-mk+1-r)}{(m+1-r)!(r-1)!} . \quad . \quad (31)$$

8. A Second Example: Anti-symmetric Loading

The case of symmetric loading provides the most appropriate test of the representation of a continuous load by horseshoe vortices: it is, however, desirable to show that the order of error demonstrated by equation (29) is not peculiar to this case. Accordingly, the rolling moment due to anti-symmetrical load is now examined.

Consider a wing of span $2s$ on which the circulation is defined by

$$K = -K_0 \sin 2\theta \qquad . \quad . \quad . \quad . \quad (32)$$

$$\text{with} \quad y = -s\cos\theta. \qquad . \quad . \quad . \quad . \quad (33)$$

In the usual way, the induced downwash is obtained as

$$w = -\frac{K_0}{s}\cos\theta = \frac{K_0 y}{s^2}. \qquad . \quad . \quad . \quad . \quad (34)$$

The total rolling moment L_R is

$$L_R = \frac{\pi}{4}\rho V K_0 s^2.$$

The loading (32) will now be represented by a finite set of m horseshoe vortices as before, with the induced downwash prescribed at the centre of each vortex (that is, $k=\frac{1}{2}$) by (34). This involves the solution of equation (5) with

$$w_j = \frac{K_0}{sm}(2j-1-m), \qquad . \quad . \quad . \quad . \quad (35)$$

$$\text{that is,} \quad \{K_i\} = \frac{8\pi K_0}{m^2}U^{-1}\{2j-1-m\}. \quad . \quad . \quad . \quad . \quad (36)$$

This expression provides the ordinates $\{K_i/K_0\}$ for comparison with the continuous curve of (32); the results are plotted in Fig. 4 for the cases $m=4, 5, 6$. As regards the total rolling moment, this is clearly given by

$$\sum_{i=1}^{m} \rho V K_i \frac{2s}{m}\frac{s}{m}(2i-1-m),$$

$$\text{that is, by} \qquad 2\rho V\frac{s^2}{m^2}[2i-1-m]\{K_i\}. \qquad . \quad . \quad (37)$$

In view of (35) and (36) the ratio R_m of the rolling moment due to the m horseshoe vortices to that derived from the continuous distribution may be written

$$R_m = \frac{4^3}{m^4}[2i-1-m]\,U^{-1}\{2j-1-m\}. \qquad . \quad . \quad . \quad (38)$$

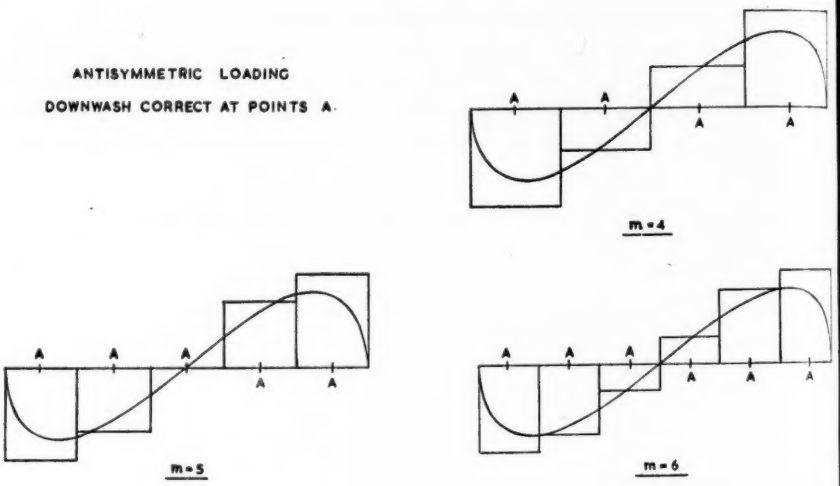

FIGURE 4.

The evaluation of this result, with m general, requires some labour: only the general lines of the analysis are given here. Since U^{-1} is determined by (19) with $n=m+1$ and $k=\frac{1}{2}$, (38) yields

$$R_m=\left(\frac{4}{m}\right)^4 \sum_{j=1}^{m}\sum_{i=1}^{m}\sum_{r=1}^{i}(i-\tfrac{1}{2}-\tfrac{1}{2}m)\,C_r,$$

where

$$C_r=\frac{(-1)^{m-j+r}(\frac{1}{2}+j-1)\ldots(\frac{1}{2}+j-m-1)(j-\frac{1}{2}-\frac{1}{2}m)(\frac{1}{2}-r+m)\ldots(\frac{1}{2}-r+1)}{(j-1)!(m-j)!(r-1)!(m+1-r)!(\frac{1}{2}-r+j)}.$$

But

$$\sum_{i=1}^{m}\sum_{r=1}^{i}(i-\tfrac{1}{2}-\tfrac{1}{2}m)\,C_r=\sum_{r=1}^{m}\frac{(r-1)(m+1-r)}{2}C_r; \quad . \quad . \quad (39)$$

thus we may write

$$R_m=\left(\frac{4}{m}\right)^4 \sum_{j=1}^{m}\frac{(-1)^{m-j+1}(\frac{1}{2}+j-1)\ldots(\frac{1}{2}+j-m-1)(j-\frac{1}{2}-\frac{1}{2}m)}{(j-1)!(m-j)!}D_r,$$

where, on cancellation of the factor $(m+1-r)$ appearing in (39),

$$D_r=\sum_{r=1}^{m}\frac{(-1)^{r-1}(\frac{1}{2}+m-r)\ldots(\frac{1}{2}+1-r)}{(r-1)!(m-r)!(\frac{1}{2}+j-r)}\,\frac{(r-1)}{2}.$$

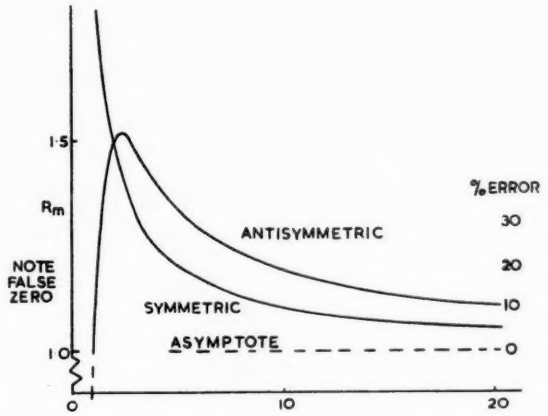

FIGURE 5.

The quantity D_r is readily evaluated by use of Theorems B and C; we find

$$D_r = \tfrac{1}{2}(j - \tfrac{1}{2} - \tfrac{1}{2}m).$$

Thus finally, with a little rearrangement

$$R_m = \frac{1}{2}\left(\frac{4}{m}\right)^4 \sum_{j=1}^{m} \frac{(-1)^j (\frac{1}{2}+m-j)\ldots(\frac{1}{2}-j)(\frac{1}{2}+\frac{1}{2}m-j)^2}{(j-1)!(m-j)!}.$$

This summation, involving as it does $(m+3)$ factors in the numerator, cannot be evaluated by means of the Theorems quoted; however, by the methods of Ref. 1 it yields finally

$$R_m = \frac{(m-1)(m+1)(m+2)}{m^3} \quad . \quad . \quad . \quad . \quad (40)$$

In Fig. 5 are plotted curves of R_m as given by (29) for the symmetric loading case and by (40) for the anti-symmetric case. Both curves show that there is considerable error unless a very large number of horseshoe vortices is employed. The anti-symmetric case is nearly twice as bad as the symmetric; this is probably due to the fact that each half-span has a continuous loading of one sign and approximates to a representation of symmetrical load by $\frac{1}{2}m$ vortices.

9. Distribution of Downwash due to Horseshoe Vortices

It is apparent from the preceding investigations that the choice of the points at which the downwash is specified in a horseshoe vortex system can profoundly affect the resultant load. This suggests that the downwash due to a horseshoe vortex system varies considerably across the span; and it is clearly of interest to examine this question.

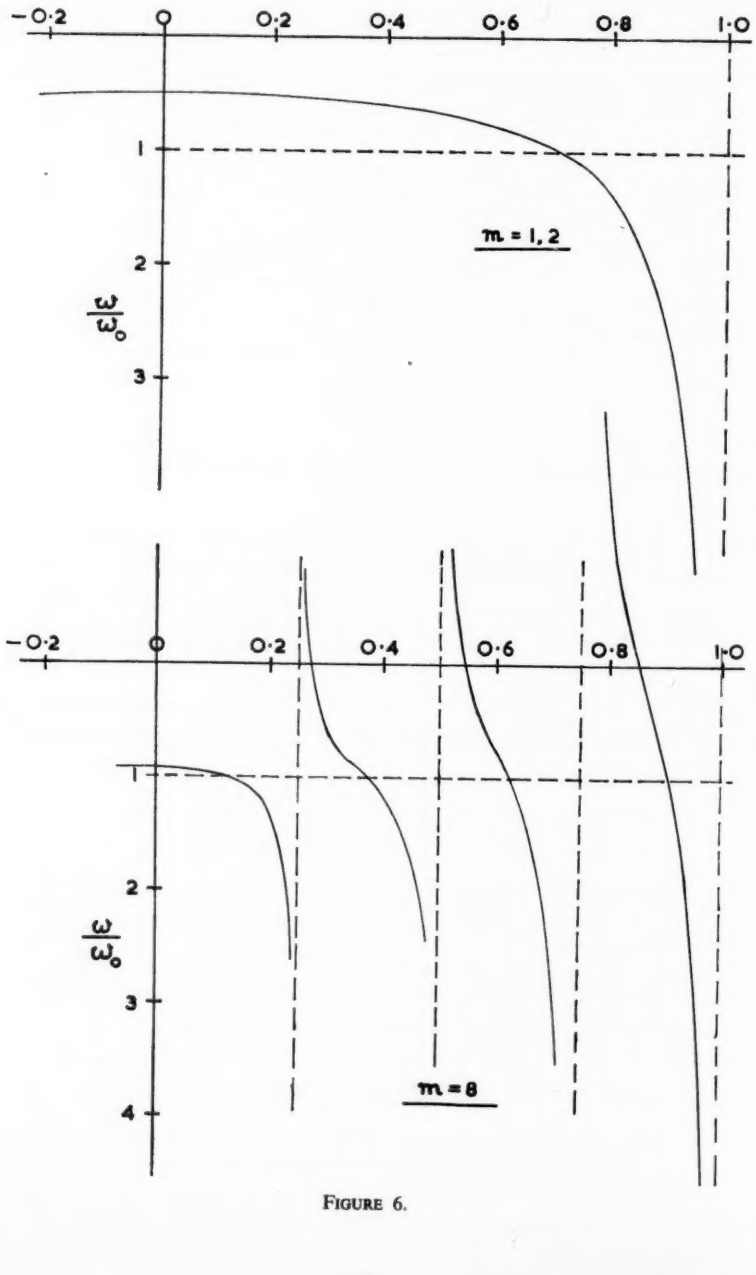

FIGURE 6.

Consider an elliptically loaded wing, and let the span $2s$ be divided into m equal parts; if the part of the elliptic load carried by the i^{th} section is L_i, the mean circulation for that section, K_i, is given by

$$L_i = \rho V K_i (2s/m).$$

If the set of circulations K_i determined in this way is now used to define a horseshoe vortex system, the total load will be correct, and the downwash for the system will be given by equation (1), in which k is now regarded as an independent variable – effectively the spanwise variable.

Values of K_i have been found in this way for a number of values of m; the downwash distribution has been calculated from equation (1). Figure 6 shows the cases $m=1$, 2 (which are identical, since for $m=2$ the two central trailing vortices cancel) and $m=8$. The downwash is expressed as w/w_0, where w_0 is the constant value for the continuous elliptic load.

As each (finite) trailing vortex is approached, the downwash tends to infinity; it is apparent that there is a very large difference from the constant value ($w/w_0=1$, shown dotted) appropriate to the continuous load. Near the centre of the wing the downwash is roughly constant but, as the tip is approached, the variation becomes exceedingly rapid; presumably this is due to the increasing strengths of the trailing vortices toward the tip.

In view of Fig. 6, it is perhaps remarkable that an arbitrary choice of position for specification of the downwash, such as $k=\frac{1}{2}$, should give a load of anything like the right order, either in magnitude or distribution. However, it is worth noting that in the case $m=8$, the intersections of the downwash lines with $w/w_0=1$ occur very near the centres of the bound vortices, except for the tip vortex, where the intersection is noticeably nearer the wing tip.

10. Practical Applications

In the foregoing analysis comparisons have been made between the loads due to continuously varying distributions of vorticity and those due to horseshoe vortex systems; they have been related solely by the induced downwash. In practice, of course, the loads are usually only partly determined by the induced downwash, and our earlier results are only partially applicable in consequence. A brief examination of this question is now attempted.

Let us consider again the elliptically loaded wing, of elliptic plan form, untwisted, and at geometric incidence α. The local load per unit length then gives, in the usual notation,

$$\tfrac{1}{2}\rho V^2 ca\left(\alpha - \frac{w}{V}\right) = \rho V K, \quad . \quad . \quad . \quad . \quad . \quad (41)$$

or $$\tfrac{1}{2}Va\left(\alpha-\frac{w}{V}\right)=\frac{K}{c}=\frac{K_0}{c_0},$$

where K_0, c_0 relate to the centre of the wing.

But $$w=K_0/(4s);$$

hence $$\tfrac{1}{2}Va\alpha=\left(\frac{ac_0}{8s}+1\right)\frac{K_0}{c_0},$$

which, with $a=2\pi$, yields the well-known result

$$\tfrac{1}{2}Vca\alpha=\left(\frac{2}{A}+1\right)K. \qquad . \quad . \quad . \quad . \quad (42)$$

The coefficient of K consists of two terms; the first, $2/A$, derives entirely from the induced downwash, and the second from the geometric incidence. Equation (42) is usually taken to mean that the lift curve slope a is reduced by the factor $A/(A+2)$; in reality, the geometric incidence is reduced by downwash from the value α to the effective value

$$\alpha-\frac{w}{V}=\alpha-\left(\frac{2}{A+2}\right)\alpha, \qquad . \quad . \quad . \quad . \quad (43)$$

so that the induced downwash angle is $2/(A+2)$ times the geometric incidence.

The representation of the continuous elliptic load by a finite set of m horseshoe vortices is now considered. The equation corresponding to (41) is

$$\tfrac{1}{2}\rho V^2c_ia\left(\alpha-\frac{w_i}{V}\right)=\rho VK_i \qquad . \quad . \quad . \quad . \quad (44)$$

with w_i determined by (3), so that

$$w=\frac{m}{8\pi s}UK.$$

Accordingly, the equation corresponding to (42) becomes

$$\tfrac{1}{2}Va\alpha c_0\left[\frac{c}{c_0}\right]\{1,\ldots,1\}=\left[\frac{1}{A}\left(\frac{m}{\pi}\right)\frac{c}{c_0}U+I\right]K, \qquad . \quad . \quad (45)$$

where c/c_0 is a diagonal matrix, with elements c_i/c_0.

Now when A is indefinitely large, the first term on the right vanishes, and K is then determined wholly by the geometric incidence; the total load due to the horseshoe vortex system is then the same as that for the continuous elliptic load.

TABLE I

ELLIPTIC WING, $m=6$: VALUES OF $R_m(A)$.

A	0	1	6	∞
Equation (45)	1·167	1·102	1·034	1·0
Equation (47)	1·167	1·105	1·037	1·0

On the other hand, when A becomes very small, the first term on the right of (42) and (45) becomes dominant. The evaluation of K then becomes precisely the problem dealt with in the earlier part of this paper, which led to the result (29).

If (29) is regarded as implying that the elements of K are, to a first approximation, each greater by the factor R_m than those corresponding to the elliptic loading, it may be inferred that (45) is approximately equivalent to

$$\tfrac{1}{2}V c a \alpha = \left(\frac{2}{AR_m}+1\right)K, \quad . \quad . \quad . \quad . \quad . \quad (46)$$

since when A is large this gives the same value for K as the elliptic load, while when A is vanishingly small K is increased by the factor R_m. For A finite and non-zero, the new ratio $R_m(A)$ is then, on comparison with (42),

$$R_m(A) = \frac{AR_m}{AR_m+2}\,\frac{A+2}{A}$$

or

$$R_m(A)-1 = \left(\frac{2}{AR_m+2}\right)(R_m-1). \quad . \quad . \quad . \quad . \quad (47)$$

When $R_m \simeq 1$ this shows that the fractional increase R_m-1, calculated for the horseshoe system when it is wholly defined by downwash, must be factored by $2/(A+2)$ approximately to give the correct fractional increase $R_m(A)-1$; the factor is the proportion of geometric incidence due to downwash, as shown by (43).

The formula (47) has been tested by calculation for the case $m=6$, for which

$$R_m = 7/6.$$

Equation (45) was solved for the circulations K_i, from which the load was found; Table I compares the results obtained by use of the approximate formula (47).

The formula (47), when equation (29) is used to define R_m, gives explicitly in terms of A and m

$$R_m(A) = \frac{(A+2)(m+1)}{(A+2)(m+1)-2} \quad . \quad . \quad . \quad . \quad . \quad (48)$$

11. Conclusions

If a set of horseshoe vortices is to be used to represent a lifting surface, the foregoing investigations suggest the following conclusions.

(*a*) If the circulations are to be wholly determined by the downwash induced, it is best specified at the centre of each vortex, except possibly near the tip.

(*b*) With the hypothesis of (*a*), a considerable error will result unless a large number of vortices is used: if the error is not to exceed 5 per cent, then not less than 20 vortices are required for a symmetric distribution, or 40 vortices for an anti-symmetric distribution.

(*c*) Correction factors based on equations (29) and (40) could be applied.

(*d*) If the circulation is determined by a geometric incidence modified by downwash, then aspect ratio will play a part and the correction to be applied is given by equations (47) and (48); if the error is to be not greater than 5 per cent, the number of horseshoe vortices should be greater than

$$m=\frac{40-A}{A+2}\,.$$

(*e*) With the hypothesis of (*d*), correction factors based on (48) could also be applied.

References

1. Collar, A. R. On the Reciprocal of a Segment of a Generalised Hilbert Matrix. *Proc. Camb. Phil. Soc.*, Vol. 47, Part. 1, 1950.

2. Glauert, H. *Aerofoil and Airscrew Theory*, Second Edition. Cambridge University Press, 1947.

A Random Distribution of Gusts Corresponding to a Measured Frequency of Vertical Gusts

M. FINE

(*Rotol Ltd.*)

SUMMARY: The paper describes a method of estimating the frequency of gust components in the plane of a propeller from measurements of *vertical* gust components, which are those generally recorded. By this means additional flight recording is avoided and the danger of under-estimating the frequency of gusts affecting the propeller is reduced. Random distribution of gusts in space is assumed. It is found that gust components in the plane of the propeller of 10 ft./sec. or more occur 2·51 times as frequently as vertical components of 10 ft./sec. or more. For speeds greater than 10 ft./sec., the ratio is higher.

1. Introduction

Accelerometers in cruising aeroplanes generally record vertical components of gusts. The propeller, however, is stressed by all components in its plane, rather than by vertical ones alone. Lateral gusts will not be recorded by an accelerometer measuring vertical components; hence available records of vertical components under-estimate the frequency of gusts affecting the propeller. The problem is to estimate the incidence of such gusts from the measured vertical components, thus avoiding additional flight recording.

NOTATION

The term "vertical gusts" is used here for "vertical components of a gust", and "propeller gust" for the "component of a gust in the plane of the propeller."

u vertical component of gust velocity (ft./sec.)

v component of gust velocity in propeller plane (ft./sec.)

θ inclination of direction of v to horizontal (radians)

$F(u)$ number of vertical components with velocity u or more for every 1,000 of 10 ft./sec. or more

$g(v)$ number of propeller gusts with velocity v or more for every 1,000 of 10 ft./sec. or more

$$R = \frac{\text{frequency of propeller gusts of 10 ft./sec. or more}}{\text{frequency of vertical gusts of 10 ft./sec. or more}}$$

Received April 1958.

$N(u)$ number of vertical gusts recorded with velocity u or more if there are 1,000 $d\theta$ propeller gusts of 10 ft./sec. or more in the directions between θ and $\theta+d\theta$

A, B, α, β constants used in the expression for g

$G(v)$ function of v used in the expression for g

p, r, w, x, y, ξ auxiliary variables

h, H auxiliary functions

$a, a_0, a_1, a_2, m, X_1, X_2, \nu$ auxiliary parameters

$$c=(2/\pi)^{0\cdot5}.$$

2. Assumptions

The vertical gusts are described by Bullen[1];

$$F(u)=27{,}800\exp(-0\cdot34411u)+878\cdot2\exp(-0\cdot20816u) \quad . \quad . \quad (1)$$

fits measured results well. (Here "vertical" means both "up" and "down.") Gusts are assumed to be randomly distributed in space and the distribution which gives vertical components agreeing with relation (1) is found.

3. Mathematical Formulation of the Problem

A gust with a component normal to the propeller is resolved into this component and one in the plane of the propeller. The components normal to the propeller are neglected for the time being; clearly the remaining components are distributed randomly. The following argument is applicable to any random distribution of vectors in a plane with records of components in one direction.

Figure 1, in the plane of the propeller, shows a component of velocity v inclined at θ to the horizontal. The vertical component is $v\sin\theta=u$, *i.e.* $v=u/\sin\theta$.

Consider an element defined by $d\theta$ and propeller gusts in the corresponding range of direction, *i.e.* these propeller gusts have no components at right angles to the direction θ. If there are 1,000 $d\theta$ propeller gusts with speed of 10 ft./sec. or more in the range given by $d\theta$ then there are $g(v)\,d\theta$ propeller gusts with speed v ft./sec. or more in this range, and $g(u/\sin\theta)\,d\theta$ propeller gusts with vertical components of u ft./sec. or more.

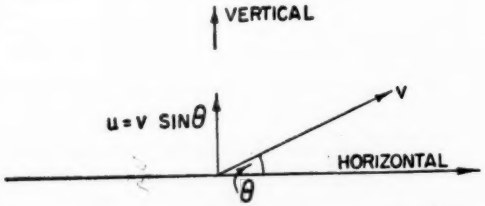

FIGURE 1.

The number of vertical gusts of u ft./sec. or more recorded by the accelerometer is

$$N(u)=2\int_0^{\pi/2} g(u/\sin\theta)\,d\theta. \quad . \quad . \quad . \quad . \quad . \quad (2)$$

The numerical factor is 2 because F, in relation (1), includes "up" and "down" gusts. The corresponding number for vertical gusts of 10 ft./sec. or more is

$$N(10)=2\int_0^{\pi/2} g(10/\sin\theta)\,d\theta. \quad . \quad . \quad . \quad . \quad (3)$$

For every 1,000 recorded vertical gusts of 10 ft./sec. or more there are 1,000 $N(u)/N(10)$ vertical gusts of u ft./sec. or more, and so

$$[2{\cdot}000/N(10)]\int_0^{\pi/2} g(u/\sin\theta)\,d\theta=F(u)$$
$$=27{,}800\exp(-0{\cdot}34411u)+878{\cdot}2\exp(-0{\cdot}20816u). \quad . \quad . \quad . \quad . \quad (4)$$

It is necessary to find g from (4), with $N(10)$ given by (3). g is the function for propeller gusts corresponding to F for vertical gusts. If g is known, R can be found.

With 1,000 $d\theta$ propeller gusts of 10 ft./sec. or more corresponding to each element $d\theta$, the total number of such gusts is

$$2\int_0^{\pi/2} 1{,}000\,d\theta=1{,}000\pi. \quad . \quad . \quad . \quad . \quad . \quad (5)$$

The accelerometer has recorded $N(10)$ vertical gusts of 10 ft./sec. or more.

$$\text{Hence} \quad R=1{,}000\pi/N(10). \quad . \quad . \quad . \quad . \quad (6)$$

The method of solving equation (4) is outlined in the Appendix.

4. Results

The solution of equation (4) is

$$g(v)=10^3\,\frac{AG(\alpha v)+BG(\beta v)}{AG(10\alpha)+BG(10\beta)}, \quad . \quad . \quad . \quad . \quad (7)$$

$$\left.\begin{array}{ll} \text{where} & A=27{,}800, \quad \alpha=0{\cdot}34411 \\ & B=878{\cdot}2, \quad \beta=0{\cdot}20816 \end{array}\right\} \quad . \quad . \quad . \quad . \quad (8)$$

$$\text{and} \quad G(x)=(2/\pi)\, xK_1(x), \quad . \quad . \quad . \quad . \quad . \quad . \quad (9)$$

$K_1(x)$ being a Bessel function* of imaginary argument[2, 3, 4];

$$R=(\pi/2{,}000)\,[AG(10\alpha)+BG(10\beta)]. \quad . \quad . \quad . \quad (10)$$

Figure 2 shows the variation of g with v and the variation of F with u. The value of R is 2·51, so that recordings of vertical gusts fall well below the number of propeller gusts.

Components normal to the propeller have been neglected; by symmetry they occur as often as vertical gusts.

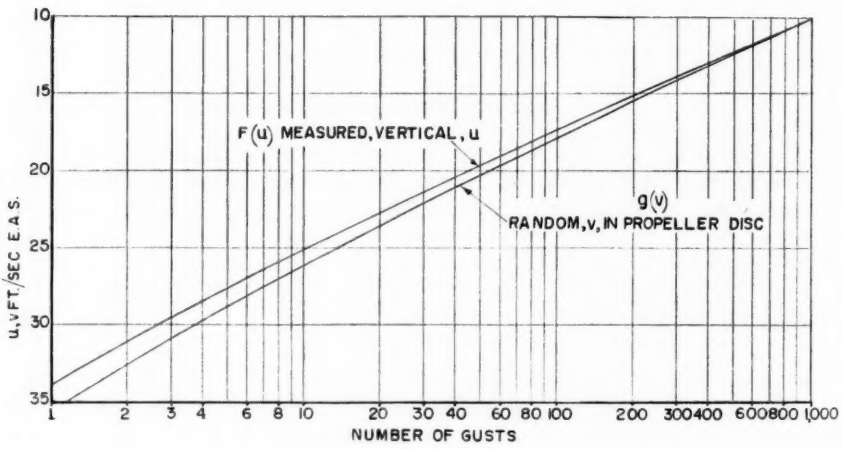

FIGURE 2.

ACKNOWLEDGMENTS

The author is grateful to N. J. Durant, British Messier Ltd., for help, particularly in obtaining the solution in terms of Bessel Functions of imaginary argument, and to other colleagues at Rotol and British Messier for helpful discussion and for the preparation of Fig. 2. Thanks are due to Messrs. Rotol for permission to publish this note.

*$K_1(x)$ used in this paper differs from that tabulated in the Mathematical Tables of the British Association by a factor of $\pi/2$.

Appendix

Method of Solving Equation (4)

If $G(v)$ satisfies $$\int_0^{\pi/2} G(v/\sin\theta)\, d\theta = \exp(-v), \quad . \quad . \quad . \quad . \quad (11)$$

then the solution of equation (4) is as stated in equations (7), (8) and (9).

$$\text{Write} \quad G(v) = c\int_0^{\infty} h(p)\cos pv\, dp, \quad . \quad . \quad . \quad . \quad (12)$$

$$\text{where} \quad c^2 = 2/\pi; \quad . \quad . \quad . \quad . \quad . \quad . \quad (13)$$

by Fourier's integral theorem

$$h(p) = c\int_0^{\infty} G(v)\cos pv\, dv. \quad . \quad . \quad . \quad . \quad (14)$$

Substituting from (12) in (11), putting

$$p = r\sin\theta, \quad . \quad . \quad . \quad . \quad . \quad . \quad (15)$$

and inverting the order of integration gives

$$c\int_0^{\infty} H(r)\cos rv\, dr = \exp(-v), \quad . \quad . \quad . \quad . \quad (16)$$

$$\text{where} \quad H(r) = \int_0^{\pi/2} h(r\sin\theta)\sin\theta\, d\theta. \quad . \quad . \quad . \quad . \quad (17)$$

Applying Fourier's integral theorem to (16) gives, with (17),

$$H(r) = c\int_0^{\infty} \exp(-v)\cos rv\, dv = c/(1+r^2) = \int_0^{\pi/2} h(r\sin\theta)\sin\theta\, d\theta \quad . \quad (18)$$

Expanding $(1+r^2)^{-1}$ and $h(r\sin\theta)$ in powers of r^2 and equating coefficients gives,

$$\text{with} \quad h(r\sin\theta) = a_0 + a_1 r^2\sin^2\theta + a_2 r^4\sin^4\theta + \ldots, \quad . \quad . \quad . \quad (19)$$

$$a_0 = c, \quad a_1 = -3c/2, \quad a_2 = (3\times 5)c/(2\times 4), \quad . \quad . \quad (20)$$

$$\text{and} \quad h(p) = c(1+p^2)^{-1\cdot 5}; \quad . \quad . \quad . \quad . \quad . \quad (21)$$

whence the step from (15) to (16) and the result (21) may be justified as follows.

$$\exp(-v) = c\int_0^{\pi/2}\left[\int_0^{\infty} h(p)\cos(pv/\sin\theta)\,dp\right]d\theta$$

$$= c\int_0^{\pi/2}\left[\int_0^{\infty} h(r\sin\theta)\cos rv\,dr\sin\theta\right]d\theta.$$

Now $$\int_0^{\pi/2}\left[\int_{X_1}^{X_2} h(r\sin\theta)\cos rv\,dr\sin\theta\right]d\theta = \int_{X_1}^{X_2}\left[\int_0^{\pi/2} h(r\sin\theta)\sin\theta d\theta\right]\cos rv\,dr.$$

With h given by (21), the last integral in square brackets is $(1+r^2)^{-1}$ if r is complex and $|r|<1$. In the strip $|\mathcal{I}(r)|<1$ the integral is an analytic function of r and, by continuation, is $(1+r^2)^{-1}$.

Hence the last double integral is

$$\int_{X_1}^{X_2}(1+r^2)^{-1}\cos rv\,dr < \int_{X_1}^{X_2} r^{-2}dr \text{ (in absolute value),}$$

which is smaller than any assigned quantity for sufficiently large X_1, X_2, and the result follows.

From relations (12), (13) and (21),

$$G(v) = (2/\pi)\int_0^{\infty}(1+p^2)^{-1\cdot 5}\cos pv\,dp \quad . \quad . \quad . \quad . \quad . \quad (22)$$

Equivalent integrals were discussed by Glaisher[5] in 1881, but his work was not seen by the author until after the solution had been found independently[6]. Using Glaisher's results gives the solution more quickly than otherwise; Ref. 6 uses rather less advanced analysis, yet provides some interesting results.

Glaisher shows that, with a slight change of notation in his work,

$$y = x^m\int_0^{\infty}\frac{\cos a\xi\,d\xi}{(x^2+\xi^2)^m} \quad . \quad . \quad . \quad . \quad . \quad . \quad . \quad (23)$$

is a solution of the Riccati equation

$$\frac{d^2y}{dx^2} - a^2y = \frac{m(m-1)\,y}{x^2} \quad . \quad . \quad . \quad . \quad . \quad . \quad (24)$$

if y is finite.

Putting $\xi = xp$ and $ax = v$ in (23) gives

$$y = \left(\frac{a}{v}\right)^{m-1} \int_0^\infty \frac{\cos pv \, dp}{(1+p^2)^m} \quad . \quad . \quad . \quad . \quad . \quad (25)$$

Hence $yv^{m-1} = (\pi/2)\, a^{m-1}\, G(v)$ if $m = 1{\cdot}5$, . . . (26)

and, from (24), y is a solution of

$$\frac{d^2y}{dv^2} - y = \frac{m(m-1)\,y}{v^2} \quad . \quad . \quad . \quad . \quad . \quad (27)$$

Following Glaisher, put $y = v^{0{\cdot}5} w$ . . . . . (28)

in (27), giving $$\frac{d^2w}{dv^2} + \frac{1}{v}\frac{dw}{dv} - \left[1 + \frac{(m-0{\cdot}5)^2}{v^2}\right] w = 0 \quad . \quad . \quad . \quad (29)$$

This has as solutions Bessel functions of order $\nu = m - 0{\cdot}5$, with imaginary argument iv. As v tends to infinity x tends to infinity and, from (23) and (28), both y and w tend to zero. This disposes of one of the solutions of (27). The behaviour of y and w when v tends to 0 gives the multiplicative constant and, for $m = 1{\cdot}5$, it is found that

$$G(v) = (2/\pi)\, vK_1(v), \quad . \quad . \quad . \quad . \quad . \quad (30)$$

where K_1 is as defined in Ref. 2.

This method may be applied to find $g(v)$ corresponding to other forms of $F(u)$ and, in addition, to find the three-dimensional distribution of gusts.

REFERENCES

1. BULLEN, N. I. B. The Variation of Gust Frequency with Gust Velocity and Altitude. A.R.C. Current Paper 324, 1957.

2. WATSON, G. N. *A Treatise on the Theory of Bessel Functions.* Cambridge University Press, 1944.

3. MCLACHLAN, N. W. *Bessel Functions for Engineers.* Oxford University Press, 1941.

4. JAHNKE, E. and EMDE, F. *Tables of Functions.* Dover Publications, New York, 1946.

5. GLAISHER, J. W. L. On Riccati's Equation and its Transformations, and on Some Definite Integrals which Satisfy Them. *Phil. Trans. Roy. Soc.*, 1881, Part III.

6. FINE, M. A Random Distribution of Gusts Corresponding to a Measured Frequency of Vertical Gusts. Rotol Performance Office Report No. 1026, April 1957.

The Influence of the Wake on the Flutter and Vibration of Rotor Blades*

J. P. JONES, Ph.D., B.Sc.(Eng.)

(*University of Southampton*)

SUMMARY: An approximate theory is described which takes into account the influence of the wake on the aerodynamic derivatives of an oscillating rotor blade. It is shown that the most important parameter is the number of cycles of the oscillation which occur during one revolution of the rotor. For integral values of this parameter the flexural damping is shown to become very small at small angles of incidence. The flutter characteristics of a simple rotor blade are calculated on the basis of this theory, and it is found that the wake causes radical changes in the critical speeds. The theory is in good qualitative agreement with experiment.

1. Introduction

1.1. Rotor Blade Bending Frequencies

Rotor blades derive much of their bending stiffness from the centrifugal force; in fact in the fundamental mode of a hinged blade the centrifugal force supplies all the stiffness. It follows that the natural bending frequencies increase with rotational speed, the increase depending upon the mode and the root conditions.

Experimentally[1], it is found that

$$f^2 = f_0^2 + \alpha\Omega^2 \quad . \quad . \quad . \quad . \quad . \quad . \quad (1)$$

where α is a constant whose value depends upon the mode and the root conditions.

Approximate values of α for hinged and encastré blades are:—

Hinged Blades		*Encastré Blades*	
Fundamental	1·0	Fundamental	1·2
1st Overtone	6·0	1st Overtone	6·5
2nd Overtone	12·0		

*The material in this paper is based on a report submitted to the Department of Scientific and Industrial Research in June 1954, which was later extended and circulated as A.R.C. Report 18,173, in January 1956. The present paper was received for *The Aeronautical Quarterly* in October 1957.

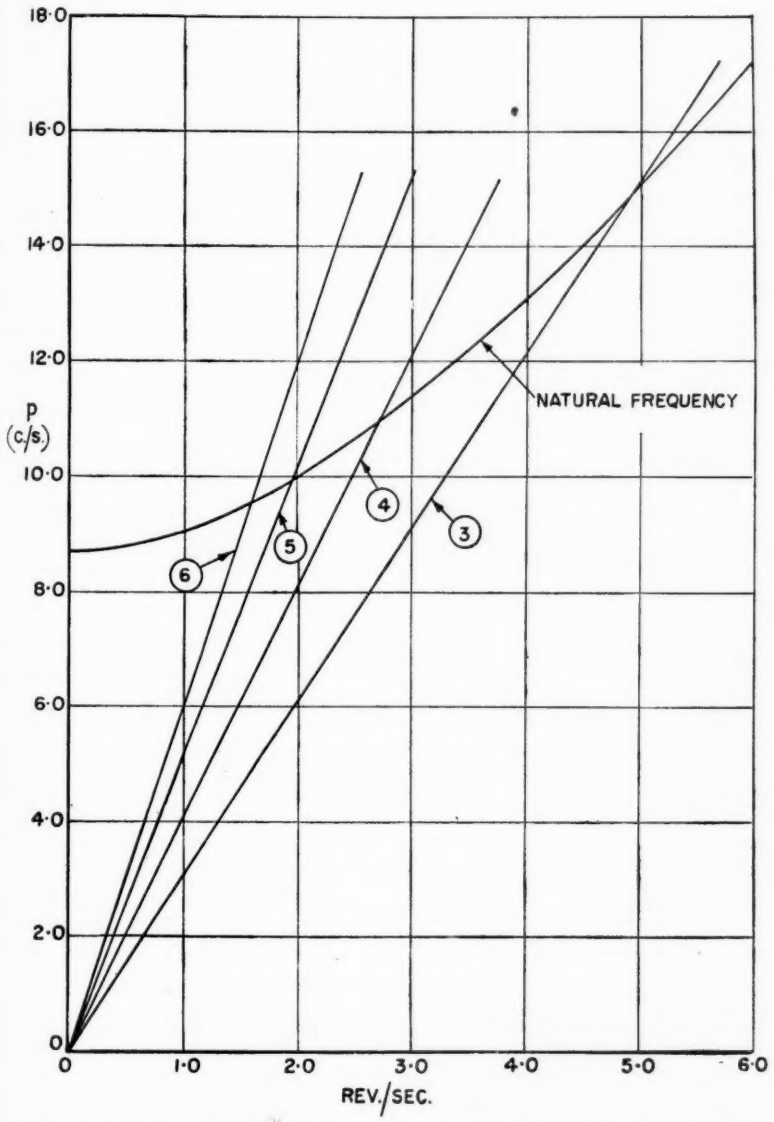

FIGURE 1. Variation of first bending frequency with rotational speed for a hinged blade.

A typical curve of natural frequency (cycles/sec.) against rotational speed (revolutions/sec.) for the first overtone mode of a hinged blade is shown in Fig. 1. It is assumed that $f_0 = 8{\cdot}65$ c./s. and $\varkappa = 6{\cdot}0$. Superimposed on the diagram are the straight lines "3," "4," "5," etc. The enclosed number denotes the slope of the

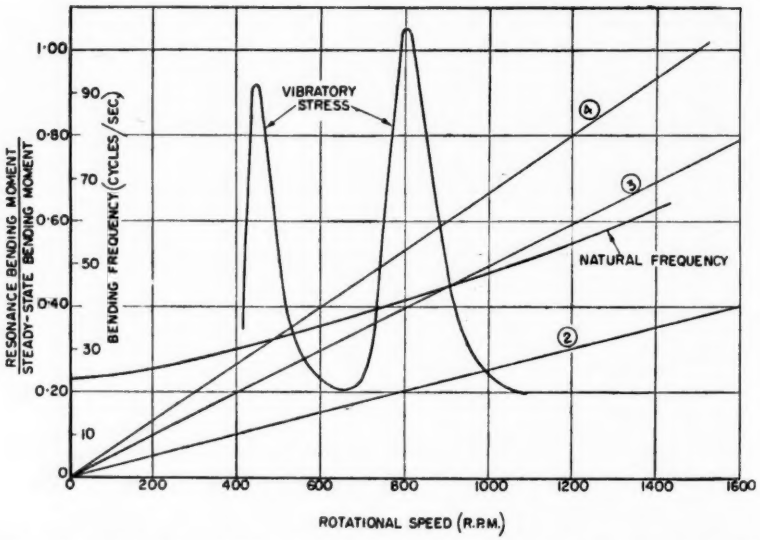

FIGURE 2. Hovering case. Hinged blade. Blade angle 12°. Variation of stress with rotational speed[3].

line in cycles per revolution. Thus, at the rotational speeds corresponding to the intersection of any of these lines with the frequency curves, the natural frequency will be such that an integral number of cycles are completed in one revolution.

1.2. EXPERIMENTAL RESULTS

Hirsch[2] and Meyer[3] have recently published the results of some experimental work on the stresses in rotor blades, and both found unexpectedly large fluctuating bending stresses, with frequencies varying from one to ten cycles per revolution. A diagram of the type shown in Fig. 1 was constructed for each blade, and it was found that the large stresses occurred at rotational speeds such that one or more of the natural bending frequencies was given by

$$\text{frequency} = \text{integer} \times \text{rotational speed}.$$

On the basis of the usual aerodynamic theory, these vibrations cannot be explained. The results certainly suggest that the blades were in resonance with exciting forces having frequencies of one per rev., two per rev., and so on, but if so, what was the source of excitation? In forward flight, the lift varies periodically as the blades rotate, but theory predicts only very small higher harmonic components, which reach a maximum at large μ, whereas the measured stresses were largest when μ was small, *i.e.* in the transition region.*

Daughaday and Kline[4] have put forward the theory, based on a paper by Mangler and Squire[5], that the excitation is produced by the variation of induced

*The "tip-speed ratio" μ is defined as $V_0/\Omega R$, where V_0 is the forward speed of the helicopter and R is the tip speed due to rotation.

velocity around the disc. By induced velocity is meant the downwash at the rotor disc due to the trailing vortex system. The agreement between theory and experiment was not good, due possibly to the difficulties of obtaining a reliable estimate of the downwash, especially near the blade tips, but more probably to the analysis being incomplete. In forward flight the induced velocity is certainly not constant around the disc, and a forced oscillation is possible; but it appears from Meyer's results that the vibrations may also be experienced on a hovering rotor (in which case the induced velocity is constant around the disc), and in the full scale tests of Ref. 2 the higher harmonic vibration was first noticed during a ground run. To investigate this phenomenon Meyer[3] carried out a comprehensive series of model tests, on hovering rotors, using both hinged and encastré blades. Figure 2 is reproduced from Meyer's report and shows (*a*) the variation of natural bending frequency with rotational speed, and (*b*) the variation of the ratio (resonance b.m.)/(steady state b.m.) with rotational speed. The most important features of the results are now described.

(*i*) Within the range of the experiments, the occurrence of the vibration was independent of the mode of oscillation and of the absolute value of the frequency. The fundamental (encastré) and first overtone (hinged) modes were excited at frequencies up to eight cycles per revolution. The peak vibratory stresses were quite large, being as much as 50 per cent† of the steady bending stress in some cases.

(*ii*) It was found that the amplitude of the vibration increased with increase of incidence but, in particular, the oscillations occurred at zero incidence with blades of symmetrical section, *i.e.* when there was no thrust, and therefore no trailing vortex system. The amplitude did not remain constant, but grew and decayed in an irregular manner.

(*iii*) Since a wide range of blade stiffnesses and frequencies was used, the possibility of the supporting structure playing an important part in the vibration could be eliminated.

(*iv*) It will be seen from Fig. 2 that the vibratory stress increases very rapidly as the frequency ratio ν (number of cycles per revolution) approaches an integral value, but that it never becomes zero. Therefore it must be assumed that a small periodic force was present at all speeds, produced either by fluctuations of torque or by slight eccentricity of the shaft and bearings. Adjustments to the balance and alignment of the rotor produced only slight changes in the amplitude of vibration.

The stress-speed curves are similar to those obtained if a lightly damped structure is in resonance with a periodic exciting force, but simple aerodynamic theory (*i.e.* assuming that the oscillation does not affect the lift-curve slope) predicts heavy damping of flexural vibrations. The possibility that the exciting force itself increases rapidly at certain rotational speeds may be ruled out, because with different blades the peak amplitudes were obtained at different rotational speeds, for the same frequency ratio.

---

†The vibratory stresses in Fig. 2 are the peak-to-peak values, *i.e.* twice the amplitude.

Thus it was concluded that the vibrations were either (*a*) self-excited, or (*b*) forced, but simple aerodynamic theory was invalid. A brief review of the evidence shows that if (*a*) is the explanation, then the vibrations were so much divorced from the usual types of instability that they must be regarded as completely new phenomena.* Whirling would involve some form of coupled motion between the rotor shaft and the blades, with perhaps as many as five critical speeds quite close together, but with the same mode of blade bending at all five speeds. For similar reasons the usual types (*i.e.* fixed-wing) of classical flexure-torsion flutter can be eliminated. The vibrations occurred in one mode only, at the natural frequency of that mode, and the several critical speeds were quite close together. The construction of the blades was such that both the flexural and inertia axes were substantially on the quarter-chord line; hence the aerodynamic and inertia couplings were very small. It is true that the rotation introduces inertia and velocity couplings which are absent from fixed wings, but in general these are small, especially at small angles of incidence. Stall flutter may be ruled out at low angles of incidence (but *see* Section 2.2).

The alternative (*b*) is the more likely explanation, *i.e.* that simple aerodynamic theory is invalid. This implies that for integral values of ν the damping becomes very small. It is known from oscillatory aerofoil theory that the flexural damping is less than that obtained if the effect of the wake is neglected. But the frequency parameter over the outer sections of a blade—where most of the lift is developed—is small, and the overall reduction of the flexural damping would not be more than 20 per cent, which is by no means sufficient to explain the sharp increase of amplitude. There is, however, a significant aerodynamic difference between fixed and rotating wings, namely the form of the wake. Behind a fixed wing it is essentially a plane surface, extending to great distances, so that the remote parts have little influence on the flow past the wing; but the wake of a rotor blade or airscrew is a helical surface and the blade actually passes over its own wake.

It is now suggested that the wake is primarily responsible for the hovering vibrations and, in the remainder of the paper, an approximate theory is developed from this idea.

NOTATION

$f/2\pi$ natural frequency of rotating blade in a given mode

$f_0/2\pi$ natural frequency of stationary blade in the given mode

Ω angular velocity of the rotor

t time

$p/2\pi$ frequency

*The possibility of the vibrations being essentially non-linear cannot be ruled out, because the amplitude did not grow without limit, and the wave form was not periodic. But if the blades had slightly different natural frequencies, then the wave form, and the fact that the amplitude had a maximum value at a certain speed, can be explained equally well by a forced oscillation.

$\nu = p/\Omega$ frequency ratio (cycles per revolution)

N integral values of the frequency ratio

δ fractional values of the frequency ratio

ε vorticity shed into wake at time t

ε_θ vorticity shed into wake at earlier instant

θ angle measured from trailing edge

$\psi = \Omega t$

c chord

r radius of blade element

δm element of mass

R tip radius

$r' = c/R$

$c\sigma$ distance of inertia axis aft of the quarter-chord line

σ_m minimum value of σ to produce flutter

ck radius of gyration of blade about the spanwise axis

ck_0 radius of gyration of mass-balanced blade about the spanwise axis

β blade flapping displacement (downward flapping positive)

χ blade pitching displacement (nose-up pitching positive)

I_F moment of inertia of the blade about the flapping hinge

I_T blade pitching moment of inertia

K_T root spring stiffness

ω_T flutter speed coefficient

ρ density

$n = 2\pi\rho cR^4/(8I_F)$, blade inertia number

$x = -\frac{1}{2}c\cos\phi$, co-ordinate of a point in the wake measured from mid-chord

$\xi = -\frac{1}{2}\cos\phi$

x_1 co-ordinate of a point on the aerofoil measured from mid-chord

$\xi_1 = -\frac{1}{2}\cos\phi_1$

$\eta = \xi - \xi_1$

$V = \Omega r$, free stream velocity at representative radius

ω' reduced frequency at representative radius $(= \rho c/2r)$

$C(i\omega') = F + iG$, Theodorsen's Function

$X_0(i\omega') = C(i\omega') I_0(i\omega') + 1 - C(i\omega') I_1(i\omega') = X + iY$

$J_0(\omega'), J_1(\omega')$ Bessel Functions

$I_0(i\omega'), I_1(i\omega')$ modified Bessel Functions

$$\Gamma_0' = 2\,[\operatorname{cosec}\phi - (1-C)\,\tfrac{1}{2}\cot\phi]$$

$$\Gamma_0'' = 2\,[\tfrac{1}{2}\cot\phi - \operatorname{cosec}\phi + i\omega'\sin\phi]$$

$$\Gamma_1 = -2\sin\phi + \tfrac{1}{2}\cot\phi + \tfrac{1}{2}i\omega'\sin 2\phi + i\omega'\sin\phi$$

$$\Gamma_n = -2\sin n\phi + i\omega'\,[\sin\{(n+1)\phi\}/(n+1) - \sin\{(n-1)\phi\}/(n-1)]$$

$$K_0' = \pi c e^{-i\omega'} X_0(i\omega'), \qquad \xi \geqslant 1$$

$$K_0'' = c\sin\phi$$

$$K_1 = \tfrac{1}{2}c\sin\phi + \tfrac{1}{2}\sin 2\phi$$

$$K_n = \tfrac{1}{2}c\,[\sin\{(n+1)\phi\}/(n+1) - \sin\{(n-1)\phi\}/(n-1)]$$

W'_{os} downwash due to vortex sheets in wake below aerofoil

P, Q, R, S, X', Y' functions of ω', h and δ defined in the text

$l_{11}, l_{21}, l_{31}, l_{12}, l_{22}, l_{32}$
$m_{11}, m_{21}, m_{31}, m_{12}, m_{22}, m_{32}$ } derivative coefficients

2. Proposed Explanation

2.1. Effect of the Wake on an Oscillating Blade

One of the many difficulties of rotor aerodynamic theory lies in the fact that there is usually more than one blade, and the mutual interference of their wakes and "bound" vorticities cannot be ignored. In vibration theory, a further complication arises from the elastic and inertia couplings which exist between the blades, through the root and rotor shaft. Thus, in order to keep the theory as simple as possible, only a single blade rotor is considered, but it is recognised that this may introduce considerable errors.

The blade is assumed to be rotating with constant angular velocity Ω and to be oscillating at a frequency of p radians per second. The oscillation is assumed to have existed for sufficient time for the wake to extend to infinity below the rotor, and for the amplitude to have become steady. Then the vorticity which is shed from the trailing edge will move along a helical path relative to the blade and, after one or more complete revolutions of the rotor, will be directly beneath the trailing edge. Since the inflow velocity through the disc is usually very small compared with the tip speed of the blade, the pitch of the helix is small, and the vortex sheet beneath the blade will be quite close to it. Thus the blade is disturbed by vorticity shed in previous revolutions, and if these disturbances were all additive they would tend to sustain the vibration, and the effective damping would be reduced. The induced effects of the wake will be a maximum if the vorticity below the blade is the same after each revolution, *i.e.* provided that an integral number of cycles of the oscillation are completed per revolution.

There are three main objections to the preceding theory:—

(*i*) The vorticity does not remain absolutely stationary in space, but tends to "slide" along the surface of the helix. Thus, after each complete revolution the vortices of equal strength would be shifted relative to each other, and the maximum induced effects would be obtained at a slightly different frequency. Meyer's results show that this is not critical, since the vibrations occurred over a range of rotor speeds on either side of that which produced maximum amplitude.

(*ii*) The vorticity diffuses with time. This is a more serious objection which obviously depends upon the rate of diffusion, but those parts of the wake in which an appreciable reduction of strength has occurred will be several chords length below the blade; hence the total error may not be large.

(*iii*) The influence of the wake must decrease with increase of incidence, but the experiments showed that the amplitude of vibration increased with incidence. It is not possible at present to give a precise reason for this, but there are two probable explanations:—

(*a*) If the vibrations were excited by small variations of the driving torque, then the amplitude of the forcing function would increase with incidence. The torque fluctuations cause small changes in the rotational speed, and hence fluctuations of the total lift, but the steady lift coefficient increases with incidence; hence the oscillatory lift component due to changes in the rotational speed will increase with incidence.

(*b*) At the greater of the two incidences (0° and 12°) investigated, large areas of the blade may have been stalled, especially since the Reynolds number was very low. There is some confirmation of this from the Cornell Aeronautical Laboratory (C.A.L.) experiments (*see* Section 2.2), which were conducted at a greater Reynolds number, but stall flutter was obtained at a blade angle of 12° (in some cases 9°).

2.2. Effect of the Wake on Flutter

A further problem which arises from the foregoing theory concerns the effect of the wake on the flutter derivatives of a rotor blade. Assuming that the flexural damping can become very small at certain frequency ratios, there is no *a priori* reason why the remaining derivatives should not change radically at some value of ν, and a recent paper from the Cornell Aeronautical Laboratory[6] suggests that this may actually happen. At about the time this theory was being worked out, further experimental work was done at the C.A.L. on the flutter of a single blade model rotor and, through the courtesy of Mr. H. Daughaday, a copy of the report has been made available to the author.

The model blade was free to flap about a hinge on the axis of rotation, and to pitch about a spanwise axis. The pitching motion was restrained by springs at the root, but in flapping the restoring moment was provided mainly by the centrifugal force. At the root an elastic coupling was introduced between flapping and pitch, and the pitching moment of inertia and chordwise c.g. position could be varied by

means of internal balance weights. Three blades were used, one of very high torsional and bending stiffnesses, so that the motion was substantially that of a rigid blade, and two others of equal (low) bending, but different torsional stiffnesses.

Two principal types of flutter were recorded, namely, classical flapping-pitch and a much milder vibration, which occurred only at small angles of incidence and at a frequency ratio of approximately 2·0. To account for the latter type of flutter, Daughaday and Kline put forward an explanation similar to that already given, but the modes of vibration, and the conditions under which it was obtained, differed considerably from those of Ref. 3. No single-degree-of-freedom vibrations were found, it was always necessary to provide some coupling (inertia or elastic) between flapping and pitch, and the frequency ratio corresponded to that of the coupled motion ($\nu \simeq 2{\cdot}0$).

In some cases it was found that a small change in root spring stiffness caused a jump in the frequency ratio, from $\nu = 1{\cdot}8$ to $\nu = 2{\cdot}2$ and even from $\nu = 1{\cdot}7$ to $\nu = 2{\cdot}6$, *i.e.* for a small change in one of the parameters it was possible to jump from one type of flutter to another.

It is possible, however, that the method of recording used by Meyer was more sensitive—or at least more revealing—than the C.A.L. technique, since the latter merely measured the rotation of the blade about its hinges, whereas Meyer's models were extensively strain-gauged along the span. On the other hand, it is likely that torque fluctuations were less on the C.A.L. models, since the rotor was driven through a gear box, flywheel and a long shaft of appreciable moment of inertia.

The elasticity of the blades was shown to have an important influence on the critical speeds, but it appeared that, for the configuration chosen, flexure was of more importance than torsion. (But *see* Section 5.4).

In several of their investigations into classical flutter, Daughaday and Kline obtained the curious result that ν remained virtually constant at about 1·50, independent of the incidence or coupling. This was not in agreement with calculated solutions, based on quasi-steady theory (*i.e.* the influence of cast-off vortices is completely neglected), which showed a substantial variation of ν, and it must be concluded that the aerodynamic theory was at fault.

In the next section an approximate theory is described which allows for the effect of the wake on the aerodynamic forces, and which gives results in good agreement with experiment.

3. Theory

3.1. An Approximate Representation of the Blade and its Wake

The forces and moments on an oscillating rotor blade may be calculated by a straightforward extension of the theory of oscillating wings of finite span, but this would be a very laborious process and some form of automatic computer would be essential. The greatest difficulty lies in the evaluation of the downwash integrals for a helical wake. Again, until it can be established that the wake does have an

important influence on the derivatives, and that the assumptions involved are acceptable, the labour necessary to obtain an exact solution cannot be justified. However, it is possible to cut down the labour considerably if the three-dimensional problem can be reduced to one in two dimensions, but which preserves the essential features of the former.

This is a common process in aerodynamics, but especially in propeller theory, where it has been used by Prandtl[7] to estimate tip losses, and by Joukowski to study the "cascade" interference between blades. The helicopter rotor is especially suited to this type of reduction, since the aspect ratio is high and the blade may be regarded as an oscillating aerofoil of infinite span.

Now the radius of curvature of the outer sections of a blade—where the relative velocity is greatest—is large; hence, for a considerable angular rotation the outer blade elements may be assumed to move in straight lines. The linear distance travelled will be large compared with the chord, and since the pitch of the helix is very small—only a chord's length or so at moderate incidence—it can be assumed that the wake is plane for several chords' length ahead of, and behind, the aerofoil. Thus the successive turns of the wake which are beneath the blade can be regarded as equally-spaced, plane vortex sheets, parallel to that attached to the trailing edge of the blade. The sheets are not horizontal, but are inclined at the mean pitch angle of the helix, *i.e.* parallel to the relative wind. But if the aerodynamic forces are calculated on the assumption that the blade is vibrating about zero mean incidence, then the simplified configuration shown in Fig. 3 is valid. The relative wind (velocity V) is assumed to be horizontal, and the vortex sheets are spaced a distance $hc/2$ apart, where c is the chord and h is a function of the mean incidence of the non-vibrating blade. It is convenient in the analysis to assume that the vortex sheets extend to infinity in both directions; hence it will be seen that the problem has been reduced to that of finding the forces on an oscillating, two-dimensional aerofoil, but with additional vortex sheets extending to infinity ahead of, behind, and below it.

So far the distribution of vorticity in these sheets has not been considered, but if ν is an integer, then the free vorticity at a distance x from the aerofoil (measured positive to the rear and from the mid-chord) will be the same in each sheet, but if ν is not an integer it is necessary to consider the vorticity distribution in the helical wake.

3.2. The Distribution of Vorticity in the Wake

Assume a system of cylindrical polar co-ordinates (r, θ, z) to be associated with the rotor; z is measured parallel to the axis of rotation and θ is measured from the position of the blade trailing edge at time t. If the oscillations are simple harmonic, then the vorticity shed into the wake at time t and radius r is

$$\varepsilon = \varepsilon(r)\, e^{ipt} \quad . \quad . \quad . \quad . \quad . \quad . \quad (2)$$

where $\varepsilon(r)$ is the amplitude of the vorticity at radius r.

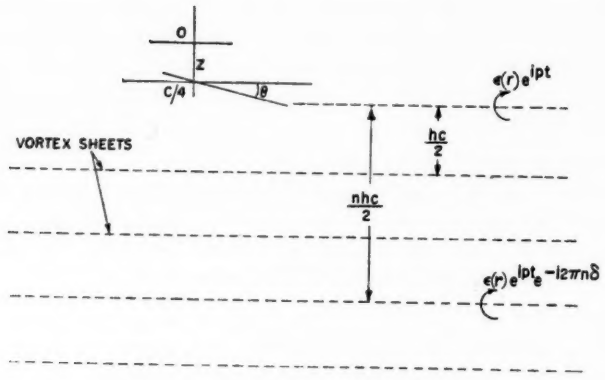

FIGURE 3. Aerofoil and vortex sheets.
Note: O is not the origin for measurement of x. The mid-chord is the origin in Section 4.1.

Then the vorticity cast off at this radius, but at some earlier time, is

$$\varepsilon_\theta = \varepsilon(r)\, e^{ip(t-\theta/\Omega)} \quad . \quad . \quad . \quad . \quad . \quad (3)$$

If $\theta = 2n\pi$, $n = 1, 2, 3 \ldots .$, then this will be the magnitude of the free vorticity in successive sheets directly below the trailing edge.

Also, putting $p/\Omega = \nu = N + \delta$, where $N = 1, 2, 3 \ldots .$, and $0 < \delta < 1{\cdot}0$, then

$$\varepsilon_{2n\pi} = \varepsilon(r)\, e^{ipt} e^{-i(N+\delta)2n\pi}$$

$$= \varepsilon(r)\, e^{ipt} e^{-i2n\pi\delta}, \quad . \quad . \quad . \quad . \quad (4)$$

i.e. in neighbouring sheets the points of equal strength are displaced relative to each other by an amount which depends upon the frequency ratio.

This result can be transferred directly to the approximate representation if it is assumed that the curved path of the blade can be represented by a straight line.

$$\text{Put} \quad \theta = (x - c/2)/r = c(\xi - 1)/(2r). \quad . \quad . \quad . \quad . \quad (5)$$

$$\text{Then} \quad \varepsilon_\theta = \varepsilon(r)\, e^{ipt} e^{-i\nu c(\xi-1)/(2r)}$$

$$= \varepsilon_1(r)\, e^{-i\omega'\xi} e^{ipt}, \quad . \quad . \quad . \quad . \quad . \quad . \quad (6)$$

where $\varepsilon_1(r)$ is the peak value of the vorticity at the trailing edge.

For the sheet which is attached to the trailing edge $1 \leqslant \xi \leqslant \infty$, and for the remaining sheets $-\infty < \xi < \infty$.

If the blade path is straight, then the strength of the vorticity at any point in the sheet attached to the trailing edge ($n=0$) is

$$\varepsilon_1(r)\,e^{ipt}\,e^{-i\omega'\xi}, \qquad (7)$$

and the free vorticity at the same value of ξ in the n^{th} sheet is

$$\varepsilon_1(r)\,e^{ipt}\,e^{-i\omega'\xi}\,e^{-i2\pi n\delta}. \qquad (8)$$

The free vorticity at the trailing edge can be obtained from the usual theory of oscillating aerofoils.

4. Theoretical Analysis

4.1. Formulae for the Lift and Moment Coefficients

This section is based on the theory of oscillating aerofoils as described by W. P. Jones[8].

If z_1 is the downward displacement of any point x_1 on the chord at time t, it is necessary to satisfy the boundary condition of tangential flow at the surface, *i.e.* the equation

$$\frac{\partial z_1}{\partial t} + V\frac{\partial z_1}{\partial x_1} = w(x_1, z_1, t) \qquad (9)$$

where $w(x_1, z_1, t)$ is the downward induced velocity due to the bound and free vorticity.

If the frequency of the oscillation is $p/(2\pi)$ c./s., then we may put

$$z_1 = \frac{c}{2}z'(\xi)\,e^{ipt}. \qquad (10)$$

and we assume that

$$\left.\begin{aligned} \text{the bound vorticity } \gamma &= \Gamma\,e^{ipt} \\ \text{free vorticity } \varepsilon &= E\,e^{ipt} \\ \text{total circulation } k &= K\,e^{ipt} \\ \text{and the downwash } w &= W\,e^{ipt} \end{aligned}\right\} \qquad (11)$$

Γ is written in the form

$$\Gamma = V[C_0(\Gamma_0' + \Gamma_0'') + C_1\Gamma_1 + C_2\Gamma_2 + \ldots . C_n\Gamma_n], \qquad (12)$$

where the functions Γ_0', Γ_0'', Γ_1, and so on, are defined in the Notation, and the constants C_0, C_1, and so on, are to be determined.

It can be shown that for points on the aerofoil

$$K = \frac{c}{2} e^{-i\omega'\xi} \int_{-1}^{\xi} \Gamma e^{i\omega'\xi} d\xi \quad . \quad . \quad . \quad . \quad (13)$$

and for points in the wake

$$K = \frac{c}{2} e^{-i\omega'\xi} \int_{-1}^{+1} \Gamma e^{i\omega'\xi} d\xi \quad . \quad . \quad . \quad . \quad (14)$$

Hence, from each of the functions Γ_0', Γ_0'', and so on, the corresponding functions K_0', K_0'', and so on, can be derived (*see* Notation). With the exception of K_0', the K_n are zero in the wake.

The downwash $w(x_1, z_1, t)$ at the aerofoil is obtained from

$$2\pi W = \int K \frac{\partial}{\partial x} \left\{ \frac{x - x_1}{(x - x_1)^2 + (\frac{1}{2}nhc - z_1)^2} \right\} . dx \quad . \quad . \quad (15)$$

and $z_1 \longrightarrow 0$.

For an aerofoil of infinite span it is found that

$$W_0' = 0, \quad W_0'' = 1{\cdot}0, \quad W_1 = \tfrac{1}{2} + \cos\phi, \quad W_n = \cos n\phi, \quad . \quad . \quad (16)$$

but in the present case $W_0' \neq 0$ because of the induced effects of the additional sheets. Let the induced velocity of these sheets be W'_{0S}; then

$$W'_{0S} = \frac{1}{2\pi} \int_{-\infty}^{+\infty} \frac{\partial K_0'}{\partial x} \sum_{n=1}^{n=\infty} \frac{x - x_1}{\{(x - x_1)^2 + n^2h^2c^2/4\}} dx. \quad . \quad . \quad . \quad (17)$$

where $$K_0' = \pi c X_0 e^{-i\omega'\xi} e^{-i2n\pi\delta} \quad . \quad . \quad . \quad . \quad . \quad . \quad . \quad (18)$$

and $$X_0 = C(i\omega') I_0(i\omega') + [1 - C(i\omega')] I_1(i\omega') \quad . \quad . \quad . \quad (19)$$

Then $$W'_{0S} = i\omega' X_0 e^{-i2n\pi\delta} \int_{-\infty}^{+\infty} \Sigma \frac{e^{-i\omega'\xi}[\xi - \xi_1]}{\{(\xi - \xi_1)^2 + n^2h^2\}} d\xi \quad . \quad . \quad . \quad (20)$$

and, if we put $$\xi - \xi_1 = \eta, \quad . \quad . \quad . \quad . \quad . \quad . \quad (21)$$

$$W'_{0s} = i\omega' X_0 \, e^{-i\omega'\xi_1} e^{-i2n\pi\delta} \int_{-\infty}^{+\infty} \sum_{n=1}^{n=\infty} \frac{e^{-i\omega'\eta}\eta}{\{\eta^2 + n^2h^2\}} \, d\eta \quad . \quad . \quad . \quad (22)$$

In the Appendix it is shown that

$$\int_{-\infty}^{+\infty} \frac{\eta \, e^{-i\omega'\eta}}{\{\eta^2 + n^2h^2\}} \, d\eta = -i\pi e^{-i\omega' nh} \quad . \quad . \quad . \quad . \quad . \quad (23)$$

Hence $$W'_{0s} = \pi\omega' X_0 \, e^{-i\omega'\xi_1} \sum_{n=1}^{n=\infty} e^{-n\zeta} \quad . \quad . \quad . \quad . \quad (24)$$

where $$\zeta = \omega' h + i2\pi\delta.$$

Now $$\sum_{n=1}^{n=\infty} e^{-n\zeta} = \frac{1}{e^{\zeta} - 1} = \frac{1}{e^{\omega' h} e^{2i\pi\delta} - 1} \cdot \quad . \quad . \quad . \quad . \quad (25)$$

Hence $$W'_{0s} = \pi\omega' X_0 \, e^{-i\omega'\xi_1} (R + iS) \quad . \quad . \quad . \quad . \quad (26)$$

where $$R = \frac{e^{\omega' h} \cos 2\pi\delta - 1}{\{[e^{\omega' h} \cos 2\pi\delta - 1]^2 + [e^{\omega' h} \sin 2\pi\delta]^2\}} \quad . \quad . \quad (27)$$

and $$S = \frac{-e^{\omega' h} \sin 2\pi\delta}{\{[e^{\omega' h} \cos 2\pi\delta - 1]^2 + [e^{\omega' h} \sin 2\pi\delta]^2\}} \quad . \quad . \quad (28)$$

Now $$e^{-i\omega'\xi_1} = e^{i\omega' \cos\phi_1} = \cos(\omega' \cos\phi_1) + i \sin(\omega' \cos\phi_1) \quad . \quad (29)$$

and it may be shown that

$$\cos(\omega' \cos\phi_1) = J_0(\omega') - 2\{J_2(\omega') \cos 2\phi_1 - J_4(\omega') \cos 4\phi_1 + \ldots\}$$

$$\sin(\omega' \sin\phi_1) = 2\{J_1(\omega') \cos\phi_1 - J_3(\omega') \cos 3\phi_1 + \ldots\},$$

where $J_0(\omega')$, $J_1(\omega')$, and so on, are Bessel functions of the first kind.

Because of the high aspect ratios of rotor blades, the reduced frequency is usually small ($\omega' < 0{\cdot}25$). If attention is restricted to small ω', then, to a good approximation,

$$e^{-i\omega'\xi_1} = J_0(\omega') + 2iJ_1(\omega') \cos\phi_1 \quad . \quad . \quad . \quad . \quad (30)$$

and $$W'_{0s} = \pi\omega' X_0 \, e^{-i\omega'\xi_1} (R + iS) = X'J_0 - 2J_1 Y' \cos\phi_1 + i(Y'J_0 + 2X'J_1 \cos\phi_1) \quad (31)$$

where $$X' = \frac{\{X[e^{\omega' h} \cos 2\pi\delta - 1] + Y e^{\omega' h} \sin 2\pi\delta\} \pi\omega'}{\{[e^{\omega' h} \cos 2\pi\delta - 1]^2 + [e^{\omega' h} \sin 2\pi\delta]^2\}} \quad . \quad . \quad . \quad . \quad (32)$$

and $$Y' = \frac{\{Y\,[e^{\omega' h}\cos 2\pi\delta - 1] - X\,e^{\omega' h}\sin 2\pi\delta\}\,\pi\omega'}{\{[e^{\omega' h}\cos 2\pi\delta - 1]^2 + [e^{\omega' h}\sin 2\pi\delta]^2\}} \quad . \quad . \quad . \quad . \quad . \quad (33)$$

Then at some point ϕ_1 on the chord, the downwash is given by

$$W(\phi_1, z_1, t) = V\,[C_0\,(1 + W'_{0s}) + C_1\,(\tfrac{1}{2} + \cos\phi_1) + C_2\cos 2\phi_1] + \ldots \quad . \quad . \quad . \quad . \quad (34)$$

and the constants C_0, C_1, C_2, and so on, can be obtained from the relation (*see* equation (9))

$$W(\phi_1, z_1, t) = i\omega' z' + \partial z'/\partial \xi_1 \quad . \quad . \quad . \quad . \quad . \quad (35)$$

When the C_n are known, the downward force L and moment M, about the quarter-chord, per unit span, can be obtained from

$$-L = \tfrac{1}{2}\rho V c \int_0^{\pi} \Gamma \sin\phi\, d\phi \quad . \quad . \quad . \quad . \quad . \quad . \quad . \quad (36)$$

$$-M = \tfrac{1}{4}\rho V c^2 \int_0^{\pi} \Gamma \sin\phi\,\{\tfrac{1}{2} - \cos\phi\}\, d\phi \quad . \quad . \quad . \quad . \quad (37)$$

Putting $$C_L = \frac{L}{\tfrac{1}{2}\rho V^2 c}, \qquad C_M = \frac{M}{\tfrac{1}{2}\rho V^2 c^2}, \quad . \quad . \quad . \quad (38)$$

it is convenient to express C_L and C_M in the form

$$C_L = 2\pi\,\{l_{11} z/c + l_{21}\dot{z}/V + l_{31}\ddot{z}c/V^2 + l_{12}\chi + l_{22}c\dot{\chi}/V + l_{32}c^2\ddot{\chi}/V^2\} \quad . \quad (39)$$

$$C_M = (\pi/4)\{m_{11} z/c + m_{21}\dot{z}/V + m_{31}\ddot{z}c/V^2 + m_{12}\chi + m_{22}c\dot{\chi}/V + m_{32}c^2\ddot{\chi}/V^2\}, \quad (40)$$

where z is the downward displacement of the quarter-chord axis and χ is the rotation (positive nose-up) about the quarter-chord axis.

The quantities l_{12}, l_{21}, and so on, will be referred to as the derivative coefficients and in Section 4.2 they are evaluated for the case of a blade performing combined translational and rotational oscillations. The first number in the suffix refers to the type of derivative, *i.e.* displacement, velocity or acceleration, and the second number to the type of motion, *i.e.* translation or rotation.

4.2. Calculation of the Derivative Coefficients

Let the downward displacement z of the quarter-chord axis be

and let $$\left.\begin{aligned} z &= \tfrac{1}{2}c\bar{z}\,e^{ipt} \\ \chi &= \chi_0\,e^{ipt} \end{aligned}\right\} \quad . \quad . \quad . \quad . \quad . \quad . \quad (41)$$

Then the tangential flow equation (35) can be written

$$W/V = i\omega' \bar{z} + \chi_0 \left[i\omega' \left(\tfrac{1}{2} - \cos\phi \right) + 1 \right] \quad . \quad . \quad . \quad (42)$$

or $$C_0 (1 + W'_{0s}) + C_1 \left(\tfrac{1}{2} + \cos\phi \right) + \ldots = i\omega' \bar{z} + \chi_0 \left\{ i\omega' \left(\tfrac{1}{2} - \cos\phi \right) + 1 \right\} \quad . \quad (43)$$

Substituting for W'_{0s} from (31), and equating the coefficients of the trigonometrical functions, gives

$$C_0 = (P + iQ) \left[i\omega' \bar{z} + \chi_0 (1 + i\omega') \right] \quad . \quad . \quad . \quad . \quad (44)$$

and $$C_1 = -i\omega'\chi_0 + 2J_1(\omega') \left[Y'P + QX' - i(PX' - QY') \right] \left[i\omega'\bar{z} + \chi_0 (1 + i\omega') \right] \quad (45)$$

where $$P = \frac{1 + X'J_0(\omega') + Y'J_1(\omega')}{\{1 + X'J_0 + Y'J_1\}^2 + \{Y'J_0 - X'J_1\}^2} \quad . \quad . \quad . \quad . \quad . \quad . \quad (46)$$

and $$Q = \frac{-\{Y'J_0(\omega') - X'J_1(\omega')\}}{\{1 + X'J_0 + Y'J_1\}^2 + \{Y'J_0 - X'J_1\}^2} \quad . \quad . \quad . \quad . \quad . \quad . \quad (47)$$

C_2, C_3, and so on, are zero to this approximation.

Now, for a *wing* of infinite span,

$$P = 1{\cdot}0, \qquad Q = 0,$$

and, if the wing is performing translational oscillations alone, *i.e.* $\chi_0 = 0$,

$$\left.\begin{aligned} C_0 &= i\omega' \bar{z} \\ \text{and} \quad C_1 &= 0. \end{aligned}\right\} \quad . \quad . \quad . \quad . \quad . \quad (48)$$

C_1 is only different from zero if the wing is pitching, but in the present case when $\chi_0 = 0$, $C_1 \neq 0$. Thus the wake produces an apparent *rotation* of the aerofoil. Similarly, an apparent *camber change* is produced if more terms are retained in the series expansions for $\cos(\omega' \cos\phi_1)$, $\sin(\omega' \cos\phi_1)$, since then C_2, C_3, and so on, are not zero.

Now from (36), (37) and (38)

$$C_L = 2\pi \left\{ C_0 \left[C(i\omega') + \frac{i\omega'}{2} \right] + \frac{i\omega'}{4} C_1 \right\} \quad . \quad . \quad . \quad (49)$$

and $$C_M = -\frac{i\omega'\pi}{4} C_0 + \frac{C_1\pi}{4} \left[1 - \frac{i\omega'}{4} \right] . \quad . \quad . \quad . \quad . \quad (50)$$

Then, on substituting for C_0 and C_1 from (44) and (45), the following expressions are obtained for the derivative coefficients.

$$l_{12}=FP-QG-\frac{Q\omega'}{2}-\omega'QF-PG\omega'+\frac{J_1(\omega')}{2}\omega'(PX'-QY')$$

$$l_{22}=\tfrac{1}{2}\left[FP-QG-\frac{Q\omega'}{2}+P\left\{\frac{G}{\omega'}+\frac{1}{2}\right\}+\frac{QF}{\omega'}+\frac{J_1(\omega')}{2}(PY'+QX')+\right.$$
$$\left.+\frac{\omega'J_1(\omega')}{2}(PX'-QY')\right]$$

$$l_{32}=\tfrac{1}{4}\left[\frac{P}{2}-\frac{1}{4}+\frac{J_1(\omega')}{2}(Y'P+QX')\right]$$

$$l_{11}=-2\omega'(QF+PG)$$

$$l_{21}=FP-Q\omega'\left(\frac{G}{\omega'}+\frac{1}{2}\right)+\frac{\omega'J_1(\omega')}{2}(PX'-QY')$$

$$l_{31}=\tfrac{1}{2}\left[\frac{P}{2}+J_1(\omega')\frac{QX'+PY'}{2}\right]$$

$$m_{12}=\omega'Q+2J_1(\omega')\{Y'P+QX'\}+\frac{3}{2}\omega'J_1(\omega')(PX'-QY')$$

$$m_{22}=-\tfrac{1}{2}\left\{1+P-\omega'Q-\frac{3}{2}J_1(\omega')(Y'P+QX')+2J_1(\omega')\left(1+\frac{\omega'^2}{4}\right)\left(\frac{PX'-QY'}{\omega}\right)\right\}$$

$$m_{32}=\tfrac{1}{4}\left\{-P+\frac{1}{4}-\frac{J_1(\omega')}{2}(Y'P+QX')\right]$$

$$m_{11}=4J_1(\omega')\omega'(PX'-QY')$$

$$m_{21}=Q\omega'+2J_1(\omega')\left[Y'P+QX'-\frac{\omega'}{4}(PX'-QY')\right]$$

$$m_{31}=\tfrac{1}{2}\left[-P-\frac{J_1(\omega')}{2}(Y'P+QX')\right]$$

. . . . . (51)

and $C(i\omega')=F+iG$ . . . . . (52)

X', Y', P and Q are functions of incidence, reduced frequency and δ. No attempt has been made to provide comprehensive tables of these functions, but P and Q have been calculated assuming the values given in Table I.

TABLE I

ω'	h	δ
0·10	0·10	0
		0·0833
0·20	1·0	0·250
		0·50
	2·0	0·75
		0·9167

4.3. Discussion of the Results

In Table I, ω' was estimated on the assumption that the blade was moving in a straight line with the velocity of an element at about 0·75 tip radius. The three values of h correspond to zero, small and moderate incidences, also at 0·75 tip radius. No attempt has been made to deal with very large incidences. The variation of the most important derivative coefficients l_{12}, l_{21}, l_{22} with δ are shown in Figs. 4, 5. For the range of parameters of Table I, l_{11}, m_{11} are very small and will be ignored.

It will be seen that l_{21} decreases rapidly as $\delta \longrightarrow 0$ or 1·0, but that it never becomes negative. When $h=0{\cdot}10$, $\omega'=0{\cdot}10$, $\delta=0$ or 1·0, l_{21} is only about 4 per cent of the value predicted by quasi-steady theory, but when $h=1{\cdot}0$, it is about 28 per cent of the quasi-steady value.

Thus, even at a moderate incidence the amplitude of a forced oscillation at resonance will be about four times that predicted by quasi-steady theory.

When $\delta \simeq 0{\cdot}5$, l_{21} has about the same value as in quasi-steady theory, the variations with incidence and reduced frequency being quite small. In fact, only when δ is very small or very close to 1·0 does the influence of ω' and h become important.

As the incidence tends to zero, P and $Q \longrightarrow 0$ if $\delta=0$ or 1·0, but l_{21} does not vanish completely; when $\omega'=0{\cdot}10$, $l_{21}=0{\cdot}0025$ approximately, *i.e.* the damping at zero incidence is almost entirely due to structural hysteresis. On this basis, it would be expected that the amplitude would be largest at zero incidence, but insufficient is known about the variation of the exciting force with incidence, and it is unlikely that the present analysis is sufficiently exact at small blade angles. No account has been taken of the fact that the vortices must come into contact with the blades—possibly exciting an oscillation—and, if the amplitude of vibration was of the same order of magnitude as the downward displacement of the wake, non-linear effects would be important. Apart from minor numerical differences, the variation of l_{12} with δ, ω' and h is identical with that of l_{21} and needs no further comment.

The behaviour of the pitching derivative coefficients m_{21} and l_{22} is surprising; m_{21} remains virtually constant at 1·0 for all values of δ, ω' and h, thus extending one of the results of oscillatory aerofoil theory to rotor blades. But l_{22} is very much a function of δ, since it changes sign between $\delta=0{\cdot}50$ and $\delta=1{\cdot}0$ and, moreover, the peak positive and negative values, although not quite equal, are very large (about $\pm 2{\cdot}0$). The peak values decrease with increase of h, and/or of ω', but the sign change is independent of either of these parameters. It is interesting to note that whereas l_{22} and m_{21} are both determined largely by the equivalent rotation produced by the wake (*see* Section 4.2) l_{12} and l_{21} are only very slightly influenced by it.

Thus it has been established that the wake does have a great influence on the damping of flexural vibrations, especially at small angles of incidence, but further confirmation of the theory is necessary, since it is not yet possible to give a complete explanation of Meyer's results and no account has been taken of the shift and

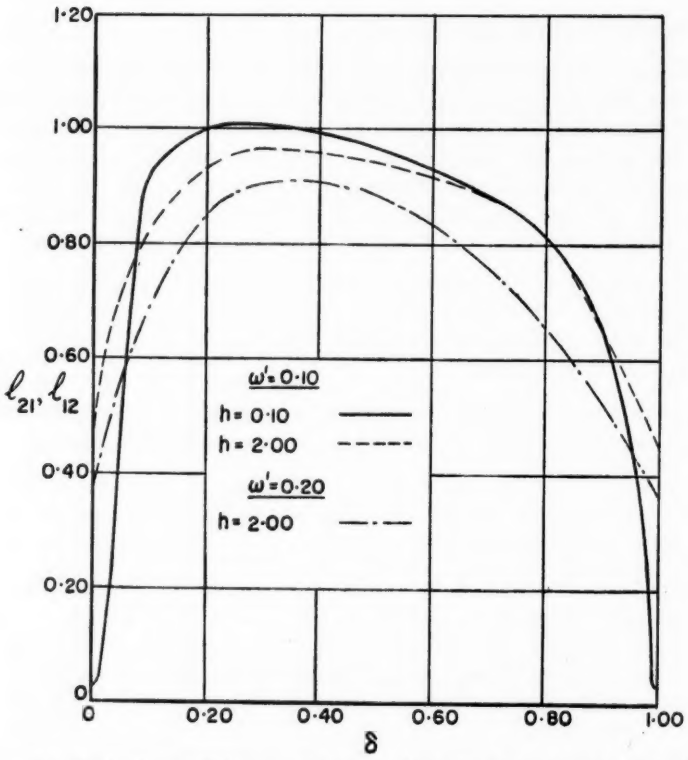

FIGURE 4. Derivative coefficients—wake theory. Variation of l_{12}, l_{21} with δ, ω' and h.

diffusion of vorticity. Fortunately the vibrations found by Meyer and by the C.A.L. were fundamentally different, since the former were forced but the latter were self-excited oscillations.

Hence it should be possible to provide independent confirmation—or otherwise—of the present theory, by calculating the flutter speeds of a typical rotor blade and comparing the results with experiment. This is the subject of the rest of this paper.

The numerical values of the critical speeds cannot be expected to be accurate, since the derivatives are not accurately known, but if the variations shown in Figs. 4 and 5 are substantially correct, then the most important experimental features should be predicted.

5. The Flutter of Rotor Blades

5.1. Derivation of the Flutter Equations

The analysis is confined to the binary flutter of a constant chord, symmetrical untwisted blade, the degrees of freedom being rigid blade flapping β about a hinge on the axis of rotation, with centrifugal force providing the restoring moment, and

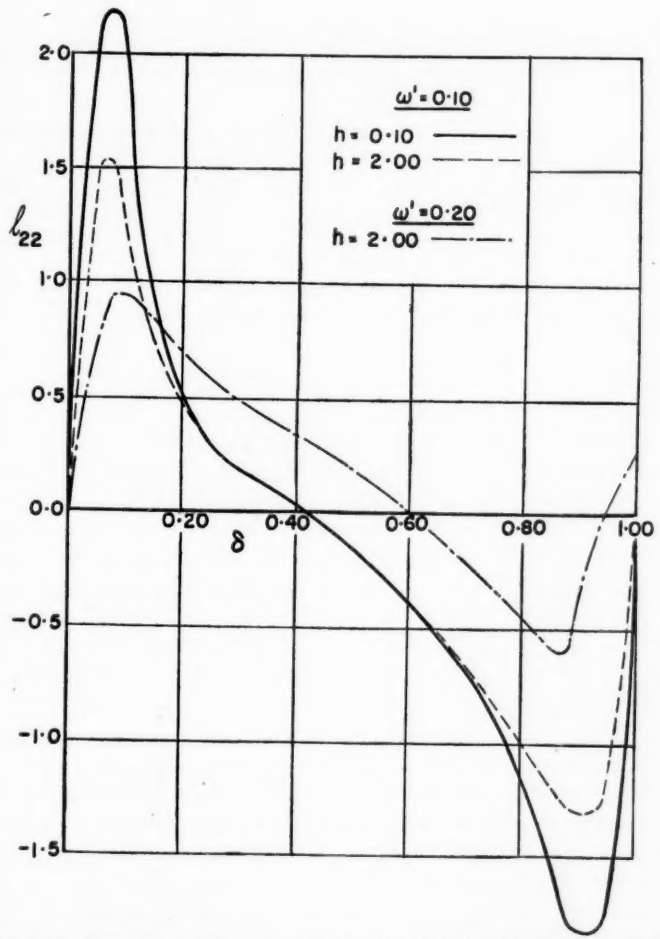

FIGURE 5. Derivative coefficients—wake theory. Variation of l_{22}, with δ, ω' and h.

rigid blade pitching χ about a spanwise axis, coincident with the quarter-chord line (*see* Fig. 6). The elastic stiffness in pitch is supplied partly by the centrifugal force, but mainly by a spring at the blade root. This simple model has been chosen for two reasons:—

(*i*) The experiments of Daughaday and Kline[4, 6] were carried out on a rotor of this type.

(*ii*) It is a close representation of an actual rotor blade, and if more freedoms (*e.g.*, bending and twisting) are taken into account, then the equations of motion are very difficult to obtain, and each of the flutter coefficients contains a number of small terms, which are functions of the pitch and coning angles, and so on.

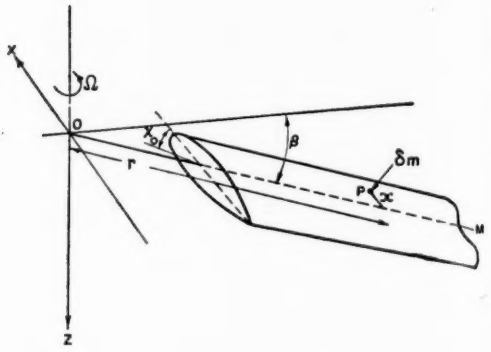

FIGURE 6. Blade configuration.

The original purpose of the C.A.L. flutter tests was to investigate the influence of an elastic coupling between flapping and pitch on the critical speeds. This was achieved by attaching a second spring to the blade, ahead of the quarter-chord axis, and some distance out along the span, *i.e.* the stiffness in flapping was partly supplied by a spring. If this coupling is included in the analysis, two more variables are introduced—the ratio of the distances of the points of attachment from the flapping hinge and the quarter-chord axis, and the spring stiffness—and the calculations become very laborious. Hence it was decided not to take this coupling into account, but to confine attention to the variation of critical speeds with inertia coupling. Sufficient tests were done under these conditions to provide a comparison between theory and experiment.

Since the derivation of the flutter equations is standard practice, the details are omitted, but some comment on the assumptions is necessary. It is assumed that the only significant aerodynamic forces are the lift and the pitching moment about the quarter-chord axis. At large angles of incidence this is not quite correct, since then the drag forces have an appreciable moment about the flapping hinge but, since neither the lift nor the moment are known to any great accuracy, the drag may be safely neglected. The aerodynamic inertias and direct aerodynamic stiffnesses are all assumed to be negligible, so that the only aerodynamic pitching moment is produced by the damping. Since the blades are of high aspect ratio, the pitching inertia coupling in the flapping equation is very small and can be neglected.

Then, putting $\psi=\Omega t$, the flutter equations reduce to

$$\ddot{\beta}+n\dot{\beta}+\beta+(4nl_{22}/3r')\dot{\chi}+nl_{12}\chi=0 \quad . \quad . \quad . \quad (53)$$

$$(r'\sigma/2k^2)(\ddot{\beta}+\beta)+\ddot{\chi}+(n/12k^2)\dot{\chi}+\omega_T{}^2\chi=0 \quad . \quad . \quad . \quad (54)$$

$$\text{where} \qquad \omega_T{}^2=K_T/(\Omega^2 I_1)+1{\cdot}0 \quad . \quad . \quad . \quad . \quad . \quad (55)$$

$$n=2\pi\rho cR^4/(8I_F), \quad . \quad . \quad . \quad . \quad . \quad (56)$$

and the dots denote differentiation with respect to ψ.

The parameter n, which in simple flapping motion is the ratio of the aerodynamic forces to the inertia forces, is known as the inertia number.

5.2. Solution of the Flutter Equations

$$\left.\begin{aligned} \text{Putting} \quad \chi &= \chi_0 \, e^{i\nu\psi} \\ \beta &= \beta_0 \, e^{i\nu\psi} \end{aligned}\right\} \quad . \quad . \quad . \quad . \quad . \quad . \quad . \quad (57)$$

then, for a given σ, the unknowns in the characteristic equations of (53) and (54) are ω_T^2 and ν. In calculations, however, it is convenient to assume ν and to solve for ω_T^2 and σ.

Then the characteristic equation reduces to

$$\omega_T^2 = (2\sigma l_{22} - m_{22}/4)(1-\nu^2)/(3k^2 l_{21}) \quad . \quad . \quad . \quad . \quad . \quad . \quad (58)$$

$$\sigma = m_{22}\{(1-\nu^2)^2 + n^2\nu^2 l_{21}^2\} / \{8(1-\nu^2) l_{22} - 6r' n l_{12} l_{21}\} . \quad . \quad . \quad (59)$$

For the usual range of values of the parameters it is found that $1{\cdot}0 < \nu < 2{\cdot}5$.

It will be recalled from Section 2.2 that in the C.A.L. experiments it was found that either an elastic or an inertia coupling was necessary to maintain flutter. In this case, the possibility of there being an elastic coupling has been ignored, but it can be seen immediately that if $\sigma = 0$ no flutter is possible. On full-scale rotor blades σ is usually made as small as is practicable, *i.e.* the inertia axis is designed to lie on the quarter-chord line, but it is of interest to know what is the tolerance on σ in a particular case. Therefore the critical values of ω_T^2 will be calculated for a range of values of σ.

5.3. Quasi-steady Theory

To estimate the influence of the wake, it will first be assumed that the derivatives are independent of ω', δ and h (quasi-steady theory). This is justifiable only when ω' is small, but in the present case it is not likely to exceed 0·10 and the derivatives can be obtained from two-dimensional theory by writing

$$C(i\omega') = 1{\cdot}0,$$

where $C(i\omega')$ is Theodorsen's Function.

Hence it is assumed that

$$m_{22} = l_{12} = l_{21} = 1{\cdot}0 \quad \text{and} \quad l_{22} = 0{\cdot}75.$$

The flutter boundaries for the two cases, (*a*) $n = 1{\cdot}414$, $r' = 10{\cdot}0$, (*b*) $n = 0{\cdot}50$, $r' = 10{\cdot}0$, have been calculated, assuming $k^2 = 0{\cdot}025 + \sigma^2$, and are shown, (marked "quasi-steady") in Figs. 7, 8, 9 and 10.

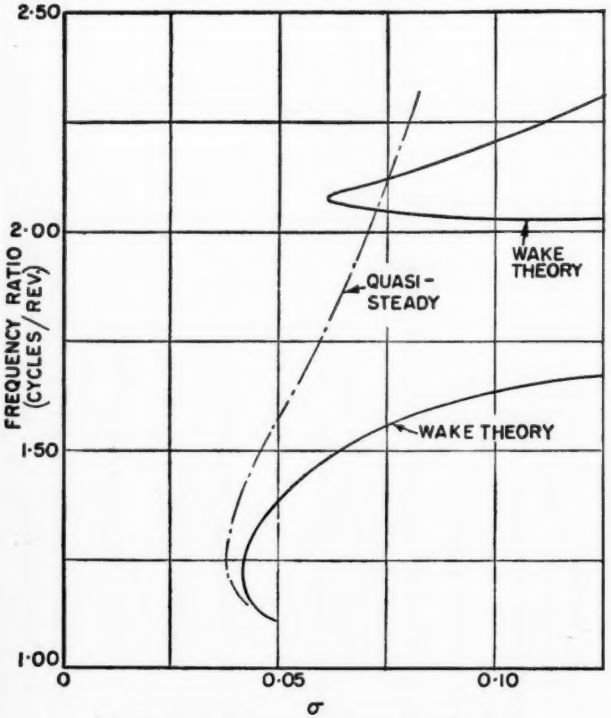

FIGURE 7. Variation of the frequency ratio with σ. Influence of the wake. $n=0{\cdot}50$, $r'=10{\cdot}0$.

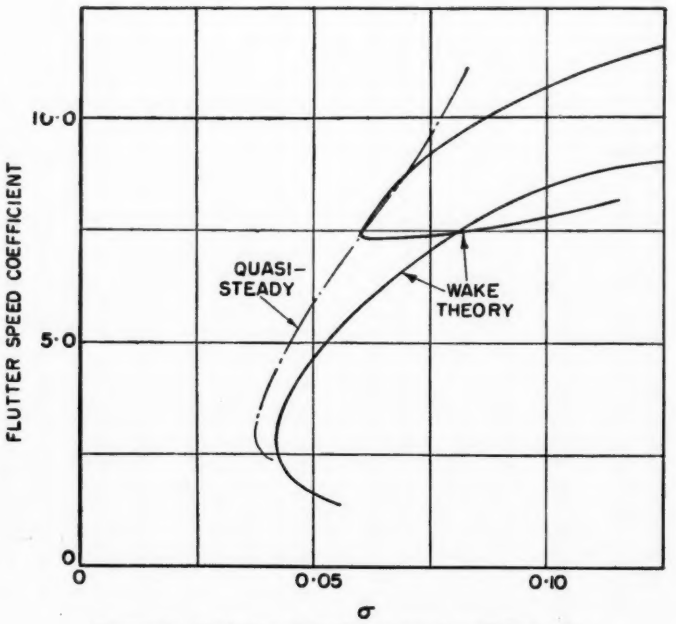

FIGURE 8. Variation of the flutter speed coefficient with σ. Influence of the wake. $n=0{\cdot}50$, $r'=10{\cdot}0$, $k_0{}^2=0{\cdot}025$.

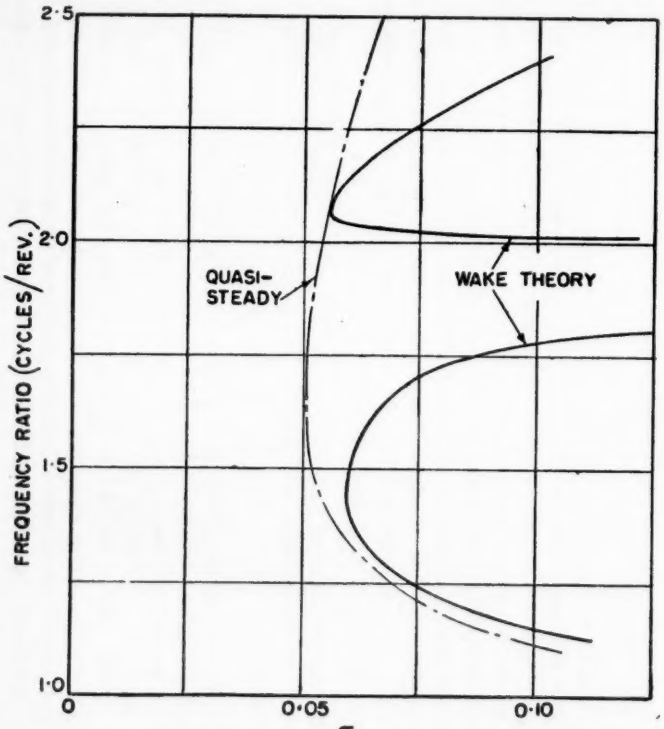

FIGURE 9. Variation of the frequency ratio with σ.
Influence of the wake. $n=1{\cdot}414$, $r'=10{\cdot}0$.

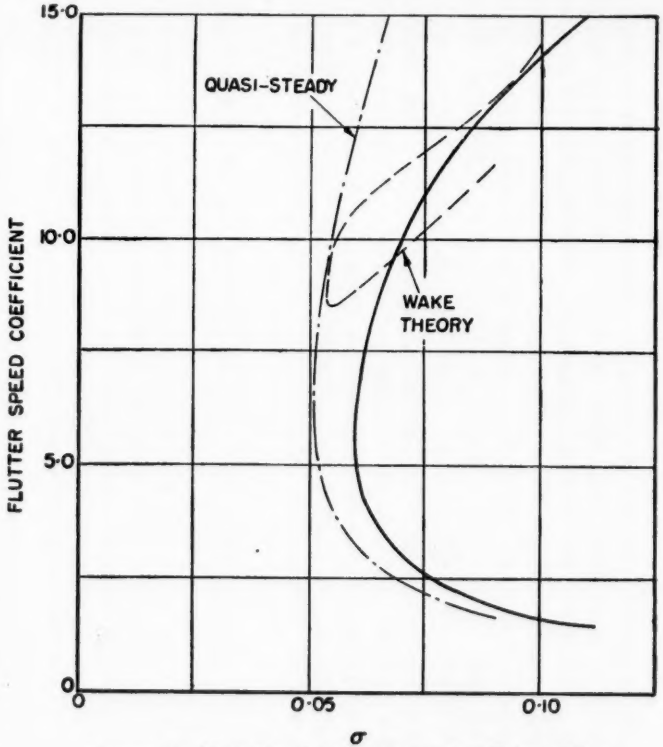

FIGURE 10. Variation of the flutter speed coefficient with σ.
Influence of the wake. $n=1{\cdot}414$, $r'=10{\cdot}0$, $k_0^2=0{\cdot}025$.

It will be seen from equation (55) that ω_T^2 is directly proportional to the spring stiffness and inversely proportional to Ω^2. In fact, it is the ratio (natural pitching frequency/rotational speed)^2, and when presenting results it is convenient to use ω_T^2 since then neither k_T, I_T nor Ω need be specified. ω_T^2 will be referred to as the flutter speed coefficient, an increase in ω_T^2 corresponding to a decrease in the critical rotational speed. The constant part (1·0) arises from the centrifugal pitching moment, which is proportional to Ω^2.

These boundaries were determined by assuming values for ν, and calculating ω_T^2 and σ by direct substitution in equations (58) and (59). (In the case of "wake" derivatives, this procedure is essential, since then l_{12}, and so on, are functions of ν). The first value of n is typical of full-scale blades. The second is more typical of models, and the chosen values of r' and k^2 are midway between model and full-scale.

It will be seen that there is a range of values of σ in which flutter is not possible, whatever the rotational speed, but the width of this range decreases with n. For any given value of σ there are two possible critical speeds, the lower one corresponding to the case in which pitching is the predominant mode. At the higher critical speed, the motion is predominantly flapping, and the frequency ratio lies close to that of pure flapping ($\nu \simeq 1{\cdot}10$). The higher critical frequency shows no tendency to remain constant, but increases rapidly with ν from about $\nu = 1{\cdot}40$, when flutter first begins.

5.4. Wake Theory

The influence of the wake can be estimated if the derivatives are calculated by the method of Section 4.2, but the theory is at best qualitative and, as the main purpose at present is to establish the characteristics of rotor blade flutter, l_{12}, l_{21}, and so on, need not be known to any great degree of accuracy. Furthermore, it has been assumed that the derivative coefficients are constants for the whole blade; hence a detailed calculation of the effects of ω' and h is not necessary, provided that the influence of δ is correctly reproduced. Therefore it will be assumed that both h and ω' are constants, and it will be seen from Figs. 4 and 5 that the derivative coefficients have reasonable mean values when $\omega' = 0{\cdot}10$, $h = 2{\cdot}0$.

The flutter boundaries for $n = 0{\cdot}50$, $n = \sqrt{2}$, $r' = 10{\cdot}0$ are shown in Figs. 7, 8, 9 and 10; the boundaries predicted by quasi-steady theory are included for comparison.

The most revealing diagrams are those showing the variation of ν with σ (Figs. 7 and 9). Quasi-steady theory predicts a continuous variation, but the "wake-theory" shows that there is a range of ν in which flutter does not occur. Flutter cannot occur for $n = 0{\cdot}50$ in the range $1{\cdot}6 < \nu < 2{\cdot}0$, and for $n = 1{\cdot}414$ when $1{\cdot}8 < \nu < 2{\cdot}0$. Flutter may be possible in these frequency ranges if σ is negative, but calculation shows that the centre of gravity must be well ahead of the quarter-chord line in the present case. Thus, the most important experimental result that two different flutter modes are possible at the same c.g. offset is amply confirmed.

For convenience, flutter when $\nu > 2{\cdot}0$ will be referred to as the high frequency or h.f. mode and flutter when $1{\cdot}0 < \nu < 1{\cdot}8$ will be referred to as the low frequency or l.f. mode. The minimum value of σ necessary to cause flutter will be denoted by σ_m.

It will be seen that σ_m is different for the two modes, the difference depending on n. (All four values are different from those predicted by quasi-steady theory, but the difference between the quasi-steady and l.f. results is quite small. This is because $l_{21} \simeq 1{\cdot}0$, and l_{22} does not have much influence on the results at these frequency ratios, *see* equation (58). When $n=0{\cdot}50$, σ_m (h.f.) is about 0·06, and σ_m (l.f.) is about 0·04, but when $n=1{\cdot}414$ the two values of σ_m are almost equal. Thus, if the range of c.g. travel in an experiment is limited, the high frequency mode may not be excited if n is small, but it may be found at larger values of n. This point is confirmed by the C.A.L. experimental results. On the rigid (*i.e.* stiff against bending) blade which had a very small value of n, the high frequency mode was not excited over the available c.g. range, but on the flexible blades this mode was produced even at 4° incidence. These blades had a value of $n \simeq 0{\cdot}75$, against 0·25 for the rigid blade. Thus, differences in the flutter characteristics of the two sets of blades cannot, as was assumed by the authors[4, 6], be attributed directly to flexibility. There can, however, be no doubt that flexibility is important at frequency ratios greater than 2·0, because this is close to a natural bending frequency.

The variation of the critical speeds with σ is quite complex, since for a given σ there may be anything up to four speeds. For $n=0{\cdot}50$, the critical speed boundaries of the two modes intersect at a certain value of σ, so that, when σ exceeds this, two critical speeds, the lower of the two for the h.f. mode and the higher for the l.f. mode speeds, will be obtained. If flutter is excited at this value of σ, three critical speeds will be obtained, one of which contains both modes, and therefore frequencies, together. For σ less than this, there may be four, three, two, one or no critical speeds. When $n=1{\cdot}414$, the range of σ in which four speeds are possible is much smaller, and beyond the intersection of the two boundaries there is not much difference between the lower critical speeds of the two modes. Also the range of *speeds* in which the high frequency mode can occur is reduced.

6. Concluding Remarks

6.1. General

There is sufficient agreement between the foregoing results and experiment, and between the calculations on damping and Meyer's experiments, for it to be claimed that the wake is primarily responsible for the observed phenomena, but the analysis is necessarily limited and there are still many points to be explained. It is probably beyond the scope of any reasonable theory to take into account all the various factors (incidence, Reynolds number, diffusion of vorticity, number of blades, and so on); only controlled experiment can do that.

The predicted variations of m_{22} (constant), l_{22} (sign change) and l_{21} could easily be detected in straightforward experiments, but the tests would have to be done in a

compressed air tunnel, to keep the Reynolds number constant, and it would be necessary to provide for an independent variation of stiffness to keep ω' constant.

Implicit in the theory of Section 3.2 is the assumption that the conditions which exist when $N \leqslant \nu \leqslant N+1$, are the same for all values of N, but it will be remembered that, whereas Meyer found vibrations for values of ν as large as 8·0, Daughaday and Kline obtained "wake flutter" only for $\nu = 2{\cdot}0$ approximately. How much of this was due to the different recording techniques is not known, but the foregoing assumption is not completely justified. The larger values of ν are obtained only at low rotational speeds, when the total energy available is small, the Reynolds number is small, and the "critical" speeds are very close together. Thus it may be difficult to excite the oscillations at large ν unless there is a strong exciting force.

6.2. Airscrew Flutter

The emphasis in the preceding sections has been on the rotor blade, but there is no reason why the wake should not influence the flutter and vibration of airscrews to some extent. The theory of Section 3.1 would not be valid, since the aspect ratio of airscrews is not as high and, except on the spinning tower, the pitch of the helix is quite large. So far no cases of "wake" flutter on airscrews have been reported as such, but the following quotations from Lynam's[9] early paper describe a vibration so similar to those of Ref. 3 that it can only be concluded that flutter of this type is possible.

> "A certain airscrew . . . . flutters in a rather unusual manner."
>
> "It has definite critical speeds at which flutter occurs and between which speeds the flutter is not so noticeable, suggesting that in this case the fundamental is below the running speed."
>
> "A special airscrew, having no pitch and symmetrical sections of the same thickness, at the same proportions of the chord, and also having the same variation of chord with radius, was constructed and spun."
>
> "Although, owing to the pitch being zero, and the sections symmetrical, the lift force was eliminated and there was no thrust, the blades fluttered at practically the same speeds as the airscrew."

Lynam states that the method of eliminating the flutter was to increase the thickness of the sections over the outer third of the blade. This had the effect of greatly increasing the natural bending (as well as torsional) frequencies, especially in rotation, and thus removed the critical speeds outside the working range.

6.3. The Rotor in Forward Flight

Finally, it is necessary to consider the influence of the wake on the blade motion of a helicopter in forward flight. Once again the theory of Section 3.1 is inapplicable, because the wake now moves rearwards as well as downwards, and the relative velocity is periodic, but it seems likely that the wake still has some influence.

The experiments showed that the vibratory stresses have a peak amplitude at low forward speeds, *i.e.* in the "transition" region, when the induced flow is not uniform around the disc. Thus an oscillation will be forced at low μ, but it is unlikely that the effects of the wake will vanish abruptly as the forward speed increases from zero. The conditions for minimum damping will no longer be realised exactly, but there will be some decrease in l_{21} at integral values of ν, and this, together with the increased forcing function, will cause an increase in the blade stresses. As the forward speed increases, the forcing function will at first decrease —after leaving the "transition" region—but will later increase rapidly. Presumably the aerodynamic damping will increase with forward speed, but the remaining blades and their wakes may play an important part in determining the aerodynamic forces, and it is not possible to draw any further conclusions without additional theoretical and/or experimental evidence.

All previous published attempts at the calculation of the forces on a blade in forward flight have assumed that the blades were in steady motion. It is now apparent that this assumption must be dropped, if reliable estimates of the stresses are to be obtained, but the labour involved would be enormous and the most satisfactory method would be to measure the derivative coefficients in a wind tunnel.

ACKNOWLEDGMENTS

The author wishes to extend his sincere thanks to Dr. W. P. Jones of the National Physical Laboratory, and to Mr. I. T. Minhinnick of the Royal Aircraft Establishment, for their kind interest and assistance.

Appendix

EVALUATION OF THE INTEGRAL $\int_{-\infty}^{+\infty} \eta e^{-i\omega'\eta} d\eta/(\eta^2+n^2h^2)$.

Integrating by parts gives

$$\left[-e^{-i\omega'\eta}\eta/\{i\omega'(\eta^2+n^2h^2)\}\right]_{-\infty}^{+\infty} + \int_{-\infty}^{+\infty} e^{-i\omega'\eta} \frac{d}{d\eta}\left[\eta/(\eta^2+n^2h^2)\right] d\eta/i\omega'$$

$$= 0 + \int_{-\infty}^{+\infty} e^{-i\omega'\eta}(\eta^2+n^2h^2-2\eta^2)\, d\eta/\{i\omega'(\eta^2+n^2h^2)^2\}$$

$$= -\int_{-\infty}^{+\infty} e^{-i\omega'\eta} d\eta/(\eta^2+n^2h^2) + 2h^2n^2 \int_{-\infty}^{+\infty} e^{-i\omega'\eta} d\eta/(\eta^2+n^2h^2)^2.$$

These integrals are standard forms and may be obtained from tables of definite integrals.

$$\int_{-\infty}^{+\infty} e^{-i\omega'\eta} d\eta/(\eta^2+n^2h^2)=\pi e^{-\omega'nh}/nh$$

$$\int_{-\infty}^{+\infty} e^{-i\omega'\eta} d\eta/(\eta^2+n^2h^2)^2=2\pi e^{-\omega'nh}\{2+2\omega'nh\}/(2nh)^3$$

Hence $$\int_{-\infty}^{+\infty} \eta e^{-i\omega'\eta} d\eta/(\eta^2+n^2h^2)=-i\pi e^{-\omega'nh}.$$

REFERENCES

1. SIMPKINSON, SCOTT H., EATHERTON, LAUREL J. and MILLENSON, MORTON B. The Influence of Centrifugal Force on the Elastic Curve of a Rotating Beam. N.A.C.A. Report 914, 1948.
2. HIRSCH, ALFRED M. The Contribution of Higher Mode Resonance to Rotor Blade Bending. *Journal of the Aeronautical Sciences*, June 1953.
3. MEYER, JOHN R. Jnr. An Investigation of Bending Moment Distribution on a Model Helicopter Blade. N.A.C.A. T.N. 2626, February 1952.
4. DAUGHADAY, H. and KLINE, J. Cornell Aeronautical Laboratory Report C.A.L.-52, November 1953.
5. MANGLER, K. and SQUIRE, H. B. The Induced Flow of a Lifting Rotor. R. & M. 2642, May 1950.
6. DAUGHADAY, H. and KLINE, J. An Investigation of the Effect of Virtual Delta-Three Angle and Blade Flexibility on Rotor Blade Flutter. Cornell Aeronautical Laboratory Report, SB-862-S-2, August 1954.
7. PRANDTL, L. Appendix to a paper by Betz in *Vier Abhandlungen zur Hydrodynamik und Aerodynamik*, Göttingen, 1927. (*See* R. & M. 1483 by Lock and Yeatman, February 1932.)
8. JONES, W. P. Aerodynamic Forces on Wings in Non-Uniform Motion. R. & M. 2117, August 1945.
9. LYNAM, E. Notes on the Flutter of Airscrew Blades. R. & M. 1258, April 1929.

The Lift on a Thin Aerofoil with a Jet-Augmented Flap

D. A. SPENCE

(Royal Aircraft Establishment)

SUMMARY: The method which was developed in an earlier paper[1] for calculating the lift on a thin jet-flapped aerofoil has been applied to the case in which the jet enters the main stream tangentially from a deflected flap. The lift derivative with respect to the (small) angle of deflection β is of the form

$$\partial C_L/\partial\beta = 2(\chi + \sin\chi + 2\pi D_0),$$

where $\chi = 2\sin^{-1}\sqrt{E}$, E being the ratio of flap length to aerofoil chord, and D_0 a function both of E and of the jet momentum coefficient C_J. In the special case $C_J = 0$, D_0 vanishes and the classical results for attached flow on flapped aerofoils without super-circulation are obtained. More generally, D_0 has been evaluated over the range $0 < C_J < 5$ for six ratios E between 0·02 and 0·50, using an electronic computer. The lift derivatives so found lie between those in the limiting cases of "deflection" ($E = 0$) and "incidence" ($E = 1$) which were calculated in Reference 1. They show that the effectiveness of the jet-flap scheme might be greatly increased by blowing over flaps of the order of 20 or 30 per cent of the chord, rather than over the small "shrouds" which have hitherto been proposed.

1. Introduction

Improvements in the lifting effectiveness of the jet-flap scheme could arise if the air were ejected over a trailing-edge flap of moderate size (flap blowing), instead of from the trailing-edge (pure jet flap), or over a small flap merely intended to turn the jet (shrouded jet flap). The author's treatment of pure jet flaps by thin aerofoil theory[1] is here extended to flap blowing, and comparative results are derived for various ratios of flap to aerofoil chord. The practical significance is discussed in Section 5 mainly in relation to jet-flap schemes, where the momentum ejected over the trailing-edge flap exceeds that required to prevent flow separation by a large amount; but brief reference is also made to more conventional boundary-layer control applications, where the excess momentum leaving the trailing edge is small.

In the earlier theoretical treatment[1], an inviscid flow solution was obtained for the case of a thin deflected jet of momentum flux coefficient C_J, emerging at a

Received August 1957

small angle β to the chord, from the trailing edge of a thin aerofoil whose surface slope is prescribed by

$$\frac{dy}{dx} = \varepsilon(x), \quad 0 < x < 1.$$

For the case of flap blowing, we now write

$$\varepsilon(x) = 0, \quad 0 < x < (1-E)$$

$$\varepsilon(x) = \beta, \quad (1-E) < x < 1$$

and allow the jet to emerge tangentially at the trailing edge.

For $C_J = 0$, the Glauert[2] theory for hinged flaps is reproduced, but the results are obtained in a more compact form, as a result of using the Carlemann[3] inversion formula for Cauchy integrals. As this treatment appears to have some intrinsic interest, and also provides a simple illustration of the general method, it is presented first in Section 2. The jet case is then presented in Section 3. Results have been computed on the Deuce electronic machine for a range of C_J values and a number of flap/chord ratios. These are summarised in Section 4 and discussed in Section 5.

Notation

The chord length is taken as unity throughout.

x, y co-ordinates of aerofoil and jet sheet in directions parallel and perpendicular to the undisturbed stream

ξ, η dummy variables over the same range as x

ρ_0, U_0 density and velocity of undisturbed stream

$w(x)$ downwash velocity on $y = 0$

$f(x)$ non-dimensional vorticity distribution on $0 \leqslant x \leqslant 1$ representing wing (*i.e.* velocities are $U_0\{1 \pm \frac{1}{2} f(x)\}$ on upper and lower surfaces)

C_J jet momentum coefficient, $= J/(\frac{1}{2}\rho_0 U_0^2)$ where J = flux of momentum

$\lambda = 4/C_J$

$g(x) = -(C_J/2)\, y'(x)$, non-dimensional vorticity distribution on $x > 1$ representing jet sheet

$\varepsilon(x)$ slope of aerofoil surface

α incidence of forward part of surface

β angular deflection of flap from forward part of surface

E ratio of lengths of flap and whole aerofoil

θ $\cos^{-1}(2x-1)$ for $0 \leqslant x \leqslant 1$

χ value of θ at hinge point, *i.e.* $\cos^{-1}(1-2E)$

$X = \{1-(1-x)^{\frac{1}{2}}\}/\{1+(1-x)^{\frac{1}{2}}\}$

$\phi = 2\cos^{-1}(x^{-\frac{1}{2}})$ for $x > 1$

$k(x)$ defined by equation (20)

$K(\phi) = [1/(2\beta)]\, g\,[1/\cos^2(\phi/2)]$

N number of pivotal points

$\phi_m = m\pi/N,\ m = 0, 1, \ldots (N-1)$

$D_0, \ldots D_{N-1}$ coefficients in Fourier series for $K'(\phi)/\sin(\phi/2)$

a_{mn}, b_{mn}, f_m coefficients in equation (26)

C_L lift coefficient

C_M nose-down pitching moment coefficient about leading edge

C_H moment coefficient of flap about hinge line

2. Attached Flow on a Thin Aerofoil with Hinged Flap (No Jet)

Consider an aerofoil on the real (x) axis from 0 to 1, with a hinge at the point $x = 1 - E$, where it is bent through a small angle β.

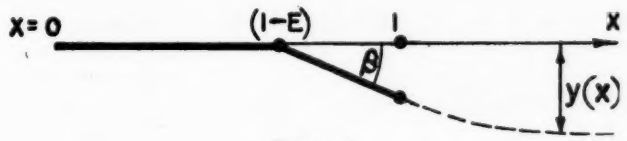

FIGURE 1.

Suppose the aerofoil is represented by a vortex distribution of strength $U_0 f(x)$ per unit length, where U_0 is the velocity at infinity.

The downwash on the axis is then given by

$$w(x) = -\frac{U_0}{2\pi}\int_0^1 \frac{f(\xi)\,d\xi}{\xi - x} \quad . \quad . \quad . \quad . \quad . \quad (1)$$

On the segment (0, 1) this is known to be

$$w(x) = 0, \qquad 0 < x < (1-E) \quad . \quad . \quad . \quad . \quad (2)$$

$$w(x) = U_0\beta, \quad (1-E) < x < 1. \quad . \quad . \quad . \quad . \quad (3)$$

Inverting equation (1) by means of Carlemann's identity[3]* gives

*The general solution of equation (1) would include a term $C/\{x^{\frac{1}{2}}(1-x)^{\frac{1}{2}}\}$ on the right-hand side of (4), C being an arbitrary constant. But, in accordance with the Joukowski hypothesis, we take $C = 0$.

$$U_0 f(x) = \frac{2}{\pi}\left(\frac{1-x}{x}\right)^{\frac{1}{2}} \int_0^1 \left(\frac{\xi}{1-\xi}\right)^{\frac{1}{2}} \frac{w(\xi)\, d\xi}{\xi - x}. \quad . \quad . \quad . \quad . \quad (4)$$

Substituting from (2) and (3)

$$\frac{f(x)}{2\beta} = \frac{1}{\pi}\left(\frac{1-x}{x}\right)^{\frac{1}{2}} \int_{1-E}^1 \left(\frac{\xi}{1-\xi}\right)^{\frac{1}{2}} \frac{d\xi}{\xi - x} \quad . \quad . \quad . \quad . \quad (5)$$

Writing $x = \frac{1}{2}(1+\cos\theta)$ . . . . . (6)

$$1 - E = \tfrac{1}{2}(1+\cos\chi), \quad . \quad . \quad . \quad . \quad (7)$$

the Cauchy integral may readily be evaluated, and the loading is given by

$$\frac{f(x)}{2\beta} = \frac{\chi}{\pi}\tan\frac{\theta}{2} + \frac{1}{\pi}\log\left|\frac{\sin(\theta+\chi)/2}{\sin(\theta-\chi)/2}\right|. \quad . \quad . \quad . \quad (8)$$

The total lift coefficient is given by

$$C_L = 2\int_0^1 f(x)\, dx. \quad . \quad . \quad . \quad . \quad . \quad (9)$$

It is found by integrating equation (8) that

$$C_L = 2\beta(\chi + \sin\chi). \quad . \quad . \quad . \quad . \quad . \quad (10)$$

(This equation may also be obtained directly by integrating equation (5). Note that with $\chi = \pi$, *i.e.* $E = 1$, it gives the usual incidence result.)

It may readily be verified that Glauert's formula for lift[2] is identical with (10), the necessary changes in notation having been made. In addition, it may be shown that the Fourier series for the loading given by Glauert has the sum given by equation (8). The various moment coefficients, on the aerofoil and flap, may also be obtained by integration of equation (8), giving the following results.

The lift coefficient on the flap (referred to the aerofoil chord) is

$$C_{L\ \text{flap}} = 2\beta\chi^2/\pi. \quad . \quad . \quad . \quad . \quad . \quad (11)$$

The nose-down pitching moment about the leading edge is

$$C_M = \beta(\tfrac{1}{2}\chi + \sin\chi + \tfrac{1}{4}\sin 2\chi). \quad . \quad . \quad . \quad . \quad (12)$$

The contribution to this pitching moment from the flap is

$$C_{M\ \text{flap}} = \frac{\beta}{2\pi}(\chi + \sin\chi)^2. \quad . \quad . \quad . \quad . \quad . \quad (13)$$

The hinge moment on the flap is

$$C_H = C_{M\ flap} - (1-E)\,C_{L\ flap}$$
$$= \frac{\beta}{2\pi}\left(\chi + \sin\chi\right)^2 - \frac{2\beta\chi^2}{\pi}\cos^2\frac{\chi}{2} \quad . \quad . \quad . \quad (14)$$

(Here the hinge moment is referred to the aerofoil chord; to make it non-dimensional in the usual way one would divide by E^2, $=\sin^4(\frac{1}{2}\chi)$.

Similarly, in linear theory the effect of incidence is directly additive; thus, with an incidence α the lift coefficient becomes

$$C_L = 2\pi\alpha + 2\,(\chi + \sin\chi)\,\beta. \quad . \quad . \quad . \quad . \quad . \quad (15)$$

3. Flap with Tangential Jet

3.1. Integral Equation for Slope of Jet

The case when a jet is blown tangentially over the flap from the hinge line may be treated precisely as if the jet emerged tangentially at the trailing edge, provided that an effectively attached flow is obtained. The effect of the jet on flow over the flap itself is merely to prevent separation, and the pressure distribution is not modified in any other way. (The pressure rise across the jet is proportional to its curvature, and thus is zero for the part in contact with the flap.)

The analysis of Ref. 1 is thus applicable to the system. In that paper the deflection of the jet below the axis is taken as $y(x)$, $(1 < x < \infty)$, and the local gradient of the aerofoil surface is $\varepsilon(x)$, $(0 < x < 1)$. The jet momentum-flux coefficient

$$C_J = J/(\tfrac{1}{2}\rho_0 U_0^2)\,. \quad . \quad . \quad . \quad . \quad . \quad (16)$$

is defined, where J is the momentum flux per second entering the jet, and ρ_0, U_0 refer to the undisturbed stream.

With the transformation

$$\left.\begin{aligned} \lambda &= 4/C_J \\ g(x) &= -\frac{2}{\lambda}\,y'(x) \end{aligned}\right\} \quad . \quad . \quad . \quad . \quad . \quad (17)$$

the following singular integral equation is obtained for the slope function $g(x)$ (equation (69) of Ref. 1) valid in $1 < x < \infty$:—

$$\frac{1}{\pi}\left(\frac{x-1}{x}\right)^{\frac{1}{2}}\int_1^1\left(\frac{\eta}{\eta-1}\right)^{\frac{1}{2}}\frac{g'(\eta)\,d\eta}{\eta-x} - \lambda g(x) = -\frac{2}{\pi}\left(\frac{x-1}{x}\right)^{\frac{1}{2}}\int_0^\infty\left(\frac{\eta}{1-\eta}\right)^{\frac{1}{2}}\frac{\varepsilon(\eta)\,d\eta}{\eta-x} \quad (18)$$

If $\varepsilon(x)$ is defined by the step function

$$\varepsilon(x)=\begin{cases}0, & 0<x<\cos^2\frac{\chi}{2}\\ \beta, & \cos^2\frac{\chi}{2}<x<1\end{cases}, \qquad . \quad . \quad . \quad . \quad (19)$$

the right hand side of (18) is found to have the value $2\beta k(x)$, say, where

$$k(x)=\frac{2}{\pi}\left\{\tan^{-1}\left[\left(\frac{x}{x-1}\right)^{\frac{1}{2}}\tan\frac{\chi}{2}\right]-\left(\frac{x-1}{x}\right)^{\frac{1}{2}}\frac{\chi}{2}\right\}, \quad . \quad . \quad . \quad (20)$$

so that equation (18) is

$$\frac{1}{\pi}\left(\frac{x-1}{x}\right)^{\frac{1}{2}}\int_1^\infty\left(\frac{\eta}{\eta-1}\right)^{\frac{1}{2}}\frac{g'(\eta)\,d\eta}{\eta-x}-\lambda g(x)=2\beta k(x), \quad . \quad . \quad (21)$$

where $k(x)$ is known and $g(x)$ unknown.

3.2. Solution of Equation (21)

This equation is of precisely the same form as that solved in Section 5 of Ref. 1; it may be transformed by writing

$$x=1/\cos^2\frac{\phi}{2} \qquad . \quad . \quad . \quad . \quad . \quad . \quad (22)$$

$$g(x)=2\beta K(\phi), \qquad . \quad . \quad . \quad . \quad . \quad . \quad (23)$$

$$\text{where} \qquad K'(\phi)=\sin\frac{\phi}{2}\sum_{n=0}^{\infty}D_n\cos n\phi. \qquad . \quad . \quad . \quad . \quad (24)$$

With this transformation, (21) becomes

$$D_0\cos^2\frac{\phi}{2}\sin\frac{\phi}{2}+\sum_{n=1}^{\infty}D_n\cos^3\frac{\phi}{2}\sin n\phi+\lambda K(\phi)=-k\,[1/\cos^2(\phi/2)]. \quad (25)$$

By satisfying this equation at N pivotal points

$$\phi=\phi_m=\frac{m\pi}{N}, \quad m=0,\ 1,\ 2\ldots\ (N-1),$$

N linear equations are obtained for $D_0 \ldots D_{N-1}$, of the form

$$\sum_{n=0}^{N-1} (a_{mn} + \lambda b_{mn})\, D_n = f_m, \quad m = 0,\ 1,\ \ldots\ (N-1), \quad . \quad . \quad . \quad (26)$$

where
$$\left.\begin{aligned} a_{m0} &= \sin\phi_m, \quad a_{mn} = (1+\cos\phi_m)\sin n\phi_m \quad \text{for} \quad n > 0 \\ b_{mn} &= \frac{4}{4n^2-1}\left(\cos n\phi_m + 2n\tan\frac{\phi_m}{2}\sin n\phi_m\right) \end{aligned}\right\} \quad . \quad . \quad (27)$$

as in Ref. 1, and

$$f_m = -2\sec\frac{\phi_m}{2}\, k\,[1/\cos^2(\phi_m/2)]$$

$$= \frac{2\chi}{\pi}\tan\frac{\phi_m}{2} - \frac{4}{\pi}\sec\frac{\phi_m}{2}\tan^{-1}\left(\tan\frac{\chi}{2}\Big/\sin\frac{\phi_m}{2}\right). \quad . \quad . \quad (28)$$

The set of equations (26) with $N=9$ has been solved for a number of values of C_J between 0·05 and 5 for flaps of flap/chord ratio E (*i.e.* $\sin^2(\frac{1}{2}\chi)$) equal to 0·02, 0·05, 0·10, 0·20, 0·30 and 0·50 on an electronic computer. The set of coefficients $\{D_n\}$ converges rapidly in each case; *e.g.* for $C_J=2$, $E=0{\cdot}3$, $D_0, D_1 \ldots D_8 = 0{\cdot}3513$, 0·3013, 0·0008, 0·0270, 0·0011, 0·0066, −0·0006, 0·0026, −0·0005.

3.3. Expressions for Lift Coefficient and Chordwise Loading

The chordwise distribution of vorticity is taken as $U_0 f(x)$, $(0 < x < 1)$, as in Section 2, and from equation (62) of Ref. 1 it is known that

$$f(x) = \frac{1}{\pi}\left(\frac{1-x}{x}\right)^{\frac{1}{2}} \left\{ \int_1^{\infty} \left(\frac{\eta}{\eta-1}\right)^{\frac{1}{2}} \frac{g'(\eta)\,d\eta}{\eta-x} + 2\int_0^1 \left(\frac{\eta}{1-\eta}\right)^{\frac{1}{2}} \frac{\varepsilon(\eta)\,d\eta}{\eta-x} \right\} \quad . \quad (29)$$

The lift coefficient is given by

$$C_L = 2\int_0^1 f(x)\,dx + \beta C_J, \quad . \quad . \quad . \quad . \quad . \quad . \quad (30)$$

the term βC_J representing the direct vertical momentum component of the jet. The contribution to the integral of the term involving the step-function $\varepsilon(\eta)$ is already known; as in Section 2, equation (10), it is $2\beta(\chi+\sin\chi)$. The contribution from the Fourier series is evaluated as in Section 6.1 of Ref. 1 and it is found that

$$\frac{2}{\pi}\int_0 dx\left(\frac{1-x}{x}\right)^{\frac{1}{2}} \int_1^{\infty}\left(\frac{\eta}{\eta-1}\right)^{\frac{1}{2}} \frac{g'(\eta)\,d\eta}{\eta-x} + \beta C_J = 4\pi\beta D_0. \quad . \quad . \quad (31)$$

TABLE I

COMPUTED VALUES OF $\partial C_L/\partial\beta$

	$E=0$	0·02	0·05	0·1	0·2	0·3	0·5	1·0
$C_J=0$	0	1·123	1·774	2·487	3·455	4·151	5·141	6·283
0·01	0·357	1·210	1·845	2·547	3·505	4·198		6·392
0·05	0·803	1·490	2·081	2·751	3·681	4·360		6·460
0·1	1·137	1·763	2·318	2·962	3·868	4·535		6·614
0·2	1·641	2·194	2·708	3·316	4·190	4·839		6·885
0·4	2·391	2·873	3·340	3·908	4·740	5·365		7·365
0·5	2·707	3·165	3·618	4·173	4·989	5·607		7·588
1	4·026	4·421	4·827	5·337	6·102	6·690	7·561	8·605
2	6·135	6·474	6·836	7·301	8·012	8·566		10·405
5	11·231	11·513	11·825	12·236	12·878	13·385	14·227	15·109

NOTE: The values for $E=0$ and $E=1$ are those of $\partial C_L/\partial\tau$ and $\partial C_L/\partial\alpha$ listed in Table 3 of Reference 1. Very close interpolations to them are provided by the formulae

$$\partial C_L/\partial\tau = 2(\pi C_J)^{\frac{1}{2}}\,[1+0{\cdot}151\,C_J^{\frac{1}{2}}+0{\cdot}139\,C_J]^{\frac{1}{2}}$$

$$\partial C_L/\partial\alpha = 2\pi[1+0{\cdot}151\,C_J^{\frac{1}{2}} \qquad +0{\cdot}219\,C_J$$

Thus the lift coefficient is given altogether by the simple formula

$$C_L = 2\,(\chi+\sin\chi+2\pi D_0)\,\beta, \qquad . \quad . \quad . \quad . \quad (32)$$

where $\chi=2\sin^{-1}\sqrt{E}$, E being the flap/chord ratio, and D_0 depends on E and C_J.

In the same way the chordwise loading is made up of a closed term coming from the solution for a Glauert type flap, equation (8), together with a series identical to that obtained in Section 6.2 of Ref. 1; in fact

$$\frac{f(x)}{2\beta} = \frac{\lambda}{\pi}\left(\frac{1-x}{x}\right)^{\frac{1}{2}} + \frac{1}{\pi}\log\left|\frac{\left(\frac{1-x}{x}\right)^{\frac{1}{2}}+\left(\frac{E}{1-E}\right)^{\frac{1}{2}}}{\left(\frac{1-x}{x}\right)^{\frac{1}{2}}-\left(\frac{E}{1-E}\right)^{\frac{1}{2}}}\right| + x^{-3/2}\left\{D_0\left(\frac{2X}{1-X}\right)+\sum_{n=1}^{\infty}D_nX^n\right\}$$

. . . . (33)

$$\text{where} \qquad X=\frac{1-(1-x)^{\frac{1}{2}}}{1+(1-x)^{\frac{1}{2}}} \qquad . \quad . \quad . \quad . \quad . \quad . \quad (34)$$

3.4. EFFECT OF OVERALL INCIDENCE

Since this is a linearised theory, the effect of an overall incidence α is directly additive; thus the expression (32) becomes

$$C_L = 2\pi\,(1+2B_0)\,\alpha+2\,(\chi+\sin\chi+2\pi D_0)\,\beta, \qquad . \quad . \quad . \quad (35)$$

where B_0 is the coefficient evaluated as a function of C_J in Ref. 1. It may be

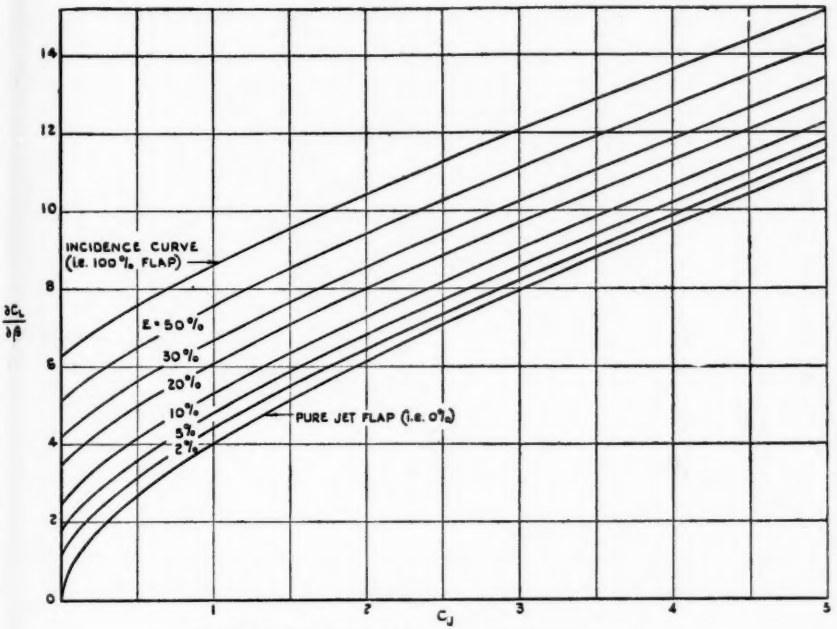

FIGURE 2. $\partial C_L/\partial\beta$ for thin wings with blown flaps.

verified that the same result is obtained by taking the step function $\varepsilon(x)$ as

$$\left.\begin{aligned} \varepsilon(x) &= \alpha, \qquad 0 < x < \cos^2\frac{\chi}{2} \\ &= \alpha+\beta, \quad \cos^2\frac{\chi}{2} < x < 1 \end{aligned}\right\} \quad . \quad . \quad . \quad . \quad (36)$$

Similarly the more general expression for chordwise loading is derived from (33) by adding $2\alpha\ \{(1-x)/x\}^{\frac{1}{2}}$ to $f(x)$ and replacing $2\beta D_n$ by $2(\alpha B_n + \beta D_n)$.

4. Results of Calculations

The computed curves of $\partial C_L/\partial\beta$ which, by (32), is given by

$$\frac{\partial C_L}{\partial\beta} = 2(\chi + \sin\chi) + 4\pi D_0 \quad . \quad . \quad . \quad . \quad (37)$$

for $E = 0{\cdot}02$, $0{\cdot}05$, $0{\cdot}10$, $0{\cdot}20$, $0{\cdot}30$ and $0{\cdot}50$ are plotted against C_J in Fig. 2, and their numerical values are given in Table I. The figure shows also the curves of $\partial C_L/\partial\alpha$ and $\partial C_L/\partial\tau$ obtained in Ref. 1. All the new curves lie between these two, and it is clear that $\partial C_L/\partial\tau$ may be regarded as the limit of $\partial C_L/\partial\beta$ as $E \longrightarrow 0$, and $\partial C_L/\partial\alpha$ as the limit when $E \longrightarrow 1$.

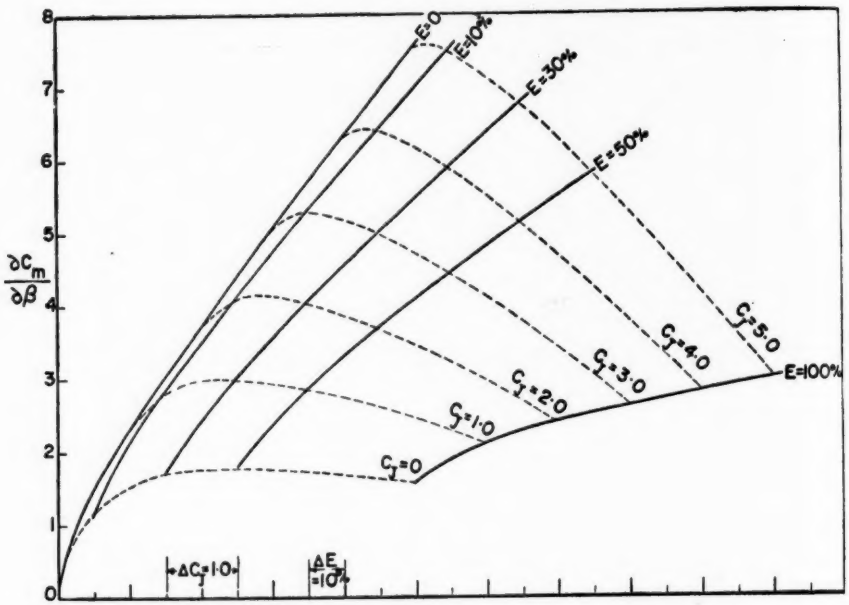

FIGURE 3. Nose-down pitching moment about leading edge on aerofoil with blown flap.

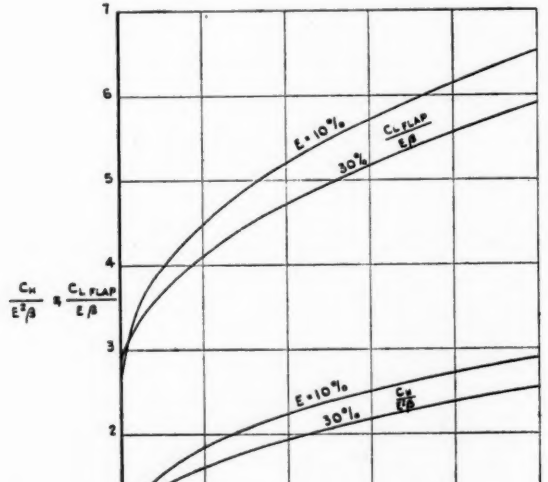

FIGURE 4. Lift and hinge moment coefficients on 10 per cent and 30 per cent blown flaps.

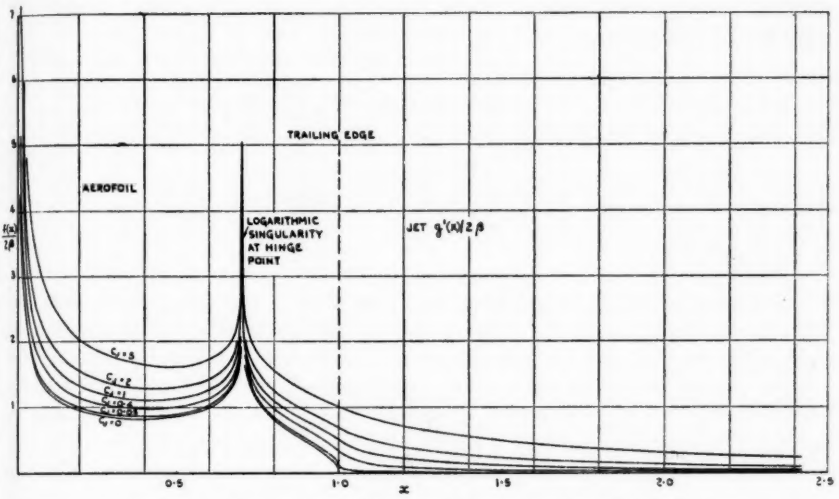

FIGURE 5. Blowing over a 30 per cent flap. Vorticity distribution.

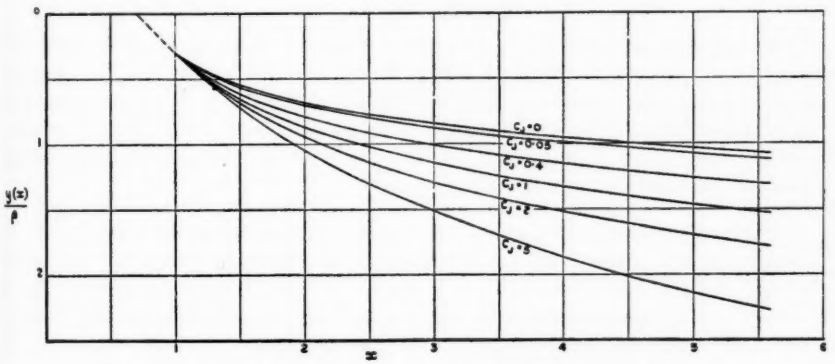

FIGURE 6. Blowing over a 30 per cent flap. Non-dimensional jet shape.

Figures 3 and 4 show the pitching moment and hinge moment curves for $E=0{\cdot}10$ and $E=0{\cdot}30$. These have been obtained by integrating the contribution of the Fourier series to the loading expression (33) numerically and using the results in Section 2 for the contributions not arising from the jet. (The sum of the series is non-singular, unlike the "Glauert" term, and the numerical integration is straightforward; for the pitching moment the integration can in any case be performed analytically, as in Ref. 1).

Figures 5 and 6 show the distribution of vorticity on the aerofoil and jet, and the jet shapes respectively, for a number of C_J values and $E=0{\cdot}30$. It is seen that the

vorticity distribution is singular at the hinge point. The singularity* comes only from the "Glauert" term

$$\frac{2\beta}{\pi}\log\left|\frac{\left(\frac{1-x}{x}\right)^{\frac{1}{2}}+\left(\frac{E}{1-E}\right)^{\frac{1}{2}}}{\left(\frac{1-x}{x}\right)^{\frac{1}{2}}-\left(\frac{E}{1-E}\right)^{\frac{1}{2}}}\right| \quad . \quad . \quad . \quad . \quad . \quad (38)$$

5. Discussion

Comment should be made about the applicability of the analysis of Ref. 1 to the present scheme. The C_J entering the analysis is the effective jet momentum flux at the trailing edge; this will obviously be rather less than the momentum emerging at the slot at the hinge point, since some momentum is transferred to the boundary layer to prevent it from separating in the adverse pressure gradient on the flap. This momentum loss is determined by the internal mechanics of the jet flow over the flap and is beyond the scope of the present treatment, which is confined to the external inviscid flow, the physical properties of the jet having entered the calculation solely by means of the value $\kappa U_0 C_J/2$ of the vortex strength on $1<x<\infty$ used in forming equation (18) (κ = curvature of sheet $\simeq d^2y/dx^2$).

The present assumptions are entirely consistent with those underlying the treatment of the pure jet flap problem in Ref. 1. Assuming an infinitely thin jet in an inviscid flow, it may be shown[4] that the variation of the momentum flux along the jet tends to zero, however the static pressure may vary. In this limiting case, therefore, there is no loss of jet momentum between the slot and the trailing edge, and the present results are strictly true.

In practice a certain "threshold" momentum must be necessary to establish the prescribed flow in either case, and this may well be greater in the case of the blown flap than for the pure jet flap itself. However, it would appear, in general, that it is the effective momentum flux at the trailing edge that determines the "super-circulation", and hence that the present results are relevant to a real flow provided that

(*i*) the prescribed "attached" flow is attained in the real flow, and

(*ii*) the relevant jet momentum flux in the real flow is taken to be that at the trailing edge.

If the "true" C_J's are defined at the slot, they must be greater than those shown in Fig. 1; how much greater would depend upon the development of the jet over the

*In fact on a plate bent through an angle β the singularity should be like that of

$$(x-x_1)^{-\beta/(\pi+\beta)}$$

at $x=x_1$, but the assumption of a step-wise discontinuity in downwash produces instead the logarithmic singularity of (38).

flap in any particular problem. For zero "true" C_J, the prescribed flow is simply not attained, because of flow separation, and the real values of $\partial C_L/\partial\beta$ would be substantially lower than the intercepts shown for $C_J=0$.

Thus certain unknown factors limit the conclusions that may be drawn from the results plotted in Fig. 1, but it appears there that, by the use of a blown flap, either

(*i*) with a given C_J and deflection, higher C_L's are obtained with larger flaps; *e.g.* for $C_J=1$, 50 per cent more lift is obtained with a 20 per cent flap than with the pure jet flap;

(*ii*) for a given C_L and deflection, the larger the flap, the smaller is the required C_J; *e.g.* for $\beta=\frac{1}{2}$ radian$=28{\cdot}6°$, $C_L=3$ could be obtained at $C_J=2$ with a pure jet flap, or at $C_J=1$ with a 20 per cent chord blown flap.

These are substantial gains which may well be attained, in part at least, in a real flow, provided that an efficient slot-flap combination can be designed. Thus it appears that the effectiveness of the jet flap scheme might be greatly increased by the use of flaps of finite size (substantially greater than the "shrouds" which have been discussed). At the opposite extreme of low C_J's, it seems that useful gains might be obtained from "super-circulation" in the conventional boundary-layer-control applications.

It may be noted that the 2 per cent flap is sufficiently different from the pure jet flap to indicate that trailing edge conditions can make a good deal of difference.

References

1. Spence, D. A. The Lift Coefficient of a Thin Jet-Flapped Wing. *Proc. Roy. Soc.*, A. Vol. 238, pp. 46-68, 1956.

2. Glauert, H. Theoretical Relationships for an Aerofoil with a Hinged Flap. R. & M. 1095, April 1927.

3. Carlemann, T. Arkiv för Matematik, Astronomi och Fysik, Vol. 16, p. 26, May 1922.

4. Maskell, E. C. and Gates, S. B. Preliminary Analysis for a Jet-Flap System in Two-Dimensional Inviscid Flow. A.R.C. Current Paper 359, June 1955.

Some Identities on Structural Flexibility after Buckling

E. H. MANSFIELD

(*Royal Aircraft Establishment*)

SUMMARY: This paper gives some identities concerning the flexibility of certain elastic structures, including flat plates, at the onset of buckling and subsequently. The identities have a useful application in determining the flexibility and the rate of change of flexibility with load for structures in which the mode in the buckled state changes continuously with load.

1. Introduction

A flat plate, on being loaded in its own plane, deforms initially in its own plane and possesses a certain flexibility. As the loading is increased, the plate may buckle out of its plane, and there will be a sudden increase in the flexibility at the onset of buckling. As the loading is further increased the out-of-plane deflections will increase, but if the out-of-plane *mode* does not alter then the flexibility will not alter, and the load-deflection and load-flexibility curves for the structure will be as in Fig. 1.

If the out-of-plane mode alters continuously with the loading, as the loading is increased beyond the initial buckling stage, then the flexibility will alter, and the load-deflection and load-flexibility curves for the structure will be as in Fig. 2.

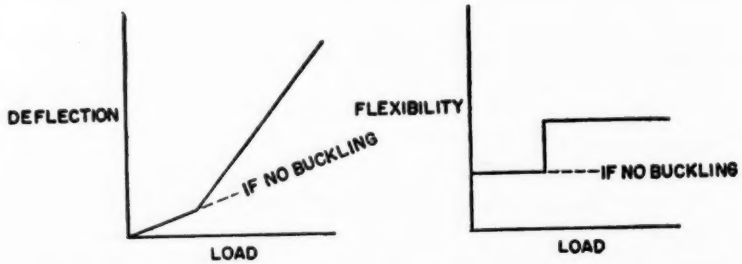

FIGURE 1. Load-deflection and load flexibility curves for structure with constant mode after buckling.

Received June 1958.

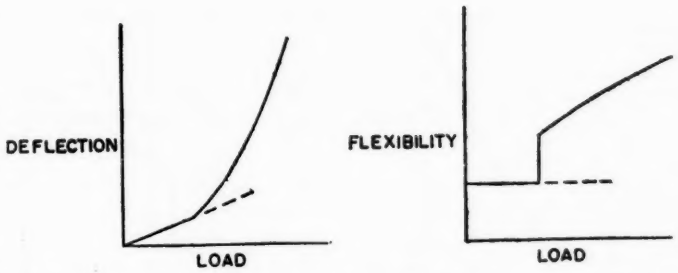

FIGURE 2. Load-deflection and load-flexibility curves for structure with varying mode after buckling.

The calculation of the flexibility for the structure considered in Fig. 2 is considerably more difficult than for that considered in Fig. 1, and it is the object in this paper to derive certain identities which enable the behaviour of such a "varying-mode" structure to be expressed in terms of the behaviour of a "constant-mode" structure. The identities were useful in an earlier paper by the author[1] in connection with the post-buckling behaviour of reinforced plane sheet under shear.

NOTATION

λ, λ' applied load

Δ deflection in the direction of λ

ϕ flexibility, $= d\Delta/d\lambda$

T work done by the applied load

ϕ_0 flexibility before buckling

λ_c actual buckling load

λ_m buckling load for the structure if it were constrained to buckle in the mode which the structure actually would have at a load λ ($\lambda > \lambda_c$)

ϕ_m flexibility of the structure constrained to buckle in the mode which the structure actually would have at a load λ

Δ' deflection not in the direction of λ

ϕ' "cross-flexibility," $= d\Delta'/d\lambda$

Suffix "c" refers to conditions at the onset of actual buckling.

2. Derivation of the Identities

2.1. General Considerations

Consider a structure subjected to a load λ', greater than λ_c, and suppose that the out-of-plane mode has altered from M_c, the initial buckling mode, to M. The state of the structure at this load is independent of the loading history and would

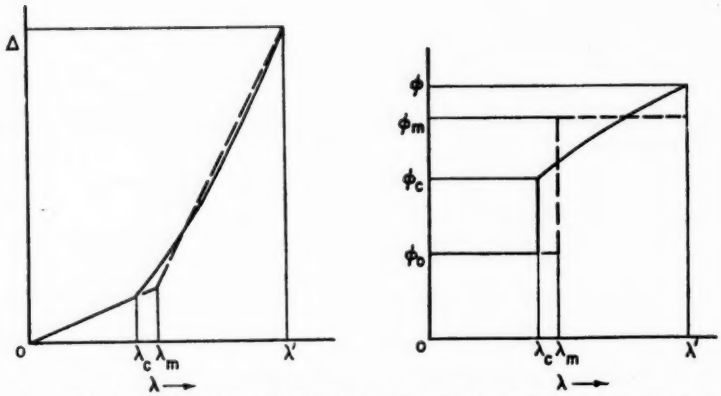

FIGURE 3. Load-deflection and load-flexibility curves for structure in constrained and unconstrained state.

be reached if there had been present in the structure constraints which prevented all out-of-plane modes except M. Such a constrained structure would buckle at a load λ_m, say, and would have a constant flexibility ϕ_m, say, after buckling. For $\lambda < \lambda_c$ there would be no difference between the unconstrained and the constrained structure. The unconstrained and constrained loading paths are indicated by the full and broken lines in Fig. 3.

The fact that the state of the structure is independent of the loading history can be expressed by the equations

$$[\Delta]_{\text{unconstrained}} = [\Delta]_{\text{constrained}} \quad . \quad . \quad . \quad . \quad . \quad (1)$$

and $$[T]_{\text{unconstrained}} = [T]_{\text{constrained}} \quad . \quad . \quad . \quad . \quad . \quad (2)$$

since the internal energy stored may be equated to the work done in each case[2].

Furthermore, Δ and T can be expressed in terms of λ' and ϕ:—

$$\left.\begin{aligned} \Delta &= \int_0^{\lambda'} \phi \, d\lambda, \\ T &= \int_0^{\lambda'} \phi\lambda \, d\lambda. \end{aligned}\right\} \quad . \quad . \quad . \quad . \quad . \quad (3)$$

Now, in the constrained state,

$$\left.\begin{aligned} \phi &= \phi_0 \text{ for } \lambda < \lambda_m \\ \phi &= \phi_m \text{ for } \lambda > \lambda_m, \end{aligned}\right\} \quad . \quad . \quad . \quad . \quad . \quad (4)$$

so that equations (1) and (2) may be combined with (3) and (4) to give

$$\int_0^{\lambda'} \phi \, d\lambda = \phi_0 \lambda_m + \phi_m (\lambda' - \lambda_m) \quad . \quad . \quad . \quad . \quad . \quad (5)$$

and $$\int_0^{\lambda'} \phi\lambda \, d\lambda = \tfrac{1}{2}\phi_0 \lambda_m^2 + \tfrac{1}{2}\phi_m (\lambda'^2 - \lambda_m^2) \quad . \quad . \quad . \quad . \quad (6)$$

Equations (5) and (6) are valid for any value of λ', and may therefore be differentiated with respect to λ' to give expressions for ϕ; furthermore, now that λ' is the independent variable it may be written for convenience as λ.

The main identities are to be derived by differentiating and combining equations (5), (6) and using the condition that, at the onset of buckling,

$$\lambda = \lambda_m = \lambda_c \quad . \quad . \quad . \quad . \quad . \quad . \quad . \quad (7)$$

2.2. The Identities

2.2.1. *Identities in the Buckled State*

$$\phi \equiv \phi_m + \tfrac{1}{2}(\lambda - \lambda_m)\frac{d\phi_m}{d\lambda} \quad . \quad . \quad . \quad . \quad . \quad (A)$$

$$(\lambda - \lambda_m)\frac{d\phi_m}{d\lambda} \equiv 2(\phi_m - \phi_0)\frac{d\lambda_m}{d\lambda} \quad . \quad . \quad . \quad . \quad (B)$$

2.2.2. *Identities at the Onset of Buckling*

$$\phi_c \equiv (\phi_m)_c \quad . \quad . \quad . \quad . \quad . \quad . \quad . \quad (C)$$

$$\left(\frac{d\lambda_m}{d\lambda}\right)_c \equiv 0 \quad . \quad . \quad . \quad . \quad . \quad . \quad . \quad (D)$$

$$\left(\frac{d\phi}{d\lambda}\right)_c \equiv \frac{3}{2}\left(\frac{d\phi_m}{d\lambda}\right)_c \quad . \quad . \quad . \quad . \quad . \quad (E)$$

$$\left(\frac{d\phi_m}{d\lambda}\right)_c \equiv 2(\phi_c - \phi_0)\left(\frac{d^2\lambda_m}{d\lambda^2}\right)_c \quad . \quad . \quad . \quad . \quad (F)$$

Identity (C) means that the flexibility at the onset of buckling is independent of the rate of change of the shape of the mode.

Identity (D) is a restatement of the fact that at the onset of buckling the true buckling mode is such as to make the buckling load a minimum[3]. For the same reason $(d^2\lambda_m/d\lambda^2)_c$ cannot be negative.

Since $\phi_c > \phi_0$ and $(d^2\lambda_m/d\lambda^2)_c$ is not negative, it follows from identities (E) and (F) that $(d\phi/d\lambda)_c$ is not negative. This means that the flexibility immediately after the onset of buckling cannot decrease with increase of load.

2.2.3. *Identities for Cross-Flexibilities*

Similar identities may be found if Δ' is a deflection in a direction different from λ, but such identities are now to be deduced only from equation (5), as equation (6) was based on equating work done.

Identities corresponding to (C) and (E) are now

$$\phi_c' \equiv (\phi_m')_c \quad . \quad . \quad . \quad . \quad . \quad . \quad . \quad . \quad . \quad \text{(G)}$$

$$\left(\frac{d\phi'}{d\lambda}\right)_c \equiv 2\left(\frac{d\phi_m'}{d\lambda}\right)_c - \tfrac{1}{2}\left(\frac{\phi_c' - \phi_0'}{\phi_c - \phi_0}\right)\left(\frac{d\phi_m}{d\lambda}\right)_c \quad . \quad . \quad . \quad \text{(H)}$$

3. Conclusions

Certain identities have been derived in which the post-buckling flexibility of a structure with a post-buckling mode that varies with the load is related to the post-buckling flexibility of a structure constrained to deflect in a constant post-buckling mode.

The identities have a useful application in determining the flexibility and the rate of change of flexibility with load at the onset of buckling.

References

1. Mansfield, E. H. On the Post-Buckling Behaviour of Stiffened Plane Sheet under Shear. R. & M. 3073, July 1958.

2. Williams, D. The Use of the Principle of Minimum Potential Energy in Problems of Static Equilibrium. R. & M. 1827. January 1938.

3. Love, A. E. H. *The Mathematical Theory of Elasticity*. Cambridge University Press. 1892. Reprinted by Dover Publications, New York, 1944.

A Note on the Drag of Wing-Body Combinations in Linearised Supersonic Flow

L. E. FRAENKEL

(Department of Aeronautics, Imperial College)

SUMMARY: In this note Ward's "area-transfer rule" is modified in order to make it more suitable for configurations with fuselages or nacelles which are neither slender nor smooth (although they are assumed to have small profile slope). The body source strength of Ward's analysis, which is appropriate only for smooth, slender bodies, is replaced by a source strength which is valid more generally. However, the drag contributions of the body multi-sources and of the interference field are still neglected, so that the theory is tentative rather than rigorous.

1. Introduction

Substantial advances towards calculation of the wave drag of whole aircraft configurations have recently been made as a result of work by Hayes[1] and others in the United States, and by Ward[2] in the United Kingdom. The present note deals with a slight modification of Ward's principal result, the so-called "area-transfer rule."

A wing-body combination free of local transverse forces may be represented by a surface distribution of sources and a line distribution of sources and multi-sources: other representations, of course, are also possible. Two sets of line singularities are required in general: those appropriate to the body alone, which will be called "body" sources and multi-sources, and those required to cancel the normal velocity induced on the body by the wing, which will be called "interference" sources and multi-sources. The strength of the wing sources is immediately known, but, in general, the strength of the line singularities, and their contribution to the drag, are not calculated so easily. However, if the body is "slender" and "smooth" considerable simplifications result: these form the basis of Ward's analysis.

A precise explanation of terms is now required. By a slender body we mean one whose maximum radius is small compared with both its length and some characteristic wing dimension, like the chord or the square root of the plan form area. Throughout this note, bodies with non-vanishing nose and base areas are

Received June 1957.

taken to be extended to infinity upstream and downstream by cylinders parallel to the free stream: a smooth body is then one such that the slope of the resulting profiles is continuous *everywhere*. Only "net" wings will be considered; that is, no hypothetical extension of the wing inside the body will be contemplated.

The simplifications already mentioned are as follows. If the body is slender, then

(*i*) the drag contribution of the interference sources and multi-sources is negligible,

(*ii*) the drag due to interaction of the body multi-sources with the wing sources is negligible.

If in addition the body is smooth, then

(*iii*) the body source strength is simply the rate of change of cross-sectional area,

(*iv*) the drag contribution of the body multi-sources is negligible.

The drag therefore consists of only three terms: the drag of the wing alone, the drag of the body sources alone, and a coupling term between the wing sources and the body sources.

Most aircraft fuselages are neither slender nor smooth; on the other hand an "exact" analysis of the drag (that is, one which is exact within the framework of linearised theory) leads to formulae which are not suitable for computing the drag of general configurations. (Such an exact analysis is made in Ref. 3 for wing-quasi-cylinder combinations). A compromise is therefore sought in the present note. The body source strength of Ward's analysis, which is appropriate only to smooth slender bodies, is replaced by a source strength which is valid more generally, but it is *assumed* that the statements (*i*), (*ii*) and (*iv*) are still approximately true. The new body source strength is calculated by combining the quasi-cylinder and slender-body source strengths in the manner already used for the pressure on the body by Lighthill (Ref. 4, p. 454), Ward (Ref. 5, p. 216) and Warren and Fraenkel[6].

The drag result of this note requires more computation than does Ward's original form, because the line source strength must be computed first, but this may not be too difficult if an electronic machine is used. A more serious defect of the new drag integral is that it is much more difficult to minimise than Ward's expression, because it involves the line source strength rather than the body geometry directly. The question of whether these new complications are worthwhile can probably be decided only by trial.

NOTATION

$B=(M^2-1)^{\frac{1}{2}}$

D drag force

$F(z)$ special function, *see* equations (3) to (5)

$g(z)$ body source strength
$H(z)$ Heaviside unit function
$h(z)$ transferred area function, *see* equation (9)
I_n, K_n modified Bessel functions of the first and second kinds
p Heaviside operator with respect to z
M free stream Mach number
$R(z)$ body radius
$\mathbf{R}$ position vector
$\mathbf{r}$ vector distance from z-axis
(r, θ, z) cylindrical co-ordinates with z-axis parallel to free stream
$S(z)$ body cross-sectional area
$T(\mathbf{R})$ wing thickness
U free stream velocity
ρ_0 free stream density
ϕ perturbation velocity potential

2. The Strength of a Line of Sources

A fundamental problem of the flow past bodies of revolution at zero incidence is: given the potential

$$\phi(r, z) = -\frac{U}{2\pi}\int_{-\infty}^{z-Br} \frac{g(z_1)}{\sqrt{[(z-z_1)^2 - B^2r^2]}}\, dz_1, \qquad (1)$$

to find the source strength $g(z_1)$ such that the boundary condition

$$\frac{\partial \phi}{\partial r}(R(z), z) = UR'(z) \qquad (2)$$

is satisfied.

With a quasi-cylinder, for which $R(z)$ is nearly constant and equal to R_0, say, the solution of this problem is as follows. We introduce the function* $F(z)$, defined by

$$\frac{e^{-p}}{pK_1(p)} \rightleftharpoons F_1(z)\, H(z) = F(z), \qquad (3)$$

where H is the Heaviside unit function.

*The derivative of this function has been roughly tabulated by Nielsen[8, 9], who denotes our $F'(z)$ by $-M_0(z)$. Since the integral in relation (8*b*) can be written in terms of F' and S', instead of F and S'', F' may, in fact, be the more useful function for practical purposes.

The behaviour of this function is indicated by

$$F(z) \sim \frac{2\sqrt{2}z^{\frac{1}{2}}}{\pi}\left(1 - \frac{1}{4}z + \frac{11}{160}z^2 \ldots\right), \quad z \ll 1, \qquad (4a)$$

$$\sim 1 - \frac{1}{2}\frac{1}{(z-1)^2} + \left[\frac{29}{8} - 3\log 2(z-1)\right]\frac{1}{(z-1)^4} \ldots, \quad z \gg 1. \qquad (4b)$$

and the function could be tabulated from the identity

$$F(z) = 1 - \int_0^\infty e^{-\lambda(z-1)} \frac{I_1(\lambda)}{K_1^2(\lambda) + \pi^2 I_1^2(\lambda)} \frac{d\lambda}{\lambda^2}. \qquad (5)$$

Then the quasi-cylinder source strength is

$$g_0(z) = \int_{-\infty}^{\infty} F\left(\frac{z - z_1}{BR_0} + 1\right) dS'(z_1). \qquad (6)$$

The source strength of a smooth slender body is

$$g_1(z) = S'(z). \qquad (7)$$

Both these results are approximately contained in each of the following, which can be shown rigorously to be valid approximations for any body of revolution with continuous radius and small profile slope:—

$$g_a(z) = \int_{-\infty}^{\infty} F\left(\frac{z - z_1}{BR(z_1)} + 1\right) dS'(z_1), \qquad (8a)$$

$$g_b(z) = \int_{-\infty}^{\infty} F\left(\frac{z - z_1}{BR(z)} + 1\right) dS'(z_1). \qquad (8b)$$

g_a and g_b, which are only two of a large number of possible functions, are equivalent because F differs significantly from unity only when its argument is not large, that is when $z - z_1$ is $O(R)$ or less, and in these regions $R(z) \simeq R(z_1)$. It might appear at first sight that g_a should correspond exactly to the Lighthill form of the pressure on the body, while g_b should correspond to the Ward and Warren-Fraenkel form, but this is not the case; further justifiable approximations are required before either of the source strengths given yields precisely either of the forms for the pressure on the body given by these authors.

It is important to notice that, in the region of the cylindrical extension behind a body of finite base area, the source strength does not vanish: sources are required in this region to make the flow parallel to the free stream, but their strength can be shown to decay like z^{-2} for large z. Behind a pointed tail g_b vanishes exactly, but g_a only approximately; g_a could, of course, be "cut off" in such a region.

The source strengths g_a and g_b are continuous: a discontinuity in $S'(z_1)$ at $z_1 = e_i$ contributes a term which behaves initially like

$$\frac{2\sqrt{2}}{\pi} \Delta S_i' \left[\frac{z-(e_i - BR_i)}{BR_i}\right]^{\frac{1}{2}}$$

and after a few radii like $\Delta S_i'$.

3. The Representation of a Wing-Body Combination by Singularities

In what follows it is assumed that the mean wing surface and the body axis are both parallel to the free stream.

The wing may be represented by sources of strength $T'(\mathbf{R})$ distributed over its mean surface. Alternatively, it may be represented by line sources and multi-sources distributed along the body axis: these give a valid representation of the flow outside a circular cylinder which is centred on the body axis and contains the wing. The line source strength in this case is

$$h(z) = \frac{1}{\pi} \iint_{|z-z_1| \leqslant Br_1} \frac{T'(\mathbf{R}_1)}{\sqrt{[B^2 r_1^2 - (z-z_1)^2]}} \, dS_1, \qquad . \quad . \quad . \quad (9)$$

which is Ward's transferred-area function and is denoted by $A'(z)$ in Ref. 2.

The former representation of the wing is useful for calculating the drag of the wing alone; the latter is useful for calculating the drag due to interaction of the wing and body fields.

The body is represented by a line of sources which satisfies the body boundary condition averaged around the body contour: the body multi-sources and the interference sources and multi-sources are neglected. If $R_m(z)$ is a mean radius, averaged in some convenient way with respect to θ, the body source strength is taken as

$$g_a(z) = \int_{-\infty}^{\infty} F\left(\frac{z-z_1}{BR_m(z_1)} + 1\right) dS'(z_1), \qquad . \quad . \quad . \quad (10)$$

or as the corresponding $g_b(z)$.

4. The Drag

Upon application of the methods of Refs. 1, 2 or 3 to the present problem the drag is found to be

$$D = -\frac{\rho_0 U^2}{4\pi}\left\{ \iint\limits_{|z_1-z_2|\geqslant B} \iint\limits_{|\mathbf{r}_1-\mathbf{r}_2|} T''(\mathbf{R}_1)\, T''(\mathbf{R}_2) \cosh^{-1}\frac{|z_1-z_2|}{B|\mathbf{r}_1-\mathbf{r}_2|}\, dS_1 dS_2 + \right.$$

$$\left. + 2\int_{-\infty}^{\infty}\int_{-\infty}^{\infty} h'(z_1)\, g'(z_2) \log|z_1-z_2|\, dz_1 dz_2 + \int_{-\infty}^{\infty}\int_{-\infty}^{\infty} g'(z_1)\, g'(z_2) \log|z_1-z_2|\, dz_1 dz_2 \right\} \quad . \quad . \quad . \quad (11)$$

$$= -\frac{\rho_0 U^2}{4\pi}\left\{ \iint\limits_{|z_1-z_2|\geqslant B} \iint\limits_{|\mathbf{r}_1-\mathbf{r}_2|} T''(\mathbf{R}_1)\, T''(\mathbf{R}_2) \cosh^{-1}\frac{|z_1-z_2|}{B|\mathbf{r}_1-\mathbf{r}_2|}\, dS_1 dS_2 + \right.$$

$$+ \int_{-\infty}^{\infty}\int_{-\infty}^{\infty} [g'(z_1)+h'(z_1)]\,[g'(z_2)+h'(z_2)] \log|z_1-z_2|\, dz_1 dz_2 -$$

$$\left. - \int_{-\infty}^{\infty}\int_{-\infty}^{\infty} h'(z_1)\, h'(z_2) \log|z_1-z_2|\, dz_1 dz_2 \right\} \quad . \quad (12)$$

A new feature of these results is that the third integrand of (11) and the second integrand of (12) vanish only outside semi-infinite (instead of outside finite) regions. But the integrals can be expressed as finite integrals by a simple change of variable. If the origin is chosen so that $g(z)$ and $h(z)$ vanish for $z \leqslant 1$, these integrals are of the form

$$I = \int_1^{\infty}\int_1^{\infty} f'(z_1)\, f'(z_2) \log|z_1-z_2|\, dz_1 dz_2 .$$

Putting $z_1 = t_1^{-1}$, $z_2 = t_2^{-1}$, we have

$$I = \int_0^1\int_0^1 \frac{d}{dt_1} f(t_1^{-1}) \frac{d}{dt_2} f(t_2^{-1}) \log|t_1-t_2|\, dt_1 dt_2 - \int_0^1 \frac{d}{dt_1} f(t_1^{-1}) \log|t_1|\, dt_1 \int_0^1 \frac{d}{dt_2} f(t_2^{-1})\, dt_2 -$$

$$- \int_0^1 \frac{d}{dt_2} f(t_2^{-1}) \log|t_2|\, dt_2 \int_0^1 \frac{d}{dt_1} f(t_1^{-1})\, dt_1$$

$$= \int_0^1\int_0^1 \frac{d}{dt_1} f(t_1^{-1}) \frac{d}{dt_2} f(t_2^{-1}) \log|t_1-t_2|\, dt_1 dt_2 \quad . \quad . \quad . \quad . \quad . \quad (13)$$

since $g(z)$ and $h(z)$ vanish at $z=1$ and $z=\infty$. $(d/dt)\, g(t^{-1})$ is $O(t)$ for $t \longrightarrow 0$ and $O((1-t)^{-\frac{1}{2}})$ for $t \longrightarrow 1$ if S' begins with a discontinuity.

The problem of minimising the second integral of (12) for given restrictions on body geometry is a difficult one. If the method of this note proves worthwhile, some progress may be made with this problem by treating the body as a quasi-cylinder for purposes of drag minimisation: in this connection it may be significant that smooth slender bodies of minimum wave drag are particular cases of quasi-cylinders of minimum wave drag. This result is due to Heaslet and Fuller[7], whose methods may prove helpful in the present context.

5. Wing-Body-Nacelle Combinations

To illustrate the application of the foregoing method to configurations with engine nacelles, we consider a configuration having a single nacelle whose axis is $\mathbf{r}=\mathbf{r}_N$. The nacelle source strength, g_N, is calculated in the same way as that of the body, g_B. The following notation is now adopted.

$$\frac{1}{\pi}\iint_{|z-z_1|\leqslant Br_1}\frac{T'(\mathbf{R}_1)}{\sqrt{[B^2r_1^2-(z-z_1)^2]}}\,dS_1+\frac{1}{\pi}\int_{|z-z_1|\leqslant Br_N}\frac{g_N(z_1)}{\sqrt{[B^2r_N^2-(z-z_1)^2]}}\,dz_1=h_{W+N}(z), \quad . \quad . \quad . \quad (14)$$

$$\frac{1}{\pi}\iint_{|z-z_1|\leqslant B|\mathbf{r}_1-\mathbf{r}_N|}\frac{T'(\mathbf{R}_1)}{\sqrt{[B^2|\mathbf{r}_1-\mathbf{r}_N|^2-(z-z_1)^2]}}\,dS_1=k_W(z), \quad . \quad . \quad (15)$$

$$-\frac{\rho_0U^2}{4\pi}\int_{-\infty}^{\infty}\int_{-\infty}^{\infty}f'(z_1)f'(z_2)\log|z_1-z_2|\,dz_1dz_2=D\{f\}. \quad . \quad . \quad (16)$$

Then, under the assumptions of Section 1, the drag is found to be

$$D=D_{Wing}+D\{g_B+h_{W+N}\}-D\{h_{W+N}\}+D\{g_N+k_W\}-D\{k_W\}. \quad . \quad . \quad (17)$$

ACKNOWLEDGMENT

The author is indebted to Mr. L. B. Jones, of the English Electric Company, Warton Aerodrome, for explaining to him the practical need for some such modification of Ward's result as is attempted here.

REFERENCES

1. HAYES, W. D. Linearized Supersonic Flow. Thesis, California Institute of Technology, North American Aviation Rep. AL-222, 1947.

2. WARD, G. N. The Drag of Source Distributions in Linearized Supersonic Flow, College of Aeronautics Report 88, 1955.

3. FRAENKEL, L. E. The Wave Drag of Wing-Quasi-Cylinder Combinations at Zero Incidenc *The Aeronautical Quarterly*, February 1958.

4. LIGHTHILL, M. J. *General Theory of High Speed Aerodynamics*: Section E. (*Edito* W. R. Sears). Oxford University Press, 1955.

5. WARD, G. N. *Linearized Theory of Steady High-Speed Flow*. Cambridge University Pre 1955.

6. WARREN, C. H. E. and FRAENKEL, L. E. A Combination of the Quasi-Cylinder and Slend Body Theories. *Journal of the Royal Aeronautical Society*, Vol. 59, pp. 305-308, April 19

7. HEASLET, M. A. and FULLER, F. B. Axially Symmetric Shapes with Minimum Wave Dra N.A.C.A. T.N. 3389, 1955.

8. NIELSEN, J. N. Supersonic Wing-Body Interference. Thesis, California Institute Technology, 1951.

9. NIELSEN, J. N. and PITTS, W. C. Wing-Body Interference at Supersonic Speeds with a Application to Combinations with Rectangular Wings. N.A.C.A. T.N. 2677, 1952.

Erratum

May 1958 (Vol. IX, Part 2)

In the paper by F. Walkden "*The Shock Pattern of a Wing-Body Combination Far from the Flight Path*" the line immediately after equation (55) on p. 183 i misprinted. This line should read

"In relation (55), s represents the distance along a ray, where the rays star from the . . . . . ."